2010

Mechanisms Of Presynaptic CaV2 Calcium Channel Localization In Caenorhabditis Elegans

Yasunori Saheki

MECHANISMS OF PRESYNAPTIC CAV2 CALCIUM CHANNEL LOCALIZATION IN CAENORHABDITIS ELEGANS

A Thesis Presented to the Faculty of

The Rockefeller University

in Partial Fulfillment of the Requirements for

the degree of Doctor of Philosophy

by

Yasunori Saheki

June 2010

MECHANISMS OF PRESYNAPTIC CAV2 CALCIUM CHANNEL LOCALIZATION IN CAENORHABDITIS ELEGANS

Yasunori Saheki, Ph.D.

The Rockefeller University 2010

Neurotransmitter release at nerve terminals is a fundamental aspect of communication in the nervous system. Voltage changes in the presynaptic membrane are sensed by presynaptic voltage-gated calcium channels that mediate calcium influx at the nerve terminals to execute exocytosis of various kinds of neurotransmitters. Defects in presynaptic calcium channels lead to many neurological disorders, emphasizing the importance of these channels in the regulation of neuronal activities in the brain. Previous physiological studies have focused on opening kinetics of the channels and their modulation by auxiliary subunits. Cell biological questions such as trafficking and clustering of the channels at the presynaptic site, however, have remained largely unanswered, partly due to a lack of an *in vivo* assay system to monitor calcium channel biogenesis in intact animals.

In my thesis, I established an *in vivo* system to visualize the UNC-2 alpha1 subunit of the *C. elegans* CaV2 channel. I showed that GFP-tagged UNC-2 is localized to presynaptic active zones of sensory and motor neurons. Using this system, I conducted a direct visual genetic screen for mutants that are defective in UNC-2 localization, identifying three genes, *calf-1*, *unc-36* and *pqn-53/calf-2*. CALF-1 is a neuronal-specific one-pass transmembrane protein that resides in the endoplasmic reticulum, and is

required for endoplasmic reticulum exit of UNC-2. Structure-function analysis revealed that the transmembrane domain and the cytosolic arginine-based basic motifs are important for the function of CALF-1. Acute induction of *calf-1* mobilizes preexisting UNC-2 for delivery to synapses, consistent with a direct trafficking role. The calcium channel alpha2-delta auxiliary subunit UNC-36 is also required for endoplasmic reticulum exit of UNC-2, but has additional functions. The polyglutamine protein *pqn-53* is localized to the nucleus; PQN-53 inhibits a non-canonical unfolded protein response pathway, and activation of this pathway in *pqn-53* mutants leads to the reduced expression of UNC-2 and other transmembrane proteins. Furthermore, *pqn-53* mutants are resistant to killing by pathogenic bacteria, potentially due to constitutive activation of the non-canonical unfolded protein response. *pqn-53* couples multipass transmembrane protein biogenesis with endoplasmic reticulum stress, and provides insights into the regulation of pathogen resistance by the endoplasmic reticulum stress-sensing pathway.

To my family and friends,
who supported my graduate studies

Acknowledgments

I am extraordinarily grateful to my thesis advisor, Cori Bargmann, for her generous support throughout my graduate studies. As a foreign graduate student from Japan, every day has been an amazing experience for me. She creates a wonderful collaborative environment in the lab that made my graduation possible. Her dedication to basic science inspired me and will continue to do so.

My committee members, Tim Ryan and Nat Heintz, have been extremely supportive. Their insightful comments and advices during my committee meetings encouraged me to do new experiments, and I always enjoyed discussing my new findings with them. I would like to thank Josh Kaplan for joining my thesis committee as an external member. His thorough studies of glutamate receptor trafficking inspired me during the course of my thesis work.

Scott Dewell at the Rockefeller Genomics Resource Center helped me analyze Illumina/Solexa mRNAsea data. Without his support, it would have been impossible to make sense of the huge amount of data. Loren Looger at the Janelia Farm provided us reagents necessary for calcium imaging and photoconversion experiments. Alison North and Shiva Bhuvanendran at the Rockefeller BioImaging Resource Center were kind enough to provide me with knowledge and techniques for using confocal microscopy.

Christian Woods is a wonderful lab manager. He manages the entire lab very efficiently and supported the progress of my project and others in many ways. Hernan Jaramillo organizes the strain lists of nematodes in our lab. He froze and thawed strains for me without complaint in spite of my infinite requests. Manoush Ardzivian provides us with plates and medium every day. There has never been a time when we were short

of plates or medium, thanks to her continuous efforts to keep up with our use. Holly Hunnicutt taught me the skills to deal with administration officers in general and helped me communicate with them whenever it was necessary. She is very efficient with all the paperwork in the lab, and she inspired me as a dedicated professional person.

I enjoyed having lunch with my wonderful lab members every day. I would like to thank Sreekanth Chalasani, Tapan Maniar, and Patrick McGrath for their insights and advice throughout my project. Conversations with my previous and current bay mates, Sarah Bauer Huang, Jason Kennerdell, Steven Flavell and Jennifer Garrison made my lab life enjoyable and fun. Andres Bendesky, Evan Feinberg, Evan Makosco, Greg Lee, Bluma Lesch, Andrew Gordus, Makoto Tsunozaki, Laura Winzenread, Heeun Jang, Navin Pokala, Elizabeth Glater, Manuel Zimmer, Andy Chang, Massimo Hilliard and Chiou-Fen Chuang all motivated me to make progress in English, and above all, I appreciated scientific as well as casual conversations with them.

My faculty house 21C roommates, Jason Schwarz, Thibaud Taillefumier, Steven Soll and Guillaume Charron, are good friends and great scientific partners to talk with. My scientific career in the U.S. originates from everyday conversations in our gigantic apartment. They provided an environment of free conversation beyond the border of countries. I would like to thank Masanori Obayashi for inspiring me, and his infinite and eternal passion continues to encourage me in my scientific career. My entire family has been always supportive, and I enjoyed their occasional visits to New York City. All my advisors and friends are extremely valuable individuals, whom I respect, and their advice has been invaluable and will continue to be in my life.

Table of Contents

List of Figures

List of Tables

Chapter 1

Introduction

Protein trafficking to proper microdomains creates functional diversity within a single neuronal cell. In neurons, different functions are associated with the soma, the axonal shaft, presynaptic terminals, and postsynaptic dendrites. In spiking neurons, the action potential travels through the axonal shaft to reach the presynaptic terminal. In the terminal, membrane depolarization activates presynaptic voltage-gated calcium channels (Pre-VGCC) to allow calcium ion flux and neurotransmitter release. In dendrites, neurotransmitters activate postsynaptic receptors and associated signaling cascades. The functional specialization of each domain is achieved by the accurate sorting and tethering of specialized molecules such as channels. How the specific localization of each synaptic protein is accomplished is an intensive focus of molecular neuroscience.

Pre-VGCC are the primary calcium source for exocytosis at the presynaptic terminal. Their functions are largely conserved over different kinds of organisms including human, rodents, flies and worms. Disruptions of Pre-VGCC function are implicated in human epilepsy, migraine, autism-spectrum disorders, and bipolar disease, underlining the importance of these channels in the regulation of neuronal excitability and function [1]. Strong loss-of-function mutations in Pre-VGCC in *Drosophila melanogaster* and *Caenorhabditis elegans* lead to lethality and severe uncoordination, respectively [2, 3]. Despite the evolutionary, clinical, and physiological importance of Pre-VGCCs, their mechanism of localization to the presynaptic terminal is unknown.

Under the supervision of Cori Bargmann, I explored the mechanism of Pre-VGCC localization in the presynaptic terminals, using a genetic approach in *Caenorhabditis elegans*.

Synapse Formation and Presynaptic Assembly

Synapses are highly organized structures. Electron microscopic analysis of presynapses has revealed electron-dense matrix associated with patches of the axonal plasma membrane surrounded by small cluster of synaptic vesicles[4, 5]. These ultrastructural specializations of the plasma membrane, named active zones, are juxtaposed to a second electron-dense specialization present in the postsynaptic membrane, the postsynaptic density. Biochemical purification of the proteins from synaptosome preparations identified several proteins associated with the presynaptic electron-dense matrix, including Bassoon, Piccolo, RIM1 and ELKS [6]. Stereotypic morphologies of the presynaptic active zones in different types of neurons suggest that the active zone is structured to tether synaptic vesicles and Pre-VGCC in a regular pattern; the presynaptic scaffold proteins must exert special constraints on the synaptic vesicle distribution as well as Pre-VGCC. A presynaptic ankyrin is required for proper synapse formation of *Drosophila* neuromuscular junctions (NMJs) through regulation of microtubules indicating the essential role of the cytoskeleton in synapse formation[7]. A link between the scaffold and synaptic membrane proteins is *Drosophila* Bruchpilot, a homolog of CAST/ELKS presynaptic scaffolding protein that localizes in donut-shaped structures at the active zone of NMJs and is required for *Drosophila* Pre-VGCC localization[8]. Below,

I will describe briefly the induction of presynapses and the assembly of presynaptic components.

The differentiation of synapses takes place in multiple steps including synapse initiation, induction and maintenance. In the mammalian CNS, the initiation or establishment of an initial contact site between an axon and a dendrite is thought to occur through cell adhesion molecules such as immunoglobulin (Ig) domain-containing proteins, leucine-rich repeat (LRR) domain-containing proteins, integrins, and members of the cadherin superfamily [9, 10]. Either on their own or through intermediate proteins, the cell adhesion proteins then trigger pre- and postsynaptic differentiation. Two complexes suggested to drive synaptic differentiation are the Beta-neurexin-neuroligin heterodimeric or synCAM homodimeric complexes. Neurexin-neuroligin and synCAM interactions drive the assembly of pre- and post-synaptic components in cell culture [11, 12]. The importance of these complexes for synapse formation *in vivo* is still being established. Neuroligin triple knockouts have defects in inhibitory synapse development, but not in all aspects of synapse formation as predicted by the initial model [13]. In *Drosophila*, neurexin is required for the proper apposition of active zones to postsynaptic densities, synapse number and synaptic transmission [14, 15]. Mouse knockouts of all the isoforms of neurexin have not been reported, but alpha-neurexin knockouts show reduced inhibitory synapse number and defective neurotransmission [16]. Nervous system phenotypes of synCAM knockouts have not been described.

Differentiation of the presynaptic terminal includes the formation of active zones, clustering of vesicles and recruitment of calcium channels. Molecules implicated as presynaptic organizers in the mammalian CNS based on cell biological studies include

neurexin, synCAM adhesion molecules, and soluble factors including WNT-7a, FGF-22 and glia-derived thrombospondin [17-20]. Scaffolding proteins such as CASK, Mint and Veli are suggested contributors to scaffolding function at presynaptic terminals [21].

A powerful route to understanding synapse initiation is through the study of genetic model systems. In *C. elegans*, the HSNL neuron, a primary component of an egg-laying circuit, specifies its synapse location by heterodimeric interactions between the immunoglobulin superfamily proteins SYG-1 and SYG-2 *in vivo* [22, 23]. The localization of SYG-1 at synapses leads to presynaptic assembly by recruiting other scaffolding proteins such as SYD-2 (liprin-alpha) and SYD-1 [24]. These induction and differentiation steps are followed by structural and functional maturation and maintenance processes, which are important for the full function of the synapses in a circuit or a network. More broadly, studies from *C. elegans* and *Drosophila melanogaster* have identified many players that coordinate synaptic vesicle clustering and active zone formation at a variety of synapses. These include SAD-1 kinase, SYD-2/liprin-alpha, SYD-1 and RPM-1/Hiw/FSN-1/dFsn ubiquitin ligase complex [25-30]. RSY-1 directly interacts with SYD-2 and inhibits its synaptic assembly function. This antagonistic regulation implicates a balance between synaptogenic factors and anti-synaptogenic factors in proper synapse formation and presynaptic assembly[31]. Glia-derived netrin acts non-cell autonomously in neurons to induce local synaptogenesis in *C. elegans* [32]. Synaptogenic proteins organize many components of the presynaptic specialization through cell biological mechanisms that are still being worked out.

Synapse maintenance and elimination

Once synapses are established, they can be maintained for weeks to months and perhaps years in mature vertebrate brains [33]. These studies indicate that synapses have mechanisms to maintain their structure over long periods of time. Some presynaptic proteins such as synapsin, actin, and Munc13 are rapidly exchanged throughout synaptic life [34, 35]. Synapses and synaptic molecules can be eliminated in active developmental processes regulated by molecules such as Wnt [36, 37], netrin [38] and complement proteins [39]. In *C. elegans*, SYG-1 interacts with the E3 ubiquitin ligase, SKR-1, and inhibits assembly of SCF complex to protect nearby synapses in HSNL neurons[40]. This study illustrates the importance of subcellular regulation of ubiquitin-mediated protein degradation in elimination of nascent synapses.

Individual presynaptic molecule can also be targets of elimination for rapid changes in synaptic communication. In mammalian CNS synapses, SCRAPPER, a synaptically-localized E3 ligase, directly binds and ubiquitinates RIM1 complex to modulate synaptic vesicle releases [41]. In addition to SCRAPPER, the anaphase-promoting complex (APC), Siah and Staring E3 ligases selectively target liprin-alpha, synaptophysin and syntaxin for degradation respectively [42-44]. The dynamic regulation of synapses is a critical feature of synapse maintenance.

Lessons from *C. elegans* studies of AMPA receptor trafficking

In the vertebrate central nervous system, fast excitatory synaptic transmission is mediated primarily by two families of glutamate receptors (GluRs): alpha-amino-3-hydroxy-5-methyl-4-isoxazole propionic acid (AMPA) receptors and N-metheyl-D-aspartate

(NMDA) receptors. Regulated trafficking of AMPA-type glutamate receptors from postsynaptic elements has been implicated as a potential mechanism for changes of synaptic strength in learning and memory [45]. Genetic studies with *C. elegans* have contributed significantly to the identification of molecular mechanisms that regulates the abundance of AMPA-type glutamate receptors. The *C. elegans* genome contains eight non-NMDA ionotropic glutamate receptor subunit genes, one of which is *glr-1*. GLR-1 is expressed in ventral cord interneurons, among other places, and it localizes to postsynaptic elements at sensory-interneuron synapses [46] as well as interneuron-interneuron synapses [47]. Studies of GLR-1 trafficking were facilitated by the use of a GFP-tagged form of GLR-1. GLR-1::GFP enabled visualization of the protein *in vivo* in live animals, allowing efficient genetic screens for molecules required for localization of the channel [47].

Trafficking of GLR-1 from cell bodies to synapses is regulated by CaMKII and voltage-gated calcium channels, suggesting that activity-dependent mechanisms regulate channel traffic[48]. Ubiquitin and the AP180 clathirn adaptor protein mediate endocytosis of GLR-1; direct ubiquitination of GLR-1 is required for endocytosis mediated by *unc-11*, the *C. elegans* homolog of AP180, suggesting that ubiquitin and clathrin-mediated endocytosis act together to regulate the abundance of GLR-1 in synapses [47]. A second ubiquitin regulation pathway is represented by LIN-23, the substrate recognition subunit of Skp1/Cullin/F Box (SCF) ubiquitin ligase which regulates the abundance of GLR-1 indirectly through ubiquitination of the beta-catenin homolog BAR-1. The effect of BAR-1 on synapse structure broadens the role of Wnt signaling in multiple aspects of synapse regulation that include synaptogenesis, synapse elimination and regulation of the

abundance of synaptic receptors [49]. UNC-108/Rab2 is also required for postendocytic trafficking of GLR-1, implicating this specific Rab GTPase in the trafficking of transmembrane receptors [50].

Mutations in the ligand-binding and pore domains of GLR-1 prevent the channel from exiting the endoplasmic reticulum [51]. This study suggests that functional maturation is important for passing the quality control system of the endoplasmic reticulum. Trafficking of GLR-1 from the endoplasmic reticulum is also regulated by phosphorylation of a PDZ protein, LIN-10. CDK-5/Cdk5 phosphorylates LIN-10/Mint-1 and regulates the abundance of GLR-1 [52]. LIN-10 negatively regulates the abundance of GLR-1; CDK-5-mediated phsphorylation of LIN-10 reduces the amount of LIN-10 at synapses, which in turn cause increased GLR-1 expression at synapses. In *cdk-5* mutants, GLR-1 is retained in the endoplasmic reticulum, indicating that LIN-10 and CDK-5 regulate efficient GLR-1 endoplasmic reticulum exit [52]. These seminal studies emphasize the strength of the genetic approach for understanding receptor trafficking and clustering at synapses.

Recent evidence regarding the mechanism of calcium channel clustering

Neuronal VGCCs are central regulators of synaptic vesicle exocytosis, dendritic integration, and calcium-dependent gene regulation [53]. A VGCC consists of one pore-forming alpha1 subunit that defines intrinsic channel properties, and auxiliary alpha2-delta, beta and sometimes gamma subunits that modify channel kinetics and channel density [54].

Specific genes in the CaV gene family encode physiologically distinct alpha1 subunits. Mammalian L-type channels with CaV1 alpha1 subunits are mainly required for gene regulation and dendritic integration, N-, P/Q- and R-type channels with CaV2 alpha1 subunits are required for neurotransmitter release and dendritic calcium transients, and T-type channels with CaV3 alpha1 subunits are required for repetitive firing [53]. CaV1, CaV2, and CaV3-related genes are found in invertebrates as well as vertebrates [55]. The fruit fly *Drosophila melanogaster* and the nematode *Caenorhabditis elegans* each have one predicted CaV2 alpha1 subunit, encoded by the *cacophony* and *unc-2* genes, respectively. Fly CaV2/*cacophony* mutants are inviable, with defects in calcium-dependent neurotransmitter release at the neuromuscular junction suggesting the loss of the presynaptic calcium current [2, 56]. A GFP-tagged Cacophony protein is localized to presynaptic active zones, consistent with a role at synapses [57]. *C. elegans* CaV2/*unc-2* mutants are uncoordinated, with defects in evoked neurotransmitter release at the neuromuscular junction [3, 58, 59]. These phenotypes suggest a conserved role for CaV2 channels as presynaptic regulators of synaptic transmission.

In mammalian systems, the localization of alpha-1 calcium channel subunits in the brain was studied by immunohistochemistry in the early nineties [60-63]. L-type, R-type and T-type calcium channels are localized to cell bodies and dendrites, and N and P/Q-type calcium channels are localized to dendrites and axon terminals. From their function and localization pattern, the N and P/Q-type channels are considered to be the Pre-VGCCs most often required for neurotransmitter release. However, this can vary in different excitable cells. For example, ribbon synapses in hair cells and photoreceptors use L-type channels as Pre-VGCCs [64, 65].

Several domains of Pre-VGCC are required for their targeting to synapses. These domains include the SH3-binding domain and the PDZ domain-binding motif of the N-type calcium channel alpha1 subunit, which work synergistically as synaptic targeting signals in cultured hippocampal neurons [66]. In addition, the auxiliary subunits can function to promote surface expression of Pre-VGCCs. The alpha2-delta auxiliary subunit increases channel activity and promotes Pre-VGCC membrane trafficking through its Von Willebrand factor-A (VWA) domain *in vitro*; mutations in the metal-ion-dependent adhesion site (MIDAS) of the VWA domain suggest an important role of divalent cation binding to this site [67]. The alpha2-delta auxiliary subunit increases synaptic expression and activity of *Drosophila* Pre-VGCC Cacophony protein *in vivo* [68, 69]. The beta auxiliary subunit increases plasma membrane expression of multiple mammalian VGCC classes [70]. Phophatidylinositol 3-kinase (PI3K) promotes the translocation of Pre-VGCC to the plasma membrane, an effect mediated by phosphorylation of the calcium channel auxiliary beta subunit by Akt-PKB [71].

Extracellular cues promote Pre-VGCC clustering as well. At the mouse NMJ, Laminin-beta2, a basement membrane component, directly binds to Pre-VGCC and induces clustering of the channels at motor nerve terminals [72]. In rat hippocampal neuronal culture, neuron-neuron contact is required for Pre-VGCC clustering, suggesting the existence of an intercellular clustering signal in the CNS [73].

Interactions of Pre-VGCC with presynaptic proteins seem to be required for Pre-VGCC clustering. In *Drosophila melanogaster*, Bruchpilot, a homolog of mammalian ELKS-1 (ERC or CAST), resides in the presynaptic terminal and is required for Pre-

VGCC clustering at the NMJ [8]. The *Drosophila* eight-transmembrane domain protein Fuseless is also important in Pre-VGCC localization, but the mechanism is not clear [74].

Trafficking and scaffolding proteins are also required for Pre-VGCC clustering. The t-complex testis-expressed 1 (tctex1) protein, a light-chain subunit of the dynein motor complex, interacts directly with Pre-VGCC. A dominant negative tctex1 protein interferes with the surface expression of Pre-VGCC in cultured hippocampal neurons [75]. Neurexin [16] and the CASK-Mint-Veli tripartite complex of presynaptic scaffolding proteins can interact with calcium channels in purified rat brain synaptosome [21, 76]. They are candidates for proteins that drive the presynaptic clustering of calcium channels. Mice lacking neurexin alpha have severe defects in presynaptic calcium channel function [16]. In mice, however, none of the knock-outs of tripartite complex proteins show clear disruption of Pre-VGCC clustering [77-79].

Calcium channel subunits in *C. elegans*

C. elegans has three predicted alpha1 calcium channel subunits, one related to CaV1 alpha1D L-type channels (EGL-19), one related to CaV2 alpha1A/alpha1B N/P/Q-type channels (UNC-2), and one related to CaV3 alpha1G T-type channels (CCA-1) [80, 81]. *C. elegans* has two alpha2/delta subunits known as UNC-36 and TAG-180 and two beta subunits termed CCB-1 and CCB-2. The existence of gamma subunits is unclear but there are numerous proteins with similarity to the superfamily that includes gamma subunits, tight junction claudins and AMPA receptor stargazin auxiliary subunits.

In vitro reconstitution of *C. elegans* calcium channels has not been reported, thus it is not clear how similar the kinetics of channel opening are between mammalian CaVs

and *C. elegans* CaVs. However, when mutations of conserved residues that occur in *unc-2* mutants are introduced into mammalian N-type channels, defective currents were observed in the mutant channels *in vitro*, suggesting evolutionary conserved structures of the CaV channels [3]. There are some sequence dissimilarities between alpha1A/alpha1B and UNC-2. For example, the synaptic protein interaction site (synprint) that binds to NSF attachment protein receptor (SNARE) proteins such as syntaxin, SNAP25, and synaptotagmin is missing in invertebrate calcium channels including *unc-2*. The synprint site was shown to be required for presynaptic localization of CaV2 and proper synaptic transmission, suggesting that binding of SNARE proteins to the synprint site is necessary for nerve terminal localization of CaV2 calcium channels [82, 83]. Detailed studies of the role of synprint sites have been complemented by invertebrate calcium channel studies. For example, fresh-water pond snail (*Lymnaea staglis*) CaV2 alpha1 subunits lack the synprint site and are unable to bind to SNARE proteins [84]. This suggests that invertebrate CaV2 does not require the synprint site for localization and functions. In contrast to the absence of the synprint site, a proline rich region that binds to SH3 domains (possibly an interaction site with CASK) and calcium channel beta subunit binding sites are conserved between vertebrate and invertebrate CaV2 calcium channels. Evolutionary analysis of presynaptic calcium channels indicates that the putative CASK binding site and beta subunit binding site was added to the ancestral proteins much earlier than the synprint site [85]. Therefore, the binding of these proteins may be more fundamental to the original function and localization of CaV2 than binding of synaptic proteins. The function of these sites in localization of presynaptic calcium channels still needs to be determined. It

will be interesting to characterize the sequence requirement for CaV2 localization using *unc-2* mutagenesis.

C. elegans lacks the voltage-gated sodium channels that are important for the generation of action potentials in other animals [81]. *C. elegans* neurons are also small compared to those of mammals, and neurons may be isopotential [86]. Thus, *C. elegans* may not require specific localization of each calcium channel for general control of membrane potential, although channels could still have unique neuronal functions such as localized calcium influx at the presynaptic terminal [3, 87]. *unc-2* is a good candidate for the Pre-VGCC alpha-1 subunit, because of its sequence homology to N and P/Q-type channels. *unc-2* is expressed specifically in neurons and null mutants in *unc-2* are defective in locomotion and neurotransmission at the NMJ, suggesting a role at synapses [3, 59]. *egl-19* is required for sensory-evoked calcium transients in the neuronal cell body, but *unc-2* is not, suggesting the existence of localized calcium sources in *C. elegans* neurons [88, 89]. Thus, determination of its localization and its function in presynaptic neurotransmitter release were critical to establish UNC-2 as a Pre-VGCC in *C. elegans.*

To complement studies of VGCCs in cultured cells, and to explore CaV2 channel traffic *in vivo*, we analyzed neuronal calcium channel localization and function in *C. elegans*. We show that a functional GFP-tagged UNC-2 is concentrated at presynaptic active zones of sensory neurons and motor neurons. In Chapter 2, I will describe the importance of the alpha2-delta subunit UNC-36 and a newly-identified endoplasmic reticulum protein, CALF-1 *(Calcium Channel Localization Factor-1)* in UNC-2 localization. In Chapter 3, I will describe a role of the voltage-gated calcium channel in the determination of left-right asymmetry of two bilateral AWC olfactory neurons. In

Chapter 4, I will describe the relationship between ER stress, innate immunity and UNC-2 localization through the study of newly-identified nuclear protein CALF-2/PQN-53. I will then discuss future directions for study in Chapter 5.

Chapter 2

Presynaptic CaV2 calcium channel traffic requires CALF-1 and the alpha(2)delta subunit UNC-36

Abstract

Presynaptic voltage-gated calcium channels provide calcium for synaptic vesicle exocytosis. We show here that a GFP-tagged alpha1 subunit of the *C. elegans* CaV2 channel, UNC-2, is localized to presynaptic active zones of sensory and motor neurons. Synaptic localization of CaV2 requires the alpha2-delta subunit UNC-36 and CALF-1 (Calcium Channel Localization Factor-1), a neuronal transmembrane protein that localizes to the endoplasmic reticulum. In *calf-1* mutants, UNC-2 is retained in the endoplasmic reticulum but other active zone components and synaptic vesicles are delivered to synapses. Acute induction of *calf-1* mobilizes preexisting UNC-2 for delivery to synapses, consistent with a direct trafficking role. The alpha2-delta subunit UNC-36 is also required for endoplasmic reticulum exit of UNC-2, but has additional functions. Genetic and cell biological interactions suggest that CALF-1 couples intracellular traffic to functional maturation of CaV2 presynaptic calcium channels.

Introduction

Neuronal voltage-gated calcium channels (VGCCs) are central regulators of synaptic vesicle exocytosis, dendritic integration, and calcium-dependent gene regulation [53]. A VGCC consists of one pore-forming alpha1 subunit that defines intrinsic channel properties, and auxiliary alpha2-delta, beta and sometimes gamma subunits that modify channel kinetics and channel density [54]. Specific genes in the CaV gene family encode physiologically distinct alpha1 subunits. Mammalian L-type channels with CaV1 alpha1 subunits are mainly required for gene regulation and dendritic integration, N-, P/Q- and R-type channels with CaV2 alpha1 subunits are required for neurotransmitter release and dendritic calcium transients, and T-type channels with CaV3 alpha1 subunits are required for repetitive firing [53]. Disruptions of VGCC function are implicated in human epilepsy, migraine, autism-spectrum disorders, and bipolar disease, underlining the importance of these channels in the regulation of neuronal excitability and function [1].

CaV1, CaV2, and CaV3-related genes are found in invertebrates as well as vertebrates [55]. The fruit fly *Drosophila melanogaster* and the nematode *Caenorhabditis elegans* each have one predicted CaV2 alpha1 subunit, encoded by the *cacophony* and *unc-2* genes, respectively. Fly CaV2/*cacophony* mutants are inviable, with defects in calcium-dependent neurotransmitter release at the neuromuscular junction suggesting the loss of the presynaptic calcium current [2, 56]. A GFP-tagged Cacophony protein is localized to presynaptic active zones, consistent with a role at synapses [57]. *C. elegans* CaV2/*unc-2* mutants are uncoordinated, with defects in evoked neurotransmitter release at the neuromuscular junction [3, 58, 59]. These phenotypes suggest a conserved role for CaV2 channels as presynaptic regulators of synaptic transmission.

The surface expression and localization of presynaptic VGCCs can be affected by channel subunit composition and by other proteins. The alpha2-delta auxiliary subunit increases channel activity and plasma membrane expression of mammalian CaV2 alpha1 subunits [67], and increases synaptic expression and activity of *Drosophila* Cacophony/CaV2 protein [68, 69]. The beta auxiliary subunit increases plasma membrane expression of multiple mammalian VGCC classes [70, 71]. Other proteins that regulate presynaptic VGCC localization *in vivo* include the *Drosophila* active zone protein Bruchpilot/ELKS [8], the *Drosophila* eight-transmembrane domain protein Fuseless [74], and the vertebrate extracellular matrix protein laminin beta2 [72]. Many additional candidate regulators of presynaptic VGCCs have been studied in cultured cells, including scaffolding proteins such as CASK, Mint and Veli [21], and the dynein light chain protein Tctex1 [75].

To complement studies of VGCCs in cultured cells, and to explore CaV2 channel traffic *in vivo*, we here analyze neuronal calcium channel localization and function in *C. elegans*. The *C. elegans* genome encodes three predicted VGCC alpha1 subunits, *egl-19* (CaV1), *unc-2* (CaV2), and *cca-1* (CaV3) [55]. UNC-2 is a candidate presynaptic voltage-gated calcium channel based on its sequence similarity to CaV2 channels, neuronal expression, and synaptic transmission defects. We show that a functional GFP-tagged UNC-2 is concentrated at presynaptic active zones of sensory neurons and motor neurons. UNC-2 localization requires the alpha2-delta subunit UNC-36 and a newly-described endoplasmic reticulum protein, CALF-1 *(Calcium Channel Localization Factor-1)*. CALF-1 and UNC-36 have partly overlapping activities in the traffic and functional maturation of UNC-2 channels.

Results

The CaV2 alpha1 subunit UNC-2 localizes to presynaptic active zones

A full-length, GFP-tagged *unc*-2 cDNA rescued the uncoordinated movement of *unc-2* mutants when expressed from a pan-neuronal promoter (see Methods). To examine its subcellular localization, GFP::UNC-2 was expressed under cell type-specific promoters together with the synaptic vesicle marker RAB-3::mCherry (hereafter, RAB-3)[24]. When expressed in AWC olfactory neurons, GFP::UNC-2 localized to axonal puncta that overlapped with RAB-3, consistent with presynaptic localization (Fig.2-1a-g). GFP::UNC-2 was also present in the cell body, but was excluded from the dendrite, cilia, and nucleus. When expressed in VD and DD GABAergic motor neurons, GFP::UNC-2 localized with RAB-3 in the ventral and dorsal nerve cords (Fig.2-1h-j). When expressed in the DA9 cholinergic motor neuron, GFP::UNC-2 localized with RAB-3 in the dorsal presynaptic region of the axon (Fig.2-1k-n). In each case, the GFP::UNC-2 protein was present in the cell body, but largely excluded from dendrites and asynaptic regions of axons.

Presynaptic calcium channels function at active zones, the plasma membrane sites of synaptic vesicle secretion. GFP::UNC-2 puncta were often more focal than RAB-3 puncta (Fig. 2-1), suggesting that UNC-2 might localize to active zones. In agreement with this idea, GFP::UNC-2 in AWC axons colocalized closely with the active zone markers ELKS-1::mCherry and SYD-2::mCherry (Fig. 2-1d-f, Supplementary Fig. 2-1a-c).

To define genes required for UNC-2 localization to synapses, we first examined candidate mutants using GFP::UNC-2 and RAB-3 expressed in AWC. Synaptic vesicle

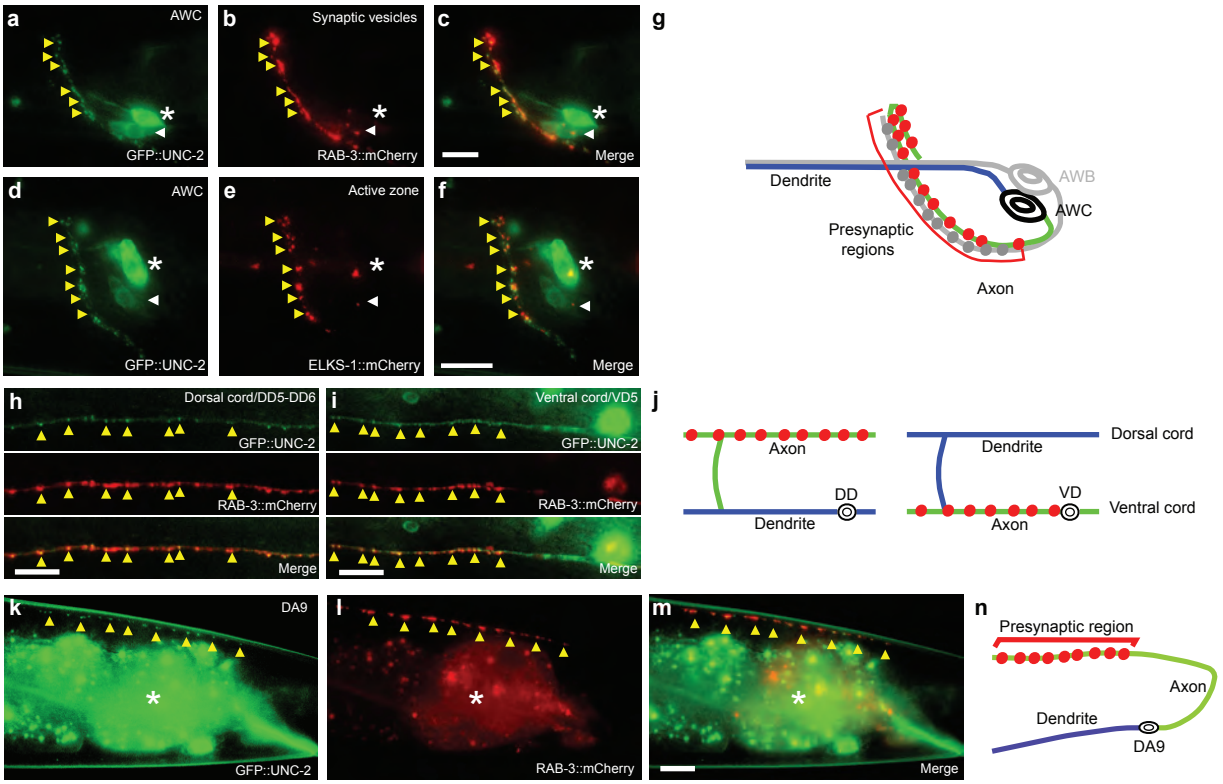

Figure 2-1. GFP-tagged UNC-2 localizes to presynaptic puncta in sensory neurons and motor neurons.
(a-c) Representative images of GFP::UNC-2 and RAB-3::mCherry in the AWC cell body (white arrowhead) and axon (yellow arrowheads). The more dorsal cell body is AWB (asterisk). (d-f) Representative images of GFP::UNC-2 and ELKS-1::mCherry. (g) Schematic of AWC processes, with synapses in red. (h,i) Representative images of GFP::UNC-2 and RAB-3::mCherry in GABAergic motor neurons: DD axons (dorsal nerve cord) and VD axons (ventral nerve cord). (j) Schematic of VD and DD processes, with synapses in red. VD has a presynaptic region in its ventral process and DD has a presynaptic region in its dorsal process. (k-m) Representative images of GFP::UNC-2 and RAB-3::mCherry in the synaptic region of DA9 cholinergic neurons. The central autofluorescent region is the intestine (asterisk). (n) Schematic of DA9 processes. In all Figures, the AWC promoter is *odr-3*, which is also expressed weakly in AWB, ASH, AWA, and ADF sensory neurons; the VD/DD promoter is *unc-25*; the DA9 promoter is *itr-1*; and all data are taken from adult animals, unless otherwise noted. Head is to the left and dorsal is up in all images unless otherwise noted. Scale bar, 10 μm.

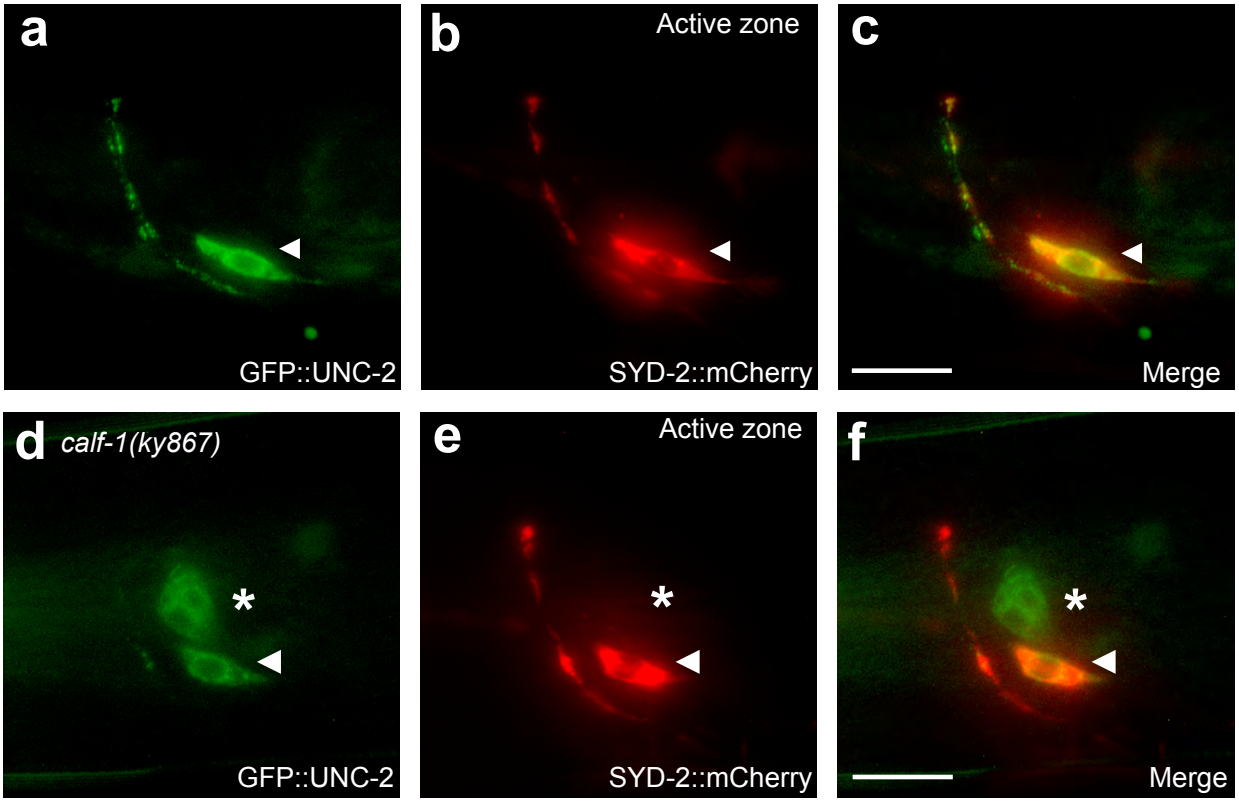

Supplementary Figure 2-1. Synaptic markers in wild type and *calf-1* animals.
(a-f) Representative images of GFP::UNC-2 and SYD-2::mCherry in AWC neurons.
(a-c) wild-type animal; (d-f) *calf-1(ky867)* mutant. Arrowheads mark AWC cell bodies.
Asterisk, AWB cell body. Scale bar, 10 μm.

clustering and active zone structure in *C. elegans* are regulated by SAD-1 kinase, SYD-2/liprin-alpha, SYD-1 and RPM-1/Hiw/Esrom/PAM [25-28]. In all of these mutants, GFP::UNC-2 puncta associated with RAB-3 in AWC axons, although there were defects in the spacing, size, and number of clusters (Supplementary Fig. 2-2a-d). Several other candidate genes had no obvious effect on GFP::UNC-2 localization in AWC: *elks-1,* the *C. elegans* homolog of *Drosophila bruchpilot* [8]*, nrx-1,* the sole *C. elegans* neurexin homolog, *lin-2/CASK, lin-7/Veli,* and *lin-10/MINT* PDZ proteins of the tripartite complex, or the synaptic exocytosis and endocytosis mutants *unc-13, unc-10/RIM, dpy-23/AP2, unc-101/AP1, unc-11/AP180,* and *unc-31/CAPS* (Supplementary Fig. 2-2e-o). A mutation in the KIF1A kinesin gene *unc-104* caused RAB-3 to disappear from AWC axons, consistent with the known requirement for KIF1A in synaptic vesicle traffic [90], but GFP::UNC-2 puncta were present and apparently normal in *unc-104* mutants (Supplementary Fig. 2-2p). Similarly, a partial loss of function mutation in the KIF5 kinesin heavy chain gene *unc-116* affected RAB-3 localization, but maintained GFP::UNC-2 colocalization with RAB-3 (Supplementary Fig. 2-2q). The absence of obvious GFP::UNC-2 phenotypes in these mutants does not exclude subtle functions, redundant functions, or functions in other classes of neurons.

unc-36 alpha2-delta mutants have uncoordinated phenotypes and other neuronal phenotypes similar to those of *unc-2* mutants [3, 91, 92]. GFP::UNC-2 was barely detectable in the AWC axons of a null *unc-36* mutant, but was still detectable in the cell body, demonstrating a requirement for UNC-36 in the sorting, folding, or localization of UNC-2 *in vivo* (Supplementary Fig. 2-2r). RAB-3 puncta were normal, suggesting that synaptic vesicle clustering was unaffected.

Supplementary Figure 2-2. GFP::UNC-2 association with RAB-3::mCherry in synaptic mutants.
Representative images of GFP::UNC-2 and RAB-3::mCherry in AWC neurons of L4 larvae. White arrowheads mark AWC cell bodies. (a-e) Presynaptic organization mutants. (a) *syd-2(ju37)* (b) *sad-1(ky289)* (c) *rpm-1(js410)* (d) *syd-1(ju82)* (e) *elks-1(tm1233)*. (f-i) Neurexin and tripartite complex mutants. (f) *nrx-1(ds1)* (g) *lin-2(n1610)* (h) *lin-7(n308cs)* (i) *lin-10(e1439)*. (j, k) Exocytosis mutants. (j) *unc-13(e51)* (k) *unc-10(e102)*. (l-n) Endocytosis and membrane trafficking mutants. (l) *dpy-23(e840)* (m) *unc-101(m1)* (n) *unc-11(ky280)*. (o) Dense core vesicle secretion mutant *unc-31(e928)*. (p, q) Kinesin mutants. (p) *unc-104(e1265)* (q) *unc-116(e2310)*. (r) VGCC alpha2-delta subunit mutant *unc-36(e251)*. Morphologically abnormal RAB-3::mCherry clusters in mutants are marked with asterisks. Note that GFP::UNC-2 still localizes to axons in all mutants except for *unc-36(e251)*, and colocalizes with abnormal RAB-3::mCherry clusters in *syd-2(ju37)*, *sad-1(ky289)* and *unc-116(e1265)* mutants. Based on molecular and genetic criteria, likely null alleles are *syd-2(ju37)* [26], *sad-1(ky289)*[25], *rpm-1(js410)*[93], *syd-1(ju82)*[28], *elks-1(tm1233)*[24], *nrx-1(ds1), dpy-23(e840)*[94], *unc-31(e928)*[95] and *unc-36(e251)*[92]. *unc-13(e51)*[96], *unc-10(e102)*[97], *unc-101(m1)*[98, 99], *lin-2(n1610), lin-7(n308cs), lin-10(e1439)*[100], *unc-104(e1265)*[90] and *unc-116(e2310)* are predicted to be reduction of function alleles, but not null. Scale bar, 10 μm.

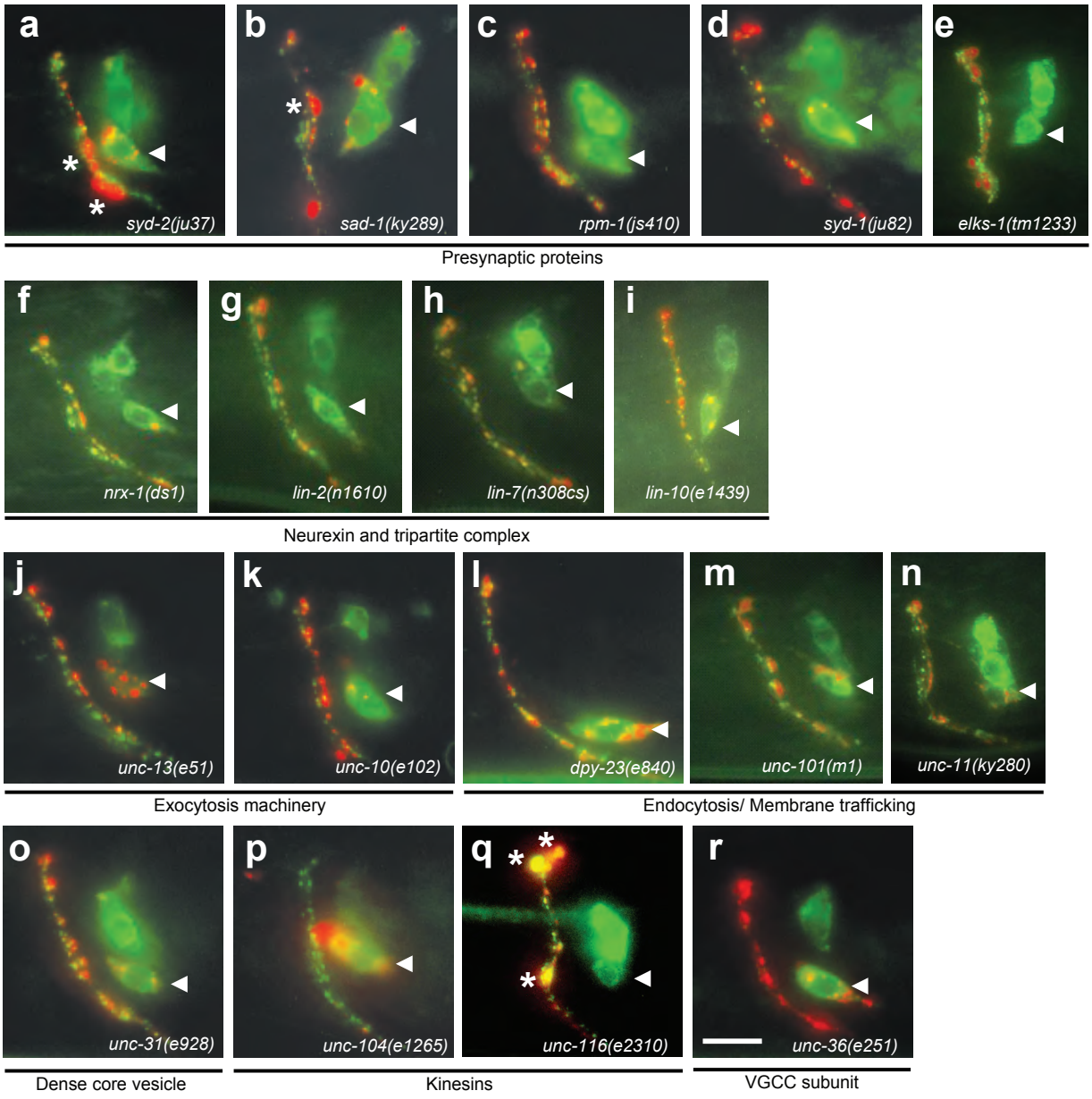

Supplementary Figure 2-2

UNC-2 synaptic puncta are reduced in *calf-1* mutants

A genetic screen for mutants with altered GFP::UNC-2 expression in AWC yielded three mutants with few axonal GFP::UNC-2 puncta, but apparently normal RAB-3 puncta (see Methods). Two mutants had an uncoordinated phenotype and failed to complement the alpha2-delta subunit mutant *unc-36(e251),* suggesting that they are mutant for *unc-36*. The third mutant affected a new gene, here named *calf-1(ky867)* or Calcium channel Localization Factor-1. In *calf-1(ky867)* mutants, GFP::UNC-2 was nearly undetectable in AWC axons, but the synaptic vesicle marker RAB-3 (Fig. 2-2a-c) and the active zone markers ELKS-1 (Fig. 2-2d-f) and SYD-2 (Supplementary Fig. 2-1d-f) appeared normal. The total fluorescence intensity of axonal GFP::UNC-2 as well as the number of puncta per axon were greatly reduced, whereas GFP::UNC-2 fluorescence in the cell body was slightly increased (Fig. 2-2g,h); minimal effects were detected upon similar quantification of RAB-3 (Fig. 2-2g,h). These results suggest that *calf-1* mutants have a selective defect in presynaptic calcium channel localization.

calf-1 also affected GFP::UNC-2 localization in motor neurons. The dorsal nerve cord of *calf-1* mutants had reduced levels of GFP::UNC-2 fluorescence and few GFP::UNC-2 puncta, but near-normal RAB-3 puncta, suggesting a loss of UNC-2 from DD synapses (Fig. 2-2i-l). In the ventral nerve cord, some GFP::UNC-2 puncta were visible, but these puncta did not localize with RAB-3 at VD synapses (Fig. 2-2j). Consistent with a defect in motor neurons, *calf-1* mutants had a distorted sinusoidal posture and moved very slowly on agar surfaces or in liquid, like *unc-2* mutants (Fig. 2-2m and data not shown).

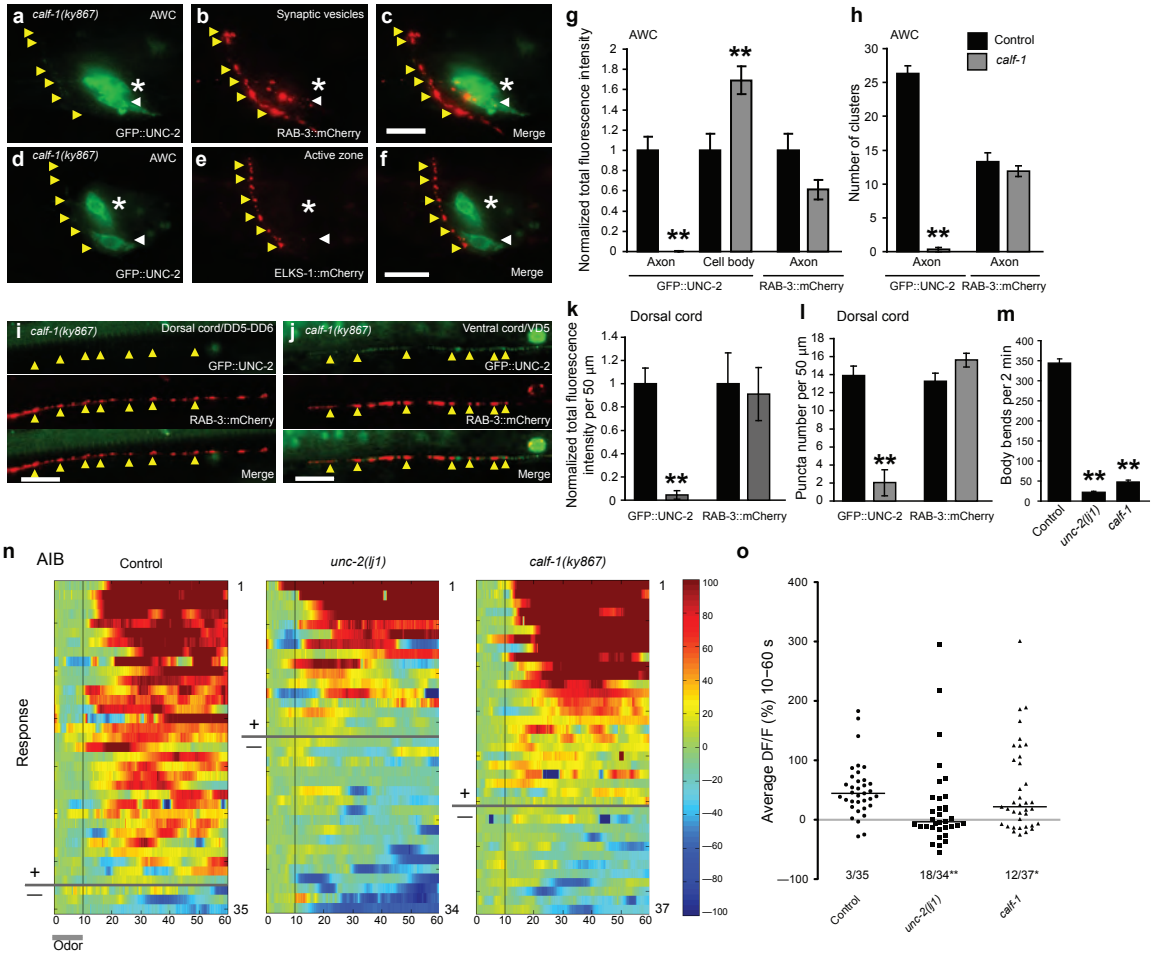

Figure 2-2. Presynaptic GFP::UNC-2 puncta are lost in *calf-1(ky867)* mutants
(a-c) Representative images of GFP::UNC-2 and RAB-3::mCherry in AWC neuron of a *calf-1(ky867)* mutant. (d-f) Representative images of GFP::UNC-2 and ELKS-1::mCherry in a *calf-1(ky867)* mutant. White arrowhead, AWC cell body; yellow arrowheads, AWC synapses; asterisk, AWB cell body. Compare Fig. 1a-f. (g, h) Quantification of GFP::UNC-2 and RAB-3::mCherry in AWC; (g) Normalized total fluorescence intensity and (h) number of fluorescent clusters. (i,j) Representative images of GFP::UNC-2 and RAB-3::mCherry in VD and DD neurons in a *calf-1(ky867)* mutant. Compare Fig. 1h,i. (k,l) Quantification of GFP::UNC-2 and RAB-3::mCherry in 50 µm covering DD5 and DD6 axons in the dorsal nerve cord; (k) Normalized total fluorescence intensity and (l) number of fluorescent puncta. Scale bar, 10 µm. (m) Quantification of swimming behavior in M9 buffer. All error bars indicate s.e.m. In g,h,k-m, asterisks indicate results different from wild-type controls by unpaired t-test at P<0.01 (**). (n) Calcium signals in AIB interneurons upon removal of the attractive odor isoamyl alcohol, which is sensed by AWC. Heat maps of individual recordings are shown for wild-type (n=35), *unc-2* (n=34), and *calf-1* (n=37) adults. Odor was removed at t=10s. AWC responses and AIB odor-on responses are in Supplementary Figure 4. (o) Average AIB response to odor removal for traces shown in (n). Lines mark median response. Neurons with an average DF/F ≤ 0 were scored as failures; both mutants were different from wild type in the fraction of failures, P<0.05 (*) or P<0.01 (**) by Chi-squared test.

In *calf-1* mutants, the GFP::UNC-2 signal in AWC cell bodies overlapped with the endoplasmic reticulum marker CP450::mCherry [101], suggesting that GFP::UNC-2 was retained in the endoplasmic reticulum (Supplementary Fig. 2-3a-c). Support for this conclusion came from examining GFP::UNC-2 in ventral cord processes of VD and DD neurons. In wild-type animals, GFP::UNC-2 in ventral cord processes was largely separated from the endoplasmic reticulum marker CP450::mCherry, but in *calf-1* mutants, GFP::UNC-2 and CP450::mCherry overlapped extensively (Supplementary Fig. 2-3d-i). These results suggest that GFP::UNC-2 preferentially accumulates in the endoplasmic reticulum or related components in *calf-1* mutants.

The functional consequences of *unc-2* and *calf-1* mutations were examined by calcium imaging of AWC sensory neurons and AIB interneurons, which are postsynaptic targets of AWC. AWC calcium levels reported by the fluorescent indicator G-CaMP fall slightly upon addition of the attractive odor isoamyl alcohol, and rise upon odor removal; similar signals are subsequently observed in AIB interneurons [102]. In *unc-2* and *calf-1* mutants, the AWC sensory responses to odors were of normal magnitude (Supplementary Fig. 2-4), but postsynaptic AIB responses to odor removal were reduced (Fig. 2-2n). Approximately half of the *unc-2* and one third of *calf-1* AIB neurons did not respond to odor removal, although those AIB neurons that did respond had similar response magnitudes to wild type (Fig. 2-2o). These results suggest that *unc-2* and *calf-1* affect neuronal signaling between AWC and AIB neurons in similar ways, reducing but not eliminating synaptic communication (see Discussion).

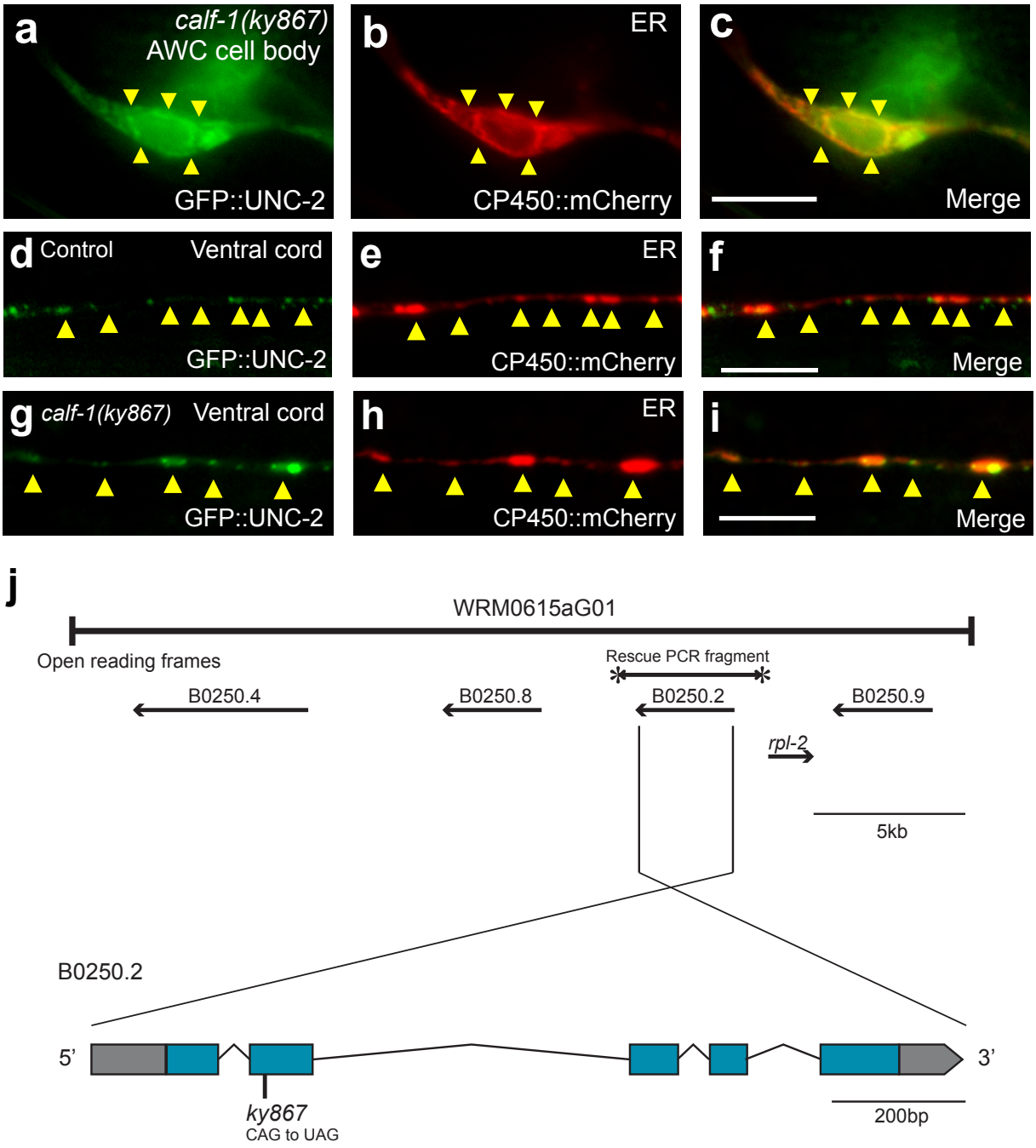

Supplementary Figure 2-3. GFP::UNC-2 is trapped in endoplasmic reticulum of *calf-1(ky867)* mutants.
(a-c) GFP::UNC-2 and the endoplasmic reticulum (ER) marker CP450::mCherry in the AWC cell body of an adult *calf-1(ky867)* mutant. Arrowheads outline the characteristic nuclear-exclusion pattern of endoplasmic reticulum. Scale bar, 10 μm. (d-i) Representative images of GFP::UNC-2 and the endoplasmic reticulum marker CP450::mCherry in ventral processes of VD and DD neurons of (d-f) a wild-type control, (g-i) a *calf-1(ky867)* mutant. Arrowheads mark location of endoplasmic reticulum. Scale bar, 5 μm. (j) Mapping and cloning of *calf-1*. A PCR fragment containing the B0250.2 gene rescued the *calf-1* mutant phenotype. The ky867 allele has a C to T transition in the second exon of B0250.2.

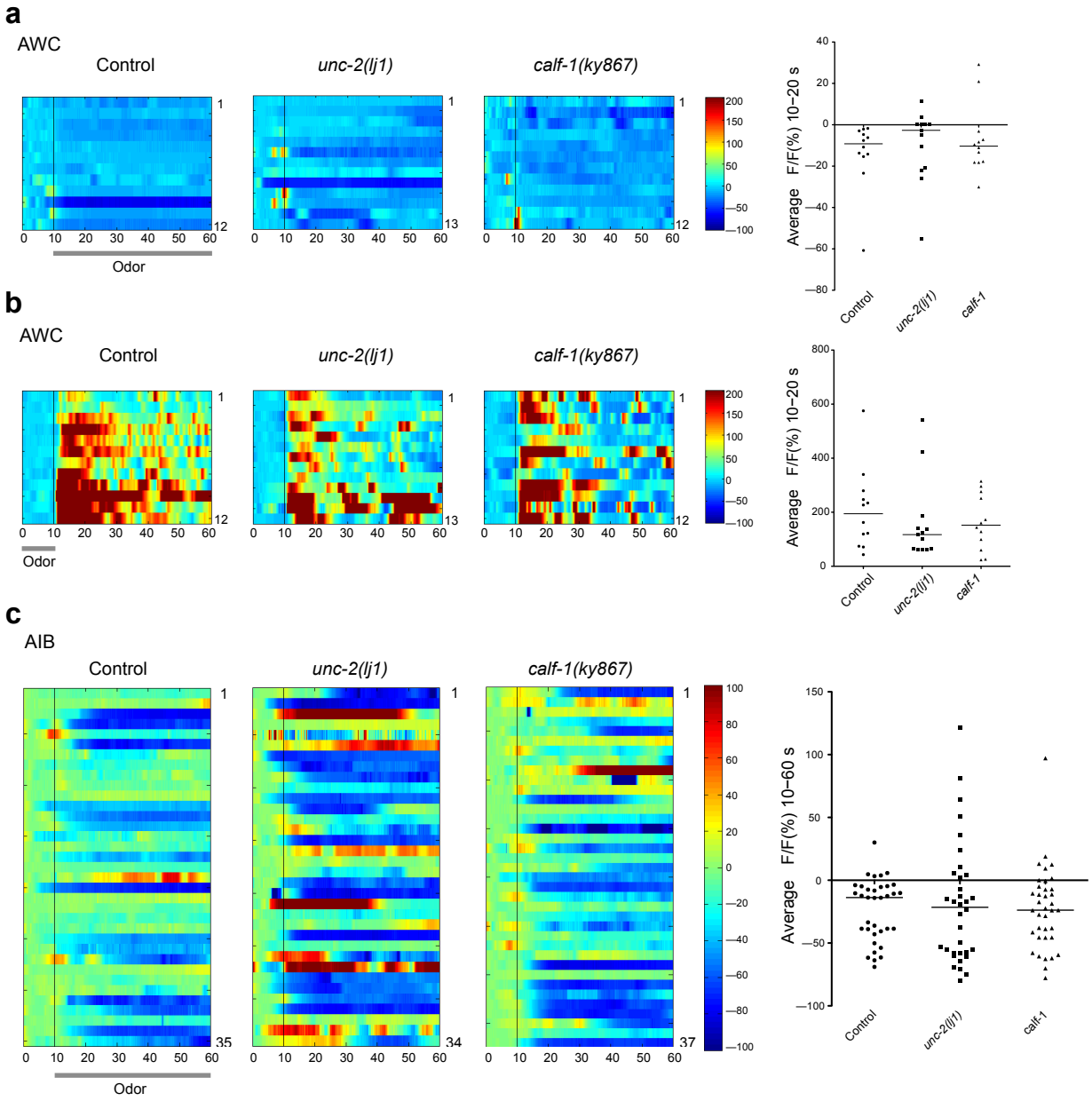

Supplementary Figure 2-4. Calcium signals in AWC and AIB.
(a-b) Calcium signals in AWC sensory neurons (a) upon addition of the attractive odor isoamyl alcohol (b) upon odor removal. Heat maps of individual recordings and average DF/F values are shown for wild type (n=12), *unc-2* (n=13) and *calf-1* (n=12). Odor was added or removed at t=10s. Mutant responses were not significantly different from wild type. (c) Calcium signals in AIB interneurons upon addition of isoamyl alcohol, same cells as in Fig. 2n,o, presented in the same order. Odor was added at t=10s. Lines mark median response of each genotype; mutants were not significantly different from wild type.

calf-1 encodes a neuronal transmembrane endoplasmic reticulum protein

Genetic mapping and transgenic rescue identified *calf-1* as the predicted gene B0250.2 (Fig. 2-3, Methods and Supplementary Fig. 2-3j). Sequencing of *calf-1(ky867)* DNA revealed a C to T mutation resulting in an early stop codon in the B0250.2 open reading frame. The *calf-1* mutant is fully recessive, and a *calf-1* gene with the *ky867* mutation did not affect GFP::UNC-2 localization or locomotion when injected into wild-type animals (data not shown). These results suggest that *ky867* is a loss of function allele of *calf-1/*B0250.2.

calf-1 encodes a predicted type I transmembrane protein with a hydrophobic membrane-spanning region, a highly basic region, and a proline-rich region (Fig. 2-3a). The region C-terminal to the transmembrane domain is predicted to be cytosolic. Homologs of *calf-1* were identified in other nematode species (Fig. 2-3b), but not in other organisms. Among nematodes, conservation of CALF-1 was highest in the predicted transmembrane domain and the adjacent basic region (Fig. 2-3c).

The uncoordinated phenotype and defective GFP::UNC-2 localization in *calf-1* mutants were rescued by a 0.5 kb *calf-1* cDNA expressed under 0.8 kb of *calf-1* upstream sequence (Fig. 2-4a,b). When the same 0.8 kb promoter was used to drive expression of GFP, fluorescence was detected in many or all neurons, but not in other tissues (Fig. 2-4c,d). Coexpression with an *odr-1::mCherry* transgene confirmed that the *calf-1* promoter drove expression in AWC neurons (Fig. 2-4e-g).

Expression of the *calf-1* cDNA under the control of the pan-neuronal *tag-168* promoter rescued the GFP::UNC-2 localization phenotypes and locomotory behavior of

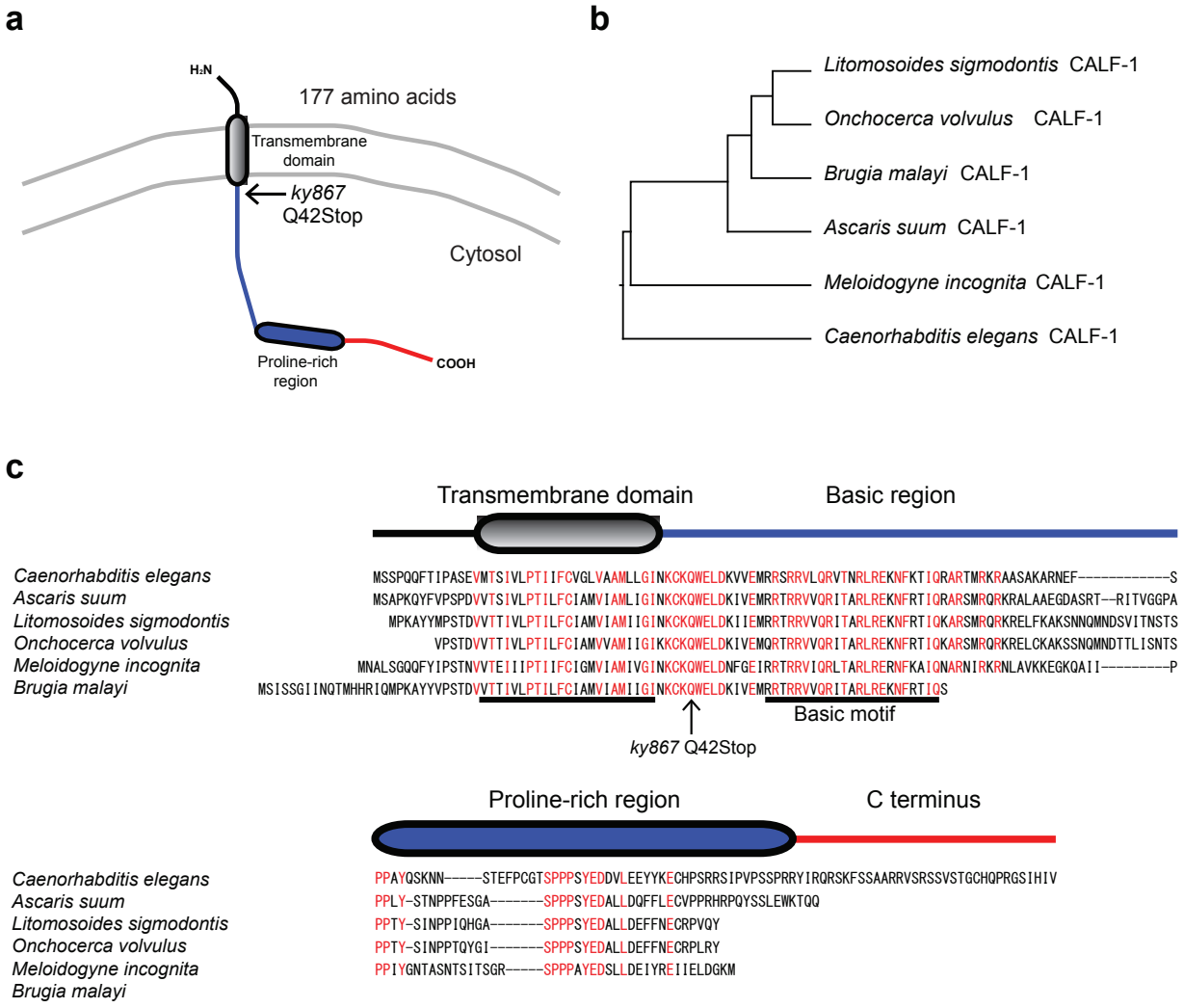

Figure 2-3. *calf-1* encodes a type I transmembrane protein.
(a) A predicted topology of CALF-1, with a transmembrane domain near its N-terminus and basic and proline-rich regions in the predicted cytosolic region. The *ky867* allele has a termination codon after the transmembrane domain. (b) Phylogenetic tree of CALF-1 in nematodes. (c) Alignment of predicted nematode CALF-1 proteins. Invariant amino acids are in red.

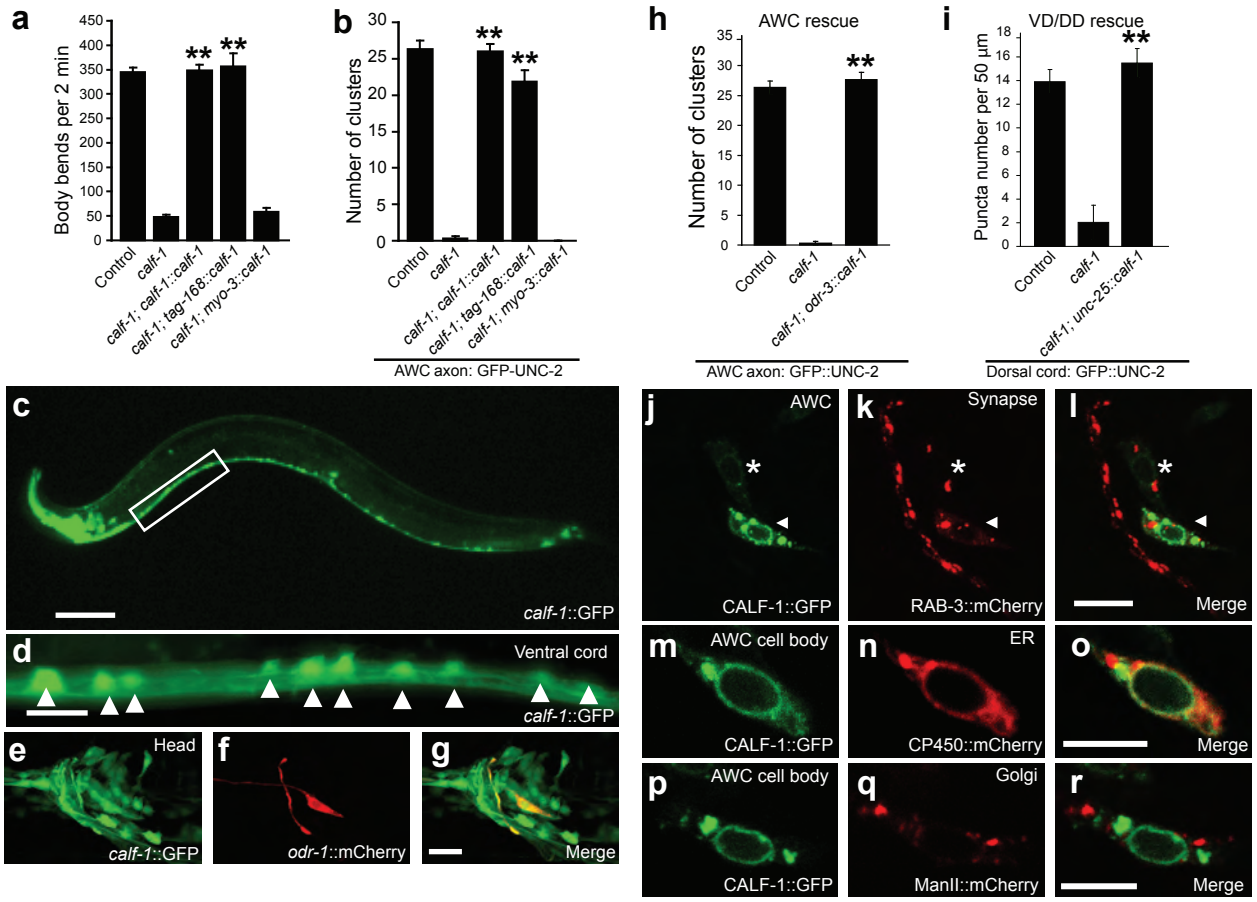

Figure 2-4. CALF-1 acts cell autonomously in neurons and localizes to endoplasmic reticulum. (a,b) Rescue of *calf-1(ky867)* mutants with *calf-1* cDNA under the endogenous *calf-1* promoter, pan-neuronal *tag-168* promoter, or muscle-specific *myo-3* promoter. (a) Swimming behavior in M9 buffer. (b) GFP::UNC-2 clusters in AWC axons. Asterisks denote strains different from *calf-1(ky867)* control by Bonferroni t-test, **= P<0.01. (c) Expression of calf-1::GFP, 0.8 kb of promoter sequence. Scale bar, 100 µm. (d) Boxed region from (c); motor neurons in the ventral nerve cord express *calf-1::GFP* (white arrowheads mark cell bodies). (e-g) AWC expresses *odr-1::mCherry* and *calf-1::GFP*. Scale bar, 10 µm. (h, i) Cell specific rescue of *calf-1(ky867)* mutants. (h) GFP::UNC-2 clusters in AWC axons, *odr-3::calf-1* rescue. (i) GFP::UNC-2 clusters in DD (dorsal cord), *unc-25::calf-1* rescue. Asterisks denote strains different from *calf-1(ky867)* controls at P<0.01 by unpaired t-test. All error bars indicate s.e.m. (j-l) Representative images of CALF-1::GFP and RAB-3::mCherry in AWC neurons. CALF-1::GFP is not visible at RAB-3-positive synapses. White arrowhead, AWC cell body; asterisk, AWB cell body. Scale bar, 10 µm. (m-r) Localization of CALF-1 in AWC cell body. (m-o) CALF-1::GFP and the endoplasmic reticulum (ER) marker CP450::mCherry in AWC. (p-r) CALF-1::GFP and the Golgi marker ManII::mCherry in AWC. Scale bar, 5 µm.

calf-1 mutants, but expression from the muscle-specific *myo-3* promoter did not (Fig. 2-4a, b). Expression of *calf-1* under the AWC-selective *odr-3* promoter rescued GFP::UNC-2 localization in AWC neurons, and expression of *calf-1* under the VD/DD motor neuron promoter *unc-25* rescued dorsal GFP::UNC-2 localization in DD neurons (Fig. 2-4h,i). These results suggest that *calf-1* acts cell autonomously to localize UNC-2.

A *calf-1* cDNA that was tagged with GFP fully rescued the locomotion defects in *calf-1* mutants (see Methods). When expressed in AWC neurons, CALF-1::GFP was exclusively localized to the cell body, and not to axons or synapses (Fig. 2-4j-l). The CALF-1::GFP signal overlapped extensively with mCherry-labeled endoplasmic reticulum markers CP450, cb5, and RAMP4 (Fig. 2-4m-o, Supplementary Fig. 2-5a-f) but not with the Golgi marker ManII::mCherry (Fig. 2-4p-r). When expressed in VD and DD motor neurons, CALF-1::GFP was present in cell bodies and in a few puncta in ventral processes; these puncta did not overlap with RAB-3 or the Golgi marker, but did overlap with an endoplasmic reticulum marker (Supplementary Fig. 2-5g-r). These results suggest that CALF-1 is a neuron-specific endoplasmic reticulum protein.

Functional motifs within CALF-1 promote endoplasmic reticulum retention

To identify sequences necessary for CALF-1 function, we tested mutant proteins for their ability to rescue either GFP::UNC-2 clusters in AWC or coordinated locomotion. Deletion of the CALF-1 transmembrane domain or replacement with the integrin PAT-3 transmembrane domain eliminated its activity (Fig. 2-5a). CALF-1 was active following individual deletion of three other regions, the basic region (deletion I), the proline-rich

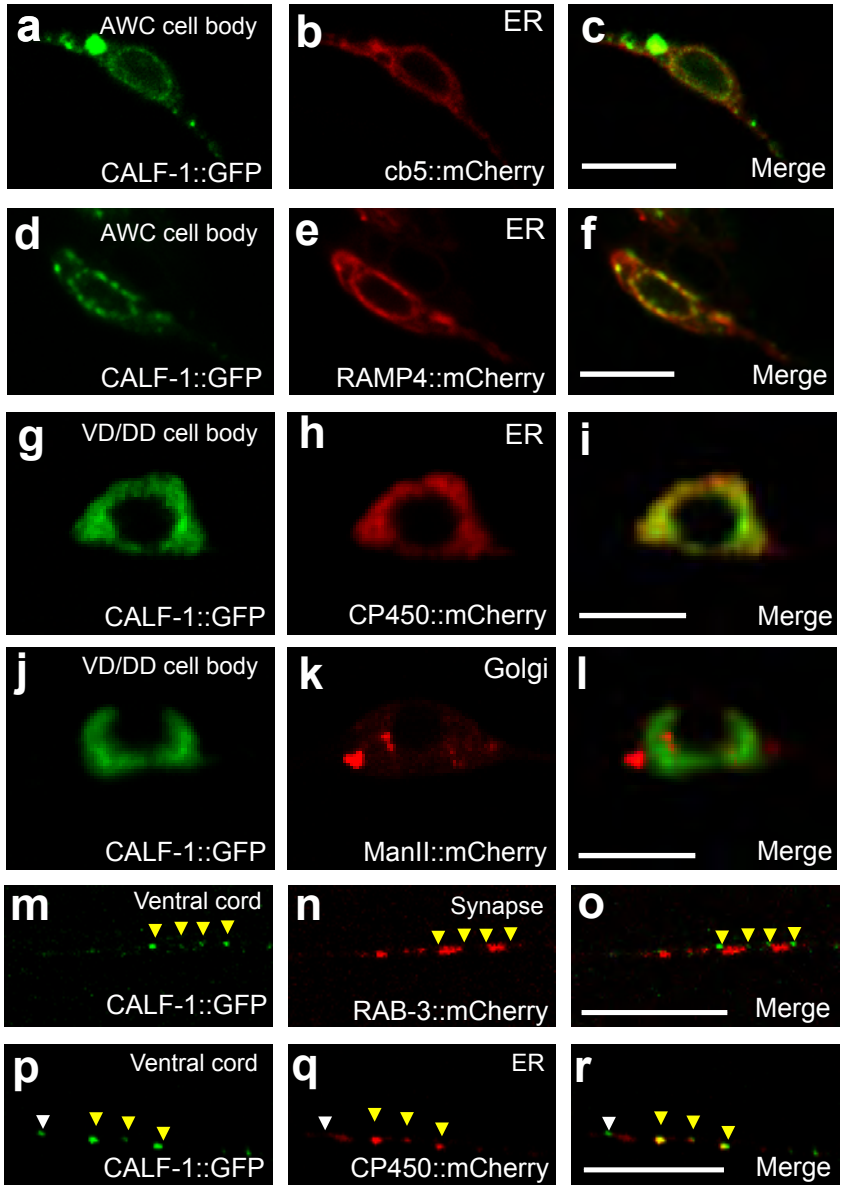

Supplementary Figure 2-5. CALF-1 is localized to endoplasmic reticulum. (a-f) CALF-1::GFP colocalization with endoplasmic reticulum markers, (a-c) cb5::mCherry or (d-f) RAMP4::mCherry in AWC cell bodies. (g-l) CALF-1::GFP and the endoplasmic reticulum (ER) marker CP450::mCherry (g-i) or the Golgi marker ManII::mCherry (j-l) in cell bodies of VD or DD neurons. (m-r) Endoplasmic reticulum localization of CALF-1 in ventral processes of VD and DD neurons. (m-o) CALF-1::GFP and RAB-3::mCherry; (p-r) CALF-1::GFP and the endoplasmic reticulum marker CP450::mCherry. Yellow arrowheads mark selected CALF-1 puncta. White arrowheads mark CALF-1 puncta that did not co-localize with CP450::mCherry. Scale bar, 5 μm.

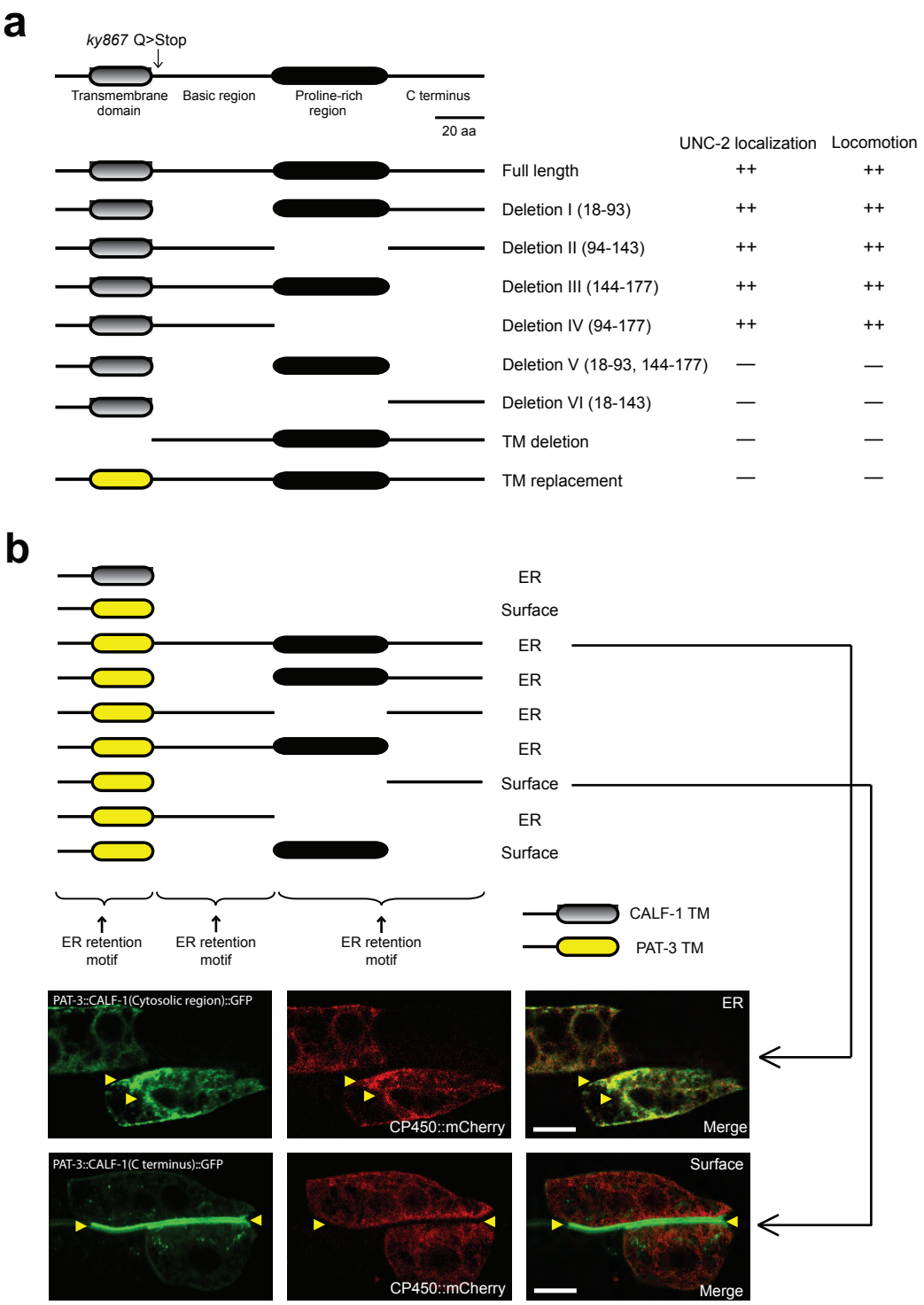

Figure 2-5. Structure-function analysis of CALF-1.
(a) Schematic representation of CALF-1 and mutants tested for rescue. For AWC axon clusters, ++, >20 GFP::UNC-2 clusters per animal; —, <3 GFP::UNC-2 clusters (compare Fig. 2h). For locomotion, ++, >250 body bends/2 min; —, <100 body bends/2 min (compare Fig. 2m).
(b) Distribution of endoplasmic reticulum (ER) retention motifs in CALF-1. Top, proteins tested by expression in intestinal epithelial cells. Bottom, plasma membrane and endoplasmic reticulum localization of representative fusion proteins in intestinal cells in L4 larva. Scale bar, 10 µm.

region (deletion II), or the C-terminal region (deletion III). Simultaneous deletion of all three regions inactivated CALF-1, but inclusion of either the basic region, or the proline-rich and C-terminal regions together, was sufficient for rescue (deletion I-VI).

Any of the three regions of CALF-1 that promote its function -- the transmembrane domain, the basic region, and the combined proline-rich and C-terminal region -- was sufficient to cause endoplasmic reticulum retention of a GFP-tagged protein in intestinal cells (Fig. 2-5b and Methods). Embedded in the basic region and C-terminal region of CALF-1 are multiple arginine-x-arginine (RXR) motifs (Fig. 2-3c), which can function as endoplasmic reticulum retention motifs in other transmembrane proteins [103]. A C-terminal truncation of CALF-1 that removed RQR and RKR motifs was competent for rescue (RKR deletion), but a larger C-terminal deletion that eliminated RQR, RKR, RAR, and RLR motifs inactivated CALF-1 (RLRE deletion) (Supplementary Fig. 2-6a-c). Interestingly, a small fusion protein consisting of the CALF-1 transmembrane domain and a 16 amino acid arginine-rich endoplasmic reticulum retention motif from the G-protein coupled alpha2 adrenergic receptor [104] partly rescued *calf-1* mutants (Supplementary Fig. 2-6a,b); similar fusions of the CALF-1 transmembrane domain to KDEL or KKYL endoplasmic reticulum retention motifs were inactive. These results suggest that arginine-rich endoplasmic reticulum retention motifs contribute to *calf-1* activity.

unc-36 affects UNC-2 maturation and function

To gain further insight into the relationships between *unc-2, calf-1,* and *unc-36*, we examined multiple phenotypes and genetic interactions in these mutants. Both canonical

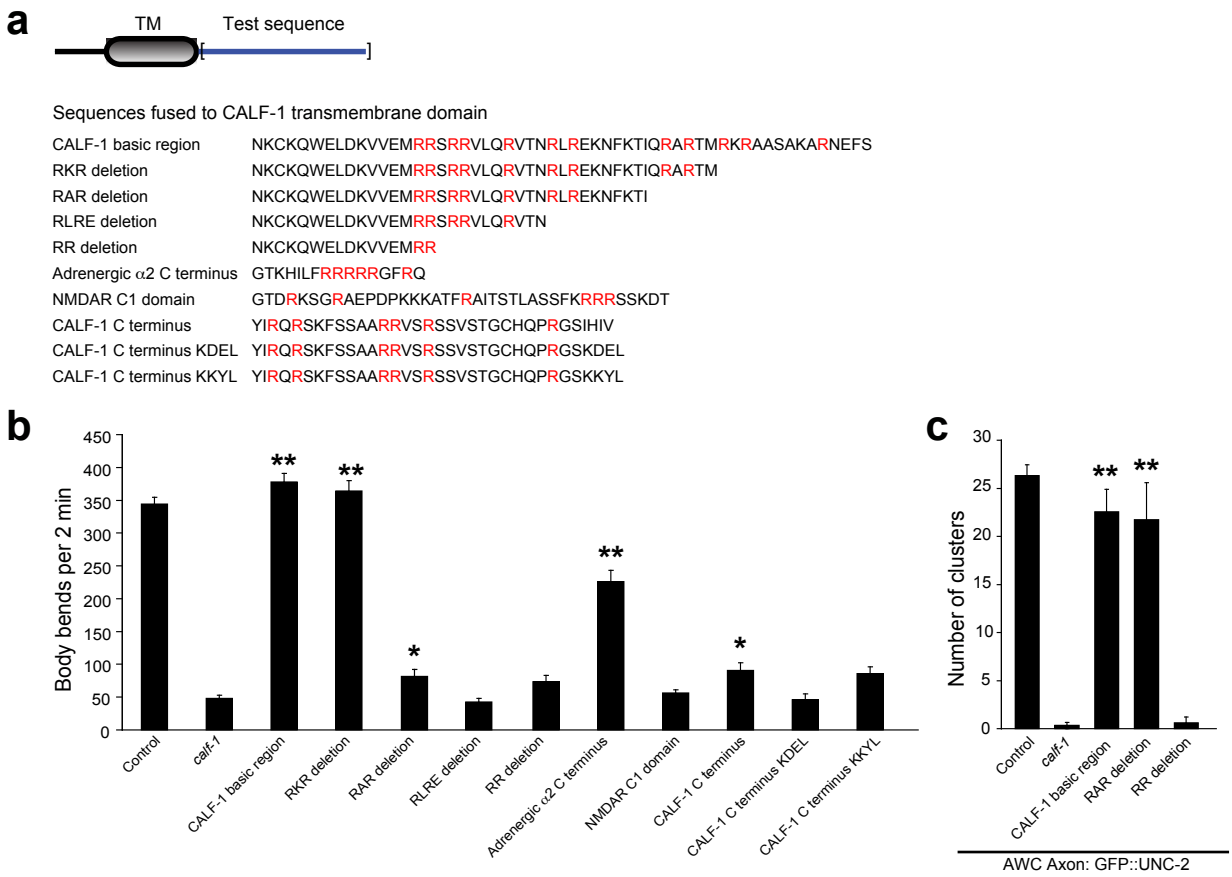

Supplementary Figure 2-6. Arginine-rich sequences enhance CALF-1 activity.
(a) Schematic and sequence of CALF-1 fusion proteins tested for rescuing activity. (b) Swimming behavior in M9 buffer. (c) GFP::UNC-2 clusters in AWC axons. Asterisks, different from *calf-1(ky867)* at P<0.05 (*) or P<0.01 (**) by Dunnett's test. The RAR deletion has an interesting phenotype reminiscent of *calf-1* overexpression in an *unc-36* mutant (Fig. 6h-k), with strong rescue of AWC UNC-2 clusters and minimal rescue of locomotion.

null *unc-36* mutations and new *unc-36* mutations from our screen caused defects in GFP::UNC-2 localization that resembled those of *calf-1* mutants: GFP::UNC-2 was absent from AWC axons and dorsal VD and DD processes, but synaptic RAB-3 localization appeared normal (Fig. 2-6a-d). In the ventral nerve cord, GFP::UNC-2 in VD/DD neurons rarely overlapped with the synaptic vesicle marker RAB-3 (Fig. 2-6e) but overlapped extensively with the endoplasmic reticulum marker CP450 (Fig. 2-6f). These observations suggest that *unc-36* mutations cause GFP::UNC-2 to accumulate in the endoplasmic reticulum. In agreement with this hypothesis, *unc-36* mutants had increased accumulation of GFP::UNC-2 in the AWC cell body and perinuclear region compared to wild type, although the effect was less marked than in *calf-1* mutants (Supplementary Fig. 2-7a-d).

A biologically active, GFP-tagged UNC-36 protein was localized both to the plasma membrane and to internal membranes of neurons, suggesting that it could function either in the endoplasmic reticulum with CALF-1, or in the synapse with UNC-2, or at both locations (Fig. 2-6g). In AWC neurons, UNC-36::GFP was largely perinuclear, and overlapped with the endoplasmic reticulum marker CP450 (Supplementary Fig. 2-7e-g); unlike GFP::UNC-2, it was not concentrated at AWC synapses. Perinuclear UNC-36::GFP localization in AWC was unchanged in *calf-1* mutants; similarly, CALF-1::GFP localization in AWC, VD, and DD was unchanged in *unc-2* and *unc-36* mutants (Supplementary Fig. 2-7h-v).

Genetic interactions were consistent with related functions of *calf-1, unc-36,* and *unc-2*. All three mutants and all double mutants were slow-moving but not paralyzed, with similar phenotypes (Fig. 2-6h). Overexpression of untagged UNC-2 from a pan-

Figure 2-6. CALF-1 and UNC-36 have related trafficking functions.
(a-c) GFP::UNC-2 and RAB-3::mCherry in AWC neuron of a *unc-36(e251)* mutant. White arrowhead, AWC cell body; yellow arrowheads, AWC synapses; asterisk, AWB cell body. (d) GFP::UNC-2 and RAB-3::mCherry in DD neurons of a *unc-36(e251)* mutant, dorsal nerve cord. (e) GFP::UNC-2 and RAB-3::mCherry in VD and DD neurons in a *unc-36(e251)* mutant, ventral nerve cord. (f) GFP::UNC-2 and the endoplasmic reticulum (ER) marker CP450::mCherry in VD and DD neurons in a *unc-36(e251)* mutant, ventral nerve cord. Compare Fig. 1a-i. (g) UNC-36::GFP expressed under the *unc-36* promoter, in the head of an adult; image analogous to panels a-c. Asterisks indicate diffuse localization of UNC-36::GFP in axons at nerve ring. Scale bar, 10 μm. (h) Swimming behavior in M9 buffer. (i) GFP::UNC-2 clusters in AWC axons. (j) GFP::UNC-2 clusters in 50 μm of dorsal cord covering DD5 and DD6 axons. In h-j, asterisks denote results different from relevant single mutant strains at $P<0.01$ (**) by unpaired t-test or Bonferroni t-test, as appropriate; error bars indicate s.e.m. (k) GFP::UNC-2 and RAB-3::mCherry in DD neurons, dorsal nerve cord, of *unc-36(e251)* mutant overexpressing *tag-168::calf-1*.

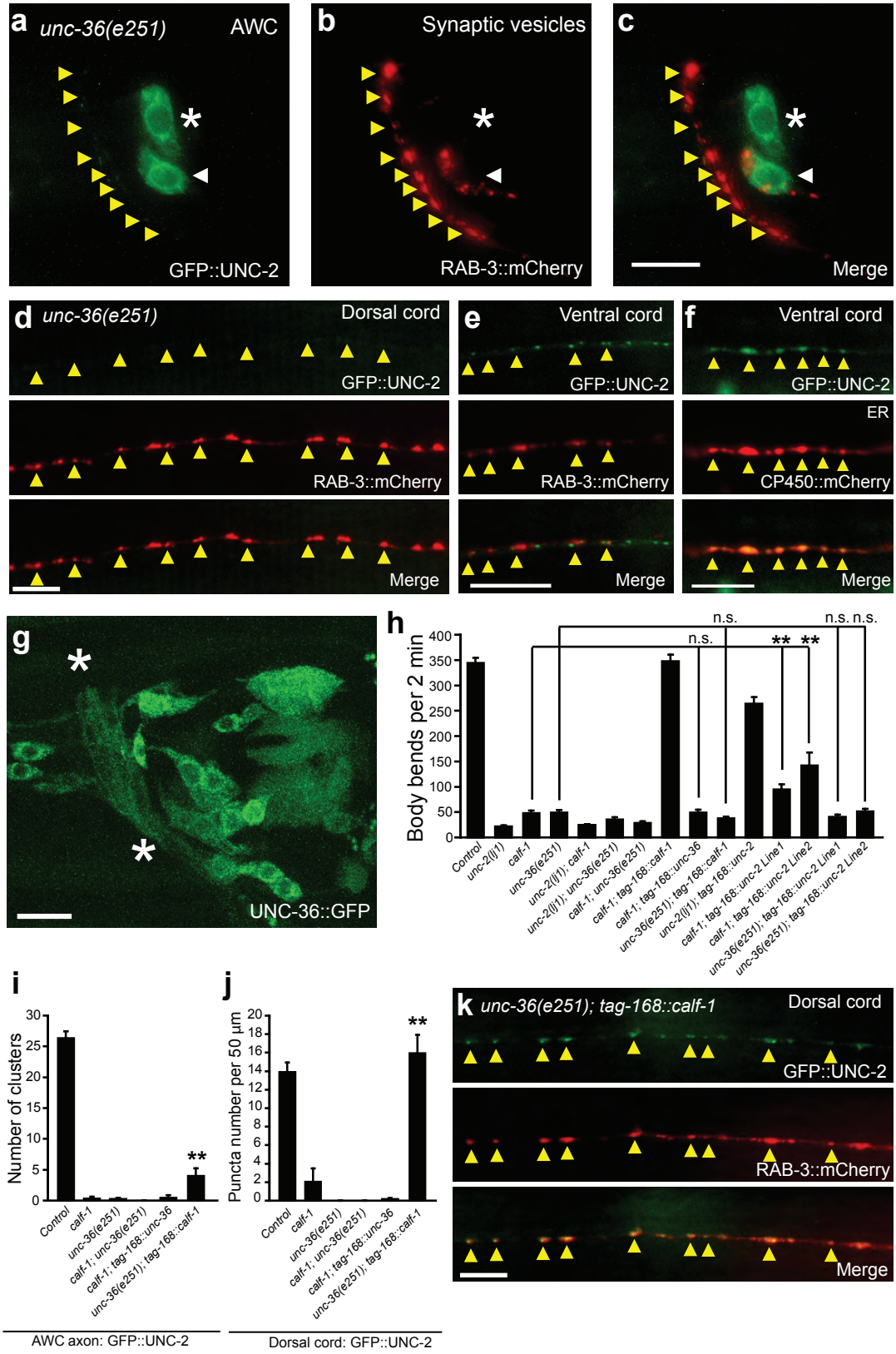
a unc-36(e251)
AWC
GFP::UNC-2
b
Synaptic vesicles
RAB-3::mCherry
c
Merge
d unc-36(e251)
Dorsal cord
GFP::UNC-2
RAB-3::mCherry
Merge
e
Ventral cord
GFP::UNC-2
RAB-3::mCherry
Merge
f
Ventral cord
GFP::UNC-2
ER
CP450::mCherry
Merge
g
UNC-36::GFP
h
Body bends per 2 min
n.s.
**
i
Number of clusters
AWC axon: GFP::UNC-2
j
Puncta number per 50 µm
Dorsal cord: GFP::UNC-2
Control
calf-1
unc-36(e251)
calf-1; unc-36(e251)
calf-1; tag-168::unc-36
unc-36(e251); tag-168::calf-1
k unc-36(e251); tag-168::calf-1
Dorsal cord
GFP::UNC-2
RAB-3::mCherry
Merge

Figure 2-6

Supplementary Figure 2-7. *unc-36(e251)* effects on localization and traffic.
(a-c) GFP::UNC-2 in AWC cell bodies of (a) wild-type control, (b) *calf-1(ky867)* mutant and (c) *unc-36(e251)* mutant. Arrowheads, perinuclear accumulation of GFP::UNC-2. (d) Perinuclear GFP::UNC-2 fluorescence in AWC cell bodies of L4 larvae. Asterisks indicate results different from wild-type controls at $P<0.05$ (*) or $P<0.01$ (**) by t-test. (e-j) UNC-36::GFP and the endoplasmic reticulum (ER) marker CP450::mCherry in AWC cell body. (e-g) wild-type animal; (h-j) *calf-1(ky867)* mutant. (k-p) CALF-1::GFP and CP450::mCherry in AWC cell body. (k-m) *unc-36(e251)* mutant; (n-p) *unc-2(lj1)* mutant. (q-v) Endoplasmic reticulum localization of CALF-1 in ventral processes of VD and DD neurons of *unc-36(e251)* mutants. (q-s) CALF-1::GFP and RAB-3::mCherry; (t-v) CALF-1::GFP and CP450::mCherry. Yellow arrowheads mark selected CALF-1 puncta. White arrowheads mark CALF-1 puncta that did not co-localize with CP450::mCherry. Scale bar, 5 μm.

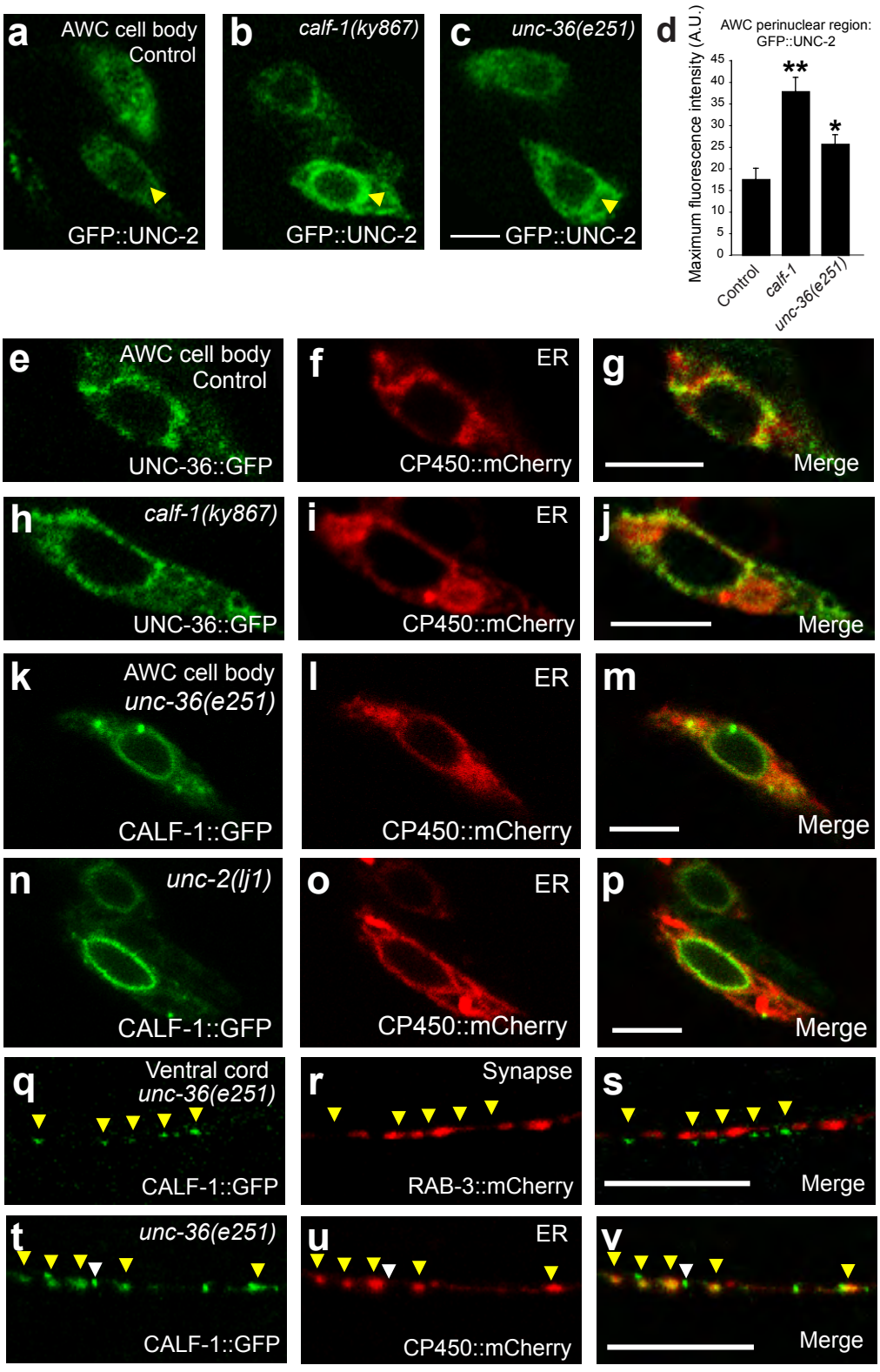

Supplementary Figure 2-7

neuronal promoter significantly improved the *calf-1* locomotion phenotype (Fig. 2-6h). This result suggests that the locomotion defect in *calf-1* is related to reduced *unc-2* activity, and supports a primary role for *calf-1* as a cofactor for *unc-2.*

Overexpression of *calf-1* from a pan-neuronal promoter rescued synaptic GFP::UNC-2 puncta in *unc-36* mutants, an effect that was weak in AWC and robust in VD and DD (Fig. 2-6i-k). However, *calf-1* overexpression did not rescue the locomotion defects of *unc-36* mutants (Fig. 2-6h), suggesting that *unc-36* mutants are defective in locomotion even when some UNC-2 is delivered to synapses. *unc-36* overexpression did not rescue GFP::UNC-2 localization or locomotion defects in *calf-1* mutants (Fig. 2-6h-j).

calf-1, unc-2, and *unc-36* also function together in a calcium-dependent developmental pathway that generates asymmetric gene expression patterns in the left and right AWC neurons [105]. Left-right asymmetry is disrupted in about 50% of *unc-2* mutants, an effect that is enhanced in *unc-2 egl-19*/CaV1 double mutants [92]. As *unc-36* mutations affect both CaV1 and CaV2 channels, *unc-36* has a stronger defect than *unc-2* [92]. *calf-1* mutants had defects in AWC gene expression that closely resembled those of *unc-2* null mutants, and an *unc-2 calf-1* double mutant was similar to the single mutants (Supplementary Table 2-1). These results suggest that the *calf-1* mutation specifically affects *unc-2* function in AWC, and not the genetically separable activities of *unc-36* and *egl-19* in the same cell.

CALF-1 acts acutely to deliver UNC-2 to synapses

The genetic analysis of *calf-1* suggests that UNC-2 accumulates in endoplasmic reticulum until CALF-1 allows its exit, but do not demonstrate a direct mobilization of

Supplementary Table 2-1

Neuronal Expression of *str-2*::GFP

	AWC neurons expressing *str-2*::GFP (% of Animals)			
Strain	2AWCs	1AWC	None	n
Wild type	0	100	0	90
unc-2(lj1)	51	45	4	155
unc-36(e251)	97	3	0	70
unc-36(e251);unc-2(lj1)	91	9	0	201
calf-1(ky867)	55	39	6	132
calf-1(ky867);unc-2(lj1)	51	41	8	110

UNC-2. To examine the acute effects of *calf-1*, we used the heat shock promoter *hsp16.2* [106] to drive expression of *calf-1* under temperature control. A three hour heat pulse in adult animals was sufficient to rescue synaptic GFP::UNC-2 localization in AWC neurons, and also restored coordinated locomotion to *calf-1* mutants (Fig. 2-7a-c). The adult rescue of *calf-1* mutants argues for a role of CALF-1 in ongoing delivery of UNC-2 to synapses, and against an essential role in synaptic development.

The rapid action of *calf-1* after heat shock made it possible to examine effects of *calf-1* on the dynamic behavior of UNC-2 protein. A pulse-chase protocol was designed to test the mobilization hypothesis directly, using *hs::calf-1* and a fluorescently labeled pool of UNC-2 protein (Fig. 2-7d). UNC-2 was tagged at its N-terminus with the photoconvertible protein Dendra2, which irreversibly changes from green to red emission upon UV irradiation [107]. Dendra2::UNC-2 protein behaved similarly to GFP::UNC-2, both before and after photoconversion; it had a synaptic location in wild-type animals, but accumulated in cell bodies of *calf-1* mutants (data not shown). In the pulse-chase experiment, a pool of Dendra2::UNC-2 protein in the cell bodies of the tail was photoconverted to red in *calf-1; hs::calf-1* animals raised at low temperatures. After photoconversion, these animals were subjected to a heat shock to induce *calf-1* expression (Fig. 2-7d,e). In 7 of 9 animals subjected to heat shock, red Dendra2::UNC-2 was mobilized from the cell bodies to puncta within the nerve ring, where many tail neurons form synapses (Fig. 2-7f). No red Dendra2::UNC-2 puncta were found in the nerve ring in the absence of heat shock (Fig 7f, n=9 animals). These results demonstrate that UNC-2 within the cell body, most likely the endoplasmic reticulum, is acutely mobilized by CALF-1. In agreement with this conclusion, the heat shock protocol

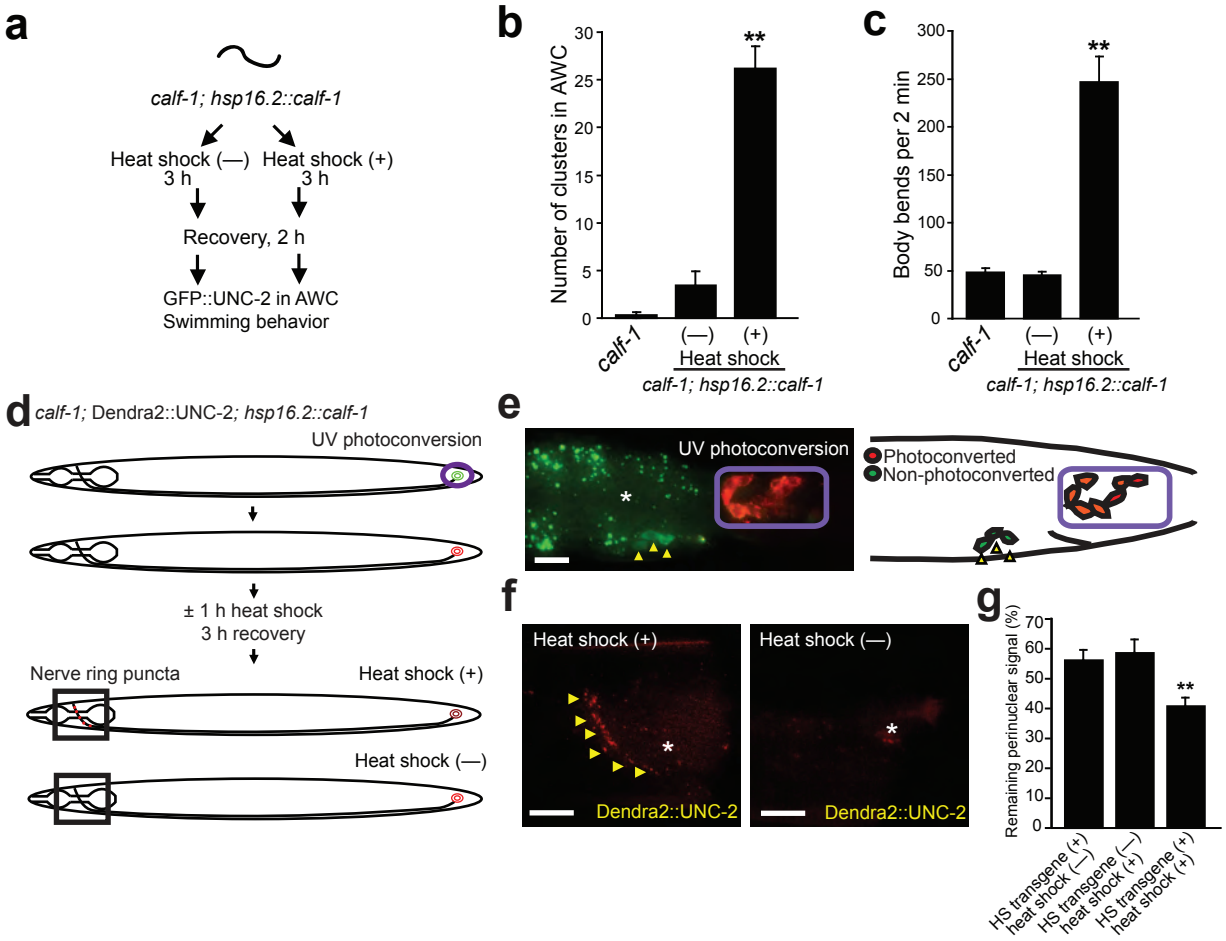

Figure 2-7. Acute CALF-1 expression transports UNC-2 from the cell body to the synapse. (a-c) Heat shock induction of *calf-1* rescues adult *calf-1(ky867)* mutants. (a) Schematic illustrating heat shock experiment. (b) GFP::UNC-2 puncta in AWC axons of heat-shocked and non-heat-shocked *calf-1; hsp16.2::calf-1* animals. (c) Swimming behavior in M9 buffer. (d) Schematic illustration of Dendra2::UNC-2 pulse-chase experiment. (e) Photoconverted Dendra2::UNC-2 in tail neurons; converted region circled in purple. Yellow arrowheads mark non-photoconverted cells. The central autofluorescence is from the intestine (asterisk). (f) Head region of heat-shocked animal and non-heat shocked animal. Arrowheads mark trafficked Dendra2::UNC-2 puncta at the nerve ring. Asterisks mark pharyngeal autofluorescence. (g) Photoconverted Dendra2::UNC-2 in the cell body. Asterisks denote results different from no heat shock controls at P<0.01 (**) by unpaired t-test. All error bars indicate s.e.m. Scale bar, 10µm.

significantly reduced the amount of red Dendra2::UNC-2 in the cell body while increasing its levels at synapses (Fig. 2-7g).

Discussion

Calcium channels in *C. elegans,* like their homologs in other animals, have distinctive functions and subcellular locations. We found that the UNC-2/CaV2 protein is highly enriched in presynaptic puncta, where it may provide calcium for exocytosis [3, 58, 59]. Signaling from AWC neurons to postsynaptic AIB neurons is reduced but not eliminated in *unc-2* mutants, indicating that UNC-2 cannot be the only source of presynaptic calcium in AWC. These observations were made by *in vivo* calcium imaging, a relatively low-resolution method, so they do not provide detailed information about synaptic mechanisms. However, the general conclusions are consistent with electrophysiological studies at the *C. elegans* neuromuscular junction showing that *unc-2* mutants have reduced synaptic release, but retain residual synaptic function (ref. 59 and J. Madison and J. Kaplan, personal communication). The axonal NCA channels are attractive candidates for a second presynaptic activity, since these mutants have variable failures in presynaptic calcium signals that are reminiscent of the variable failures in *unc-2* mutants [108]. EGL-19/CaV1 channels are also candidates; although EGL-19 is expressed mainly in the cell body (Y.S., unpublished results), inhibitory interactions between EGL-19 and UNC-2 may allow EGL-19-dependent compensation in *unc-2* mutants [92]. Homeostatic compensation may also upregulate postsynaptic glutamate receptors to potentiate the AIB response [109].

Efficient exit of a GFP-tagged UNC-2 from the endoplasmic reticulum requires both the alpha2-delta subunit UNC-36 and the endoplasmic reticulum protein CALF-1. Proteins that promote the surface expression of channels can be divided into two categories: auxiliary subunits and regulators of biogenesis [110]. Auxiliary proteins like TARPs (for glutamate receptors) and MinK (for potassium channels) first associate with the channel in the endoplasmic reticulum, but remain associated at the plasma membrane where they modify channel properties. Their function may be primarily channel modulation, and secondarily channel traffic. Our results suggest that the alpha2-delta subunit UNC-36 acts as an auxiliary subunit that regulates both UNC-2 exit from the endoplasmic reticulum and UNC-2 function (Fig. 2-8).

Alpha2-delta subunits in other animals are also implicated in CaV2 traffic. *Drosophila straightjacket* alpha2-delta mutants have a major defect in synaptic transmission, and a minor decrease in CaV2 channel levels at the synapse (25-40%) [68, 69]. Similarly mammalian alpha2-delta subunits can affect both CaV2 traffic and function; mammalian alpha2-delta-1 and alpha2-delta-2 are the primary targets of the antiepilepsy drug gabapentin, which reduces surface expression of CaV2 channels in cultured neurons and heterologous cells [67, 111]. The precise trafficking step affected by *straightjacket* and mammalian alpha2-delta subunits has not been defined, but our results indicate that one effect of UNC-36 on UNC-2 occurs during exit from the endoplasmic reticulum. Mammalian and fly alpha2-delta mutants appear to have a milder trafficking defect than *unc-36,* perhaps because of less redundancy among alpha2-delta genes: *Drosophila* has three predicted genes encoding alpha2-delta subunits, and mammals have four, but *C. elegans* has only two (*unc-36* and the uncharacterized gene *tag-180).* However, the

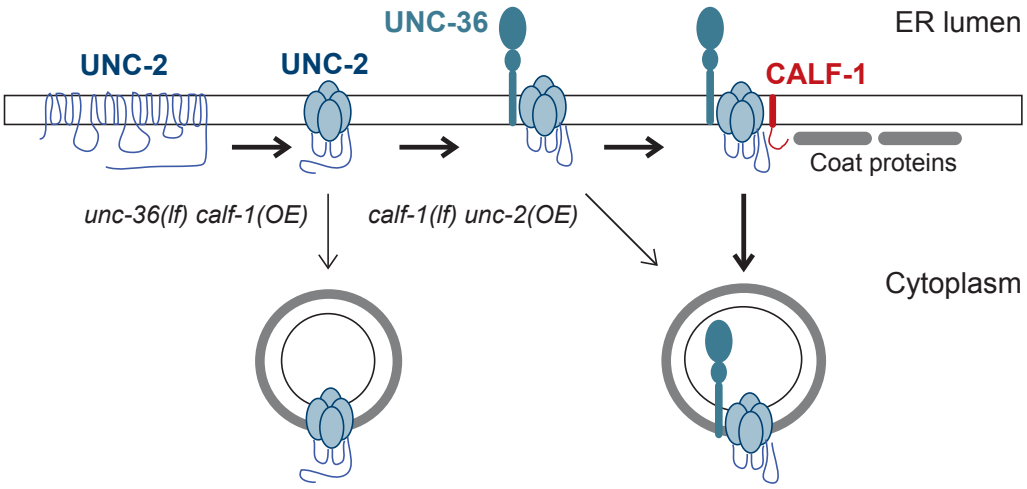

Figure 2-8. Model for UNC-2 folding, assembly with UNC-36, and regulated endoplasmic reticulum exit dependent on CALF-1.
CALF-1 may prevent UNC-2 aggregation, assist UNC-2 assembly with other subunits such as UNC-36, monitor assembly, recruit coat proteins for endoplasmic reticulum exit, or release UNC-2 from endoplasmic reticulum-retention factors. UNC-36::GFP is less prominent at synapses than GFP::UNC-2; it may be sub-stoichiometric or transiently

interpretation of our experiments and those in *Drosophila* is limited by the fact that localization was only examined using overexpressed GFP-tagged CaV2 proteins, which could have different sorting requirements from native CaV2 channels.

CALF-1 appears to function primarily in UNC-2 biogenesis, not as an auxiliary subunit (Fig. 2-8). CALF-1 resides in the endoplasmic reticulum, and CALF-1::GFP is not detectable at synapses, whereas synaptic GFP::UNC-2 is easily detected. Thus if CALF-1 remains associated with UNC-2 at the cell surface, that association is transient or sub-stoichiometric. *calf-1* acts rapidly and cell-autonomously to affect UNC-2 localization, apparently by ongoing regulation of UNC-2 exit from the endoplasmic reticulum. This activity is consistent with a role as cargo-specific chaperone, or "outfitter", for UNC-2 [112]. Among the overlapping functions of cargo-specific chaperones are protein folding activities, prevention of aggregation and retrotranslocation of transmembrane proteins from the endoplasmic reticulum into the cytosol, and recruitment of COPII vesicle proteins for endoplasmic reticulum exit [113-115].

CALF-1 contains multiple RXR motifs, sequences that were first identified for their ability to retain unfolded or partially assembled potassium channels in the endoplasmic reticulum [103, 104]. *Cis*-acting RXR motifs regulate sorting of Kir and Kv potassium channels, cystic fibrosis-associated CFTR channels, NMDA-type glutamate receptors, cardiac sodium channels, and GABA-B receptors [115]. Unlike other endoplasmic reticulum retention motifs such as KDEL, RXR motifs can stimulate endoplasmic reticulum exit in some contexts, particularly when multimerized or when bound by 14-3-3 proteins [115]. CALF-1 contains many RXR motifs, but acts in *trans* to UNC-2 and not in *cis*. In its small size, transmembrane structure, and proposed function,

it resembles the RXR-containing invariant chain that regulates MHC Class II traffic through internal membranes [116].

We suggest that CALF-1 acts at an assembly or endoplasmic reticulum exit checkpoint for UNC-2, perhaps by recruiting coat proteins or releasing UNC-2 from endoplasmic reticulum retention factors (Fig. 2-8). CALF-1-dependent endoplasmic reticulum exit normally occurs after UNC-2 and UNC-36 interact, but can occur under other circumstances when UNC-2 or CALF-1 is overexpressed. Conserved CALF-1 homologs are only recognizable in nematodes, but more distantly-related proteins in other species could have analogous activities. For example, the poorly-understood gamma subunits of mammalian calcium channels have multiple RXR motifs and multiple prolines in their C-terminal cytoplasmic domains, like CALF-1. Defining the conserved, species-specific, and cell type-specific components of presynaptic CaV2 localization is a challenge for further experiments.

Chapter 3

unc-2 CaV2 and *egl-19* CaV1 calcium channel homologs act together in AWC asymmetry

As a part of my thesis, I characterized a role of the voltage-gated calcium channel in the determination of left-right asymmetry of two bilateral AWC olfactory neurons. Together with an analysis of the RAW repeat protein OLRN-1 in AWC asymmetry conducted by Sarah Bauer Huang, this work was published in *Neural Development* as my second author paper. Below, I briefly describe my findings. The entire paper is attached to form Chapter 3.

In the adult *C. elegans* nervous system, the two bilateral AWC olfactory neurons are different in function and chemosensory receptor gene expression; in each animal, one AWC randomly takes on one identity, designated AWC^{OFF}, and the contralateral AWC becomes AWC^{ON}. Previous studies from our group had demonstrated that a stochastic lateral signaling interaction occurs between two developing AWC olfactory neurons through a gap junction network and a claudin-related protein, which inhibit a calcium-regulated MAP kinase pathway in the neuron that becomes AWC^{ON} [105, 117-119]. The precise site of action and role of calcium channels in this process, however, were unknown. Using genetic approaches such as targeted expression and genetic mosaic analysis, I showed that voltage-gated calcium channel activity is essential in AWC^{OFF}, and that signals from the calcium channels coordinate left-right asymmetry of the two AWC neurons. I showed that the calcium channels act at the transition between a

multicellular signaling network and cell-autonomous execution of the decision. We proposed that the asymmetry decision in AWC results from the intercellular coupling of voltage-regulated channels, whose cross-regulation generates distinct calcium signals in the left and right AWC neurons.

Summary

Background. The left and right AWC olfactory neurons in *Caenorhabditis elegans* differ in their functions and in their expression of chemosensory receptor genes; in each animal, one AWC randomly takes on one identity, called AWC^{OFF}, and the contralateral AWC becomes AWC^{ON}. Signaling between AWC neurons induces left-right asymmetry through a gap junction network and a claudin-related protein, which inhibit a calcium channel - Ca2+/calmodulin-dependent protein kinase II (CaMKII) - MAP kinase pathway in the neuron that becomes AWC^{ON}.

Results. We show here that a new asymmetry gene, *olrn-1*, acts downstream of the gap junction and claudin genes to inhibit the calcium – MAP kinase pathway in AWC^{ON}. OLRN-1, a novel protein with potential membrane-association domains, is related to the *Drosophila* Raw protein, a negative regulator of JNK MAP kinase signaling. *olrn-1* opposes the action of two voltage-activated calcium channel homologs, *unc-2* (CaV2) and *egl-19* (CaV1), which act together to stimulate the calcium – MAP kinase pathway. Calcium channel activity is essential in AWC^{OFF}, and the two AWC neurons coordinate left-right asymmetry using signals from the calcium channels and signals from *olrn-1*.

Conclusions. *olrn-1* and voltage-activated calcium channels are mediators and targets of AWC signaling that act at the transition between a multicellular signaling network and

cell-autonomous execution of the decision. We suggest that the asymmetry decision in AWC is made by intercellular coupling of voltage-regulated channels, perhaps through a process analogous to sinoatrial node synchronization in the vertebrate heart.

Introduction

Olfactory neurons sense environmental chemicals using large families of chemoreceptor genes that are deployed in elaborate patterns. For example, the main olfactory organs of the nematode *C. elegans* are the bilateral (left and right) amphids, which house twelve pairs of ciliated sensory neurons. Each sensory neuron expresses many receptor genes, in contrast with vertebrate olfactory neurons that generally express one receptor gene per cell [118]. Every neuron pair expresses a unique complement of receptors, and in addition, expression of some receptor genes is asymmetric on the left and right sides. For example, the left and right ASE gustatory neurons (ASEL and ASER) are structurally similar, but they express different receptor genes and sense different tastants[120, 121]. ASE asymmetry, which is established by transcription factors and microRNAs, is stereotyped and tightly coupled to the body plan [122]. The left and right AWC olfactory neurons also have distinct functions, but AWC asymmetry is variable [105, 123]. The receptor gene *str-2* is expressed stochastically in one of the AWC neurons, such that half of the animals express *str-2* in AWCL and half of the animals express *str-2* in AWCR. The AWC cell expressing *str-2* is called AWC^{ON}, while the cell lacking *str-2* expression is called AWC^{OFF}. These alternative AWC gene expression patterns correlate with different olfactory functions: the AWC^{ON} cell senses the odor butanone, while the AWC^{OFF} cell senses 2,3 pentanedione [123]. Behavioral analysis of animals with an altered complement of AWCs has demonstrated that AWC asymmetry increases olfactory discrimination and olfactory plasticity [123, 124].

Signaling between the two AWCs is required for the diversification of AWC^{ON} and AWC^{OFF}. If one AWC precursor is killed in the embryo, the surviving cell always

becomes AWC^{OFF}, suggesting that AWC^{OFF} is a ground state and AWC^{ON} is an induced state [105]. The random left-right specification and signaling between equipotential AWCs are reminiscent of developmental lateral signaling, which is usually mediated by Notch receptors and Delta/Serrate ligands [125], but Notch pathway genes have no apparent role in AWC asymmetry. Instead, the induction of AWC^{ON} requires NSY-5, an innexin gap junction protein, and NSY-4, a protein similar to claudins and the regulatory g subunits of voltage-activated calcium channels [117, 119]. NSY-5 creates a transient gap junction network essential for communication between the left and right AWCs. NSY-5-dependent ultrastructural gap junctions link the cell bodies of the embryonic AWC neurons with many additional neurons; these gap junctions are gone soon after hatching [117]. Genetic experiments indicate that AWC^{ON} induction involves contributions from both the left and right AWC neurons as well as other neurons in the network. *nsy-4,* which is related to proteins that regulate channels and cell adhesion, also has network functions – it has cell-autonomous effects within the AWC neuron that expresses it, and cell non-autonomous effects on the contralateral AWC [119]. Even in a wild-type genetic background, the level of *nsy-4* or *nsy-5* activity in one AWC neuron is sensed by the contralateral AWC, so that the neuron with higher *nsy-4* or *nsy-5* expression preferentially becomes AWC^{ON}. It is likely that the networks on the left and right are linked in the nerve ring, where axons from the left and right sides meet [105].

nsy-5 and *nsy-4* induce AWC^{ON} by repressing a kinase cascade that includes the calcium/calmodulin-dependent kinase II (CaMKII) UNC-43, the p38/JNK MAPKKK NSY-1/ASK-1, and the MAPKK SEK-1, along with the signaling scaffold protein TIR-1 [105, 126-128]. The downstream kinase cascade behaves straightforwardly and cell-

autonomously: a cell with high activity of the kinase homologs becomes AWC^{OFF} and a cell with low gene activity becomes AWC^{ON}, regardless of the kinase activity in the contralateral AWC [126, 127].

The results described above define a decision point between the *nsy-5/nsy-4* multicellular signaling network and cell-autonomous execution of the decision by the kinase homologs. In previous studies, two genes encoding subunits of a CaV2-type voltage-activated calcium channel were shown to affect AWC asymmetry upstream of the kinases [105]. Loss-of-function mutants in *unc-2,* the CaV2 pore-forming a1 subunit, result in a mixed phenotype with wild-type, 2AWC^{ON}, and 2AWC^{OFF} animals. By contrast, mutants in the regulatory alpha 2 delta subunit *unc-36* have a simple, strong 2AWC^{ON} phenotype; the reason for this difference was unknown. Here we show that *unc-2* cooperates with a second calcium channel a1 subunit, the CaV1 homolog *egl-19,* explaining the difference between *unc-2* and *unc-36*. Rescue experiments and mosaic analysis provide evidence that the calcium channels act in cell communication between AWCs. The activity of the calcium channels is opposed by the new AWC asymmetry gene *olrn-1,* which acts downstream of *nsy-5* and *nsy-4* in the induction of AWC^{ON}. *olrn-1* represses the CaMKII/MAPK kinase cascade in AWC^{ON} and provides feedback to AWC^{OFF}, allowing coordination of the left and right AWCs.

Results

The *olrn-1* gene is expressed in AWC and promotes induction of AWC^{ON}

In a screen for AWC asymmetry mutants, we isolated the mutation *olrn-1(ky626),* which was named based on the isolation of another allele, *olrn-1(ut305),* from an Olfactory Learning screen [124]. *olrn-1(ky626)* animals had a highly penetrant 2AWC^{OFF} phenotype (Fig. 3-1A, 1B, Table 3-1), and they were able to chemotax to 2,3 pentanedione, an odor sensed by AWC^{OFF}, but not butanone, an odor sensed by AWC^{ON} (Fig. 3-1C). The AWC cell fate marker *odr-1::dsRed* was normally expressed in both AWCs of *olrn-1* mutants, and AWC axon guidance was also apparently normal (Figure 3-1D). These results suggest that *olrn-1(ky626)* has one or more functional AWC^{OFF} neurons and no AWC^{ON} neurons.

A marker for the AWC^{OFF} neuron provided further evidence that *olrn-1* disrupts AWC^{OFF}/AWC^{ON} asymmetry. *srsx-3::GFP* is expressed bilaterally in the AWB neurons [129] and asymmetrically in one of the two AWC neurons (Table 3-2). In wild-type animals expressing an *srsx-3::GFP* transgene and a *str-2::dsRed* transgene, the neuron expressing *srsx-3::GFP* was invariably contralateral to the neuron expressing *str-2::dsRed* (Fig. 3-1E), indicating that *srsx-3::GFP* is expressed in AWC^{OFF}. This interpretation was confirmed by mutant analysis: *nsy-1(lf)* (ASK1/MAPKKK) and *unc-43(lf)* (CaMKII) failed to express *srsx-3::GFP* in either AWC neuron, consistent with their 2-AWC^{ON} phenotype, and *unc-43(gf)* expressed *srsx-3::GFP* in both AWC neurons, consistent with its 2AWC^{OFF} phenotype (Table 3-2). *olrn-1(ky626)* mutants expressed *srsx-3::GFP* in

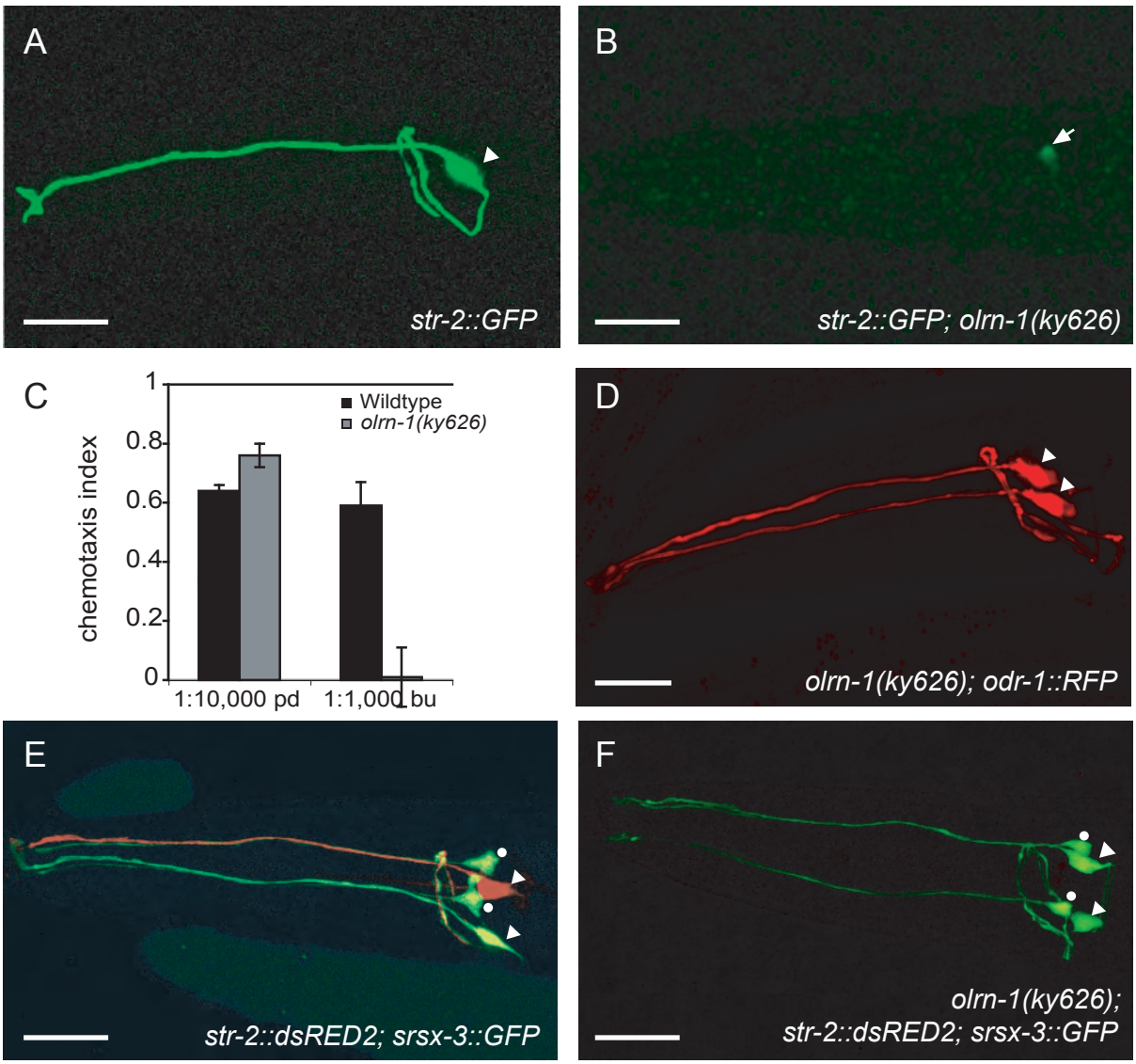

Figure 3-1. *olrn-1* mutants have two AWCOFF neurons.
(A-B) *str-2::GFP* expression in (A) wild type and (B) *olrn-1(ky626)* animals. Arrowhead, AWC, arrow, dim *str-2::GFP* expression in ASI. (C) Chemotaxis of wild type and *olrn-1(ky626)* animals to the AWCOFF sensed odorant 2,3-pentanedione (pd) and the AWCON sensed odorant butanone (bu). A chemotaxis index of 1 represents 100% animals approaching an odorant, while a chemotaxis index of 0 represents random behavior. (D) *odr-1::DsRed* expression in AWC neurons (arrowheads). (E-F) *str-2::DsRed*; *srsx-3::GFP* expression in (E) wild type and (F) *olrn-1(ky626)* mutant animals. Arrowheads indicate AWCs; dots indicate AWBs.
Scale bars, 20µm. Images are stacked confocal images.

Table 3-1 *str-2* expression in AWC in single and double mutants.

Strain	Percentage of Animals (%) 2AWC^{ON}	1AWC^{ON}/ 1AWC^{OFF}	2AWC^{OFF}	n
A. Wild type	0	100	0	158
olrn-1(ky626)	0	1	99	198
olrn-1(OE)[a]	49	51	0	218
nsy-4(OE)[a]	69	29	2	92
nsy-4(ky616)	0	34	66	98
nsy-5(OE)[a]	57	42	1	111
nsy-5(ky634)	0	3	97	124
unc-36(e251)	84	16	0	73
unc-2(lj1)	44	44	12	165
unc-2(e55)	40	37	23	75
unc-43(n1186)	81	17	2	123
tir-1(tm1111)	69	31	0	149
nsy-1(ky542)	96	4	0	103
sek-1(km4)	74	23	3	125
nsy-4(OE); olrn-1(ky626)[a]	0	16	84	51[b]
nsy-4(ky616); olrn-1(OE)[a]	80	20	0	150[b]
nsy-5(OE); olrn-1(ky626)[a]	13	38	49	160[b]
nsy-5(ky634); olrn-1(OE)[a]	70	24	6	120[b]
unc-36(e251);olrn-1(ky626)	4	18	78	88[b]
unc-2(lj1); olrn-1(ky626)	0	0	100	110
unc-2(e55); olrn-1(ky626)	0	1	99	227
unc-43(n1186); olrn-1(ky626)	87	11	2	208
tir-1(tm1111); olrn-1(ky626)	20	80	0	115[b]
nsy-1(ky542); olrn-1(ky626)	95	3	2	217
sek-1(km4); olrn-1(ky626)	81	16	3	97
B. Wild-type	0	100	0	
unc-2(lj1)	63	33	4	72
unc-36(e251)	95	5	0	110
egl-19(n582rf)	0	100	0	107
egl-19(ad695gf)	0	100	0	125
unc-2(lj1) egl-19(n582)	97	3	0	204[b]
unc-2(lj1) egl-19(ad695gf)	0	5	95	128[b]
unc-36(e251) egl-19(n582rf)	88	11	3	64
unc-36(e251) egl-19(ad695gf)	21	54	25	73[b]

[a]Overexpression from extrachromosomal transgenic arrays *kyEx914 [odr-3::olrn-1b], kyEx822 [odr-3::nsy-4]*, or *kyEx996[nsy-5 genomic fragment]*.
[b]Significantly different from either single mutant (Chi square test, significance set at $P < 0.025$ to $P < 0.006$ as Bonferroni correction for multiple comparisons).
Table 1A and Table 1B were scored at different magnifications, resulting in slightly different values for *unc-2* and *unc-36* mutants.

Table 3-2. *srsx-3::GFP* is expressed in AWC^{OFF}

	Percentage of Animals (%) expressing *srsx-3* in				
Genotype	2 AWC	1 AWC	0 AWC	2 AWB	n
Ex(srsx-3::GFP)	0	94	6	96	135
nsy-1(ag3lf); Ex(srsx-3::GFP)	0	0	100	93	89
nsy-1(ok593lf); Ex(srsx-3::GFP)	0	0	100	96	114
unc-43(n408lf); Ex(srsx-3::GFP)	0	0	100	97	144
unc-43(n498gf); Ex(srsx-3::GFP)	98	2	1	95	129

both AWC neurons, suggesting that the neurons are both specified as AWC^{OFF} (Fig. 3-1F).

ky626 was mapped using single nucleotide polymorphisms to a small region on X and was determined to be an allele of *olrn-1* by failure to complement *olrn-1(ut305)* (see Methods). *olrn-1(ut305)* corresponds to the C02C6.2 gene [124]. C02C6.2 has two isoforms, C02C6.2a and C02C6.2b (*olrn-1a* and *olrn-1b*, respectively), which differ in their first 13 or 20 amino acids due to the use of alternative first exons (Fig. 3-2A, 3-2B) [130]. A G to A mutation was identified in *ky626* mutants at position 473 in the *olrn-1a* isoform (position 466 in the *olrn-1b* isoform), resulting in a missense mutation (G →E) in both isoforms (Fig. 3-2B). *olrn-1(ut305)* is mutated at the splice acceptor site of the fourth intron [124] and, like *olrn-1(ky626),* results in a strong $2AWC^{OFF}$ phenotype (99% penetrant, n=91). A deletion allele of *olrn-1* has a lethal phenotype that is not rescued by transgenes covering C02C6.2 (data not shown); it is not clear whether the lethality is the null phenotype of *olrn-1,* or whether it results from a linked mutation in another gene.

Expression of *olrn-1* cDNAs under the AWC-selective *odr-3* promoter rescued the $2AWC^{OFF}$ phenotypes of *olrn-1(ky626)* mutants [124] (Table 3-3). Additionally, overexpression of *olrn-1b* in a wild type background caused a $2AWC^{ON}$ phenotype (*olrn-1a* was not tested)(Table 3-1A, Table 3-3). These results indicate that high *olrn-1* activity promotes the AWC^{ON} phenotype, support AWC as the likely site of *olrn-1* function, and suggest that *ky626* is a reduction-of-function allele.

To establish the potential *olrn-1* expression pattern, two regions upstream of *olrn-1* were fused to coding sequences for the fluorescent protein *mCherry* [131]. The 3.8 kb region upstream of the *olrn-1a* start site was expressed in AWC neurons as well as ASG

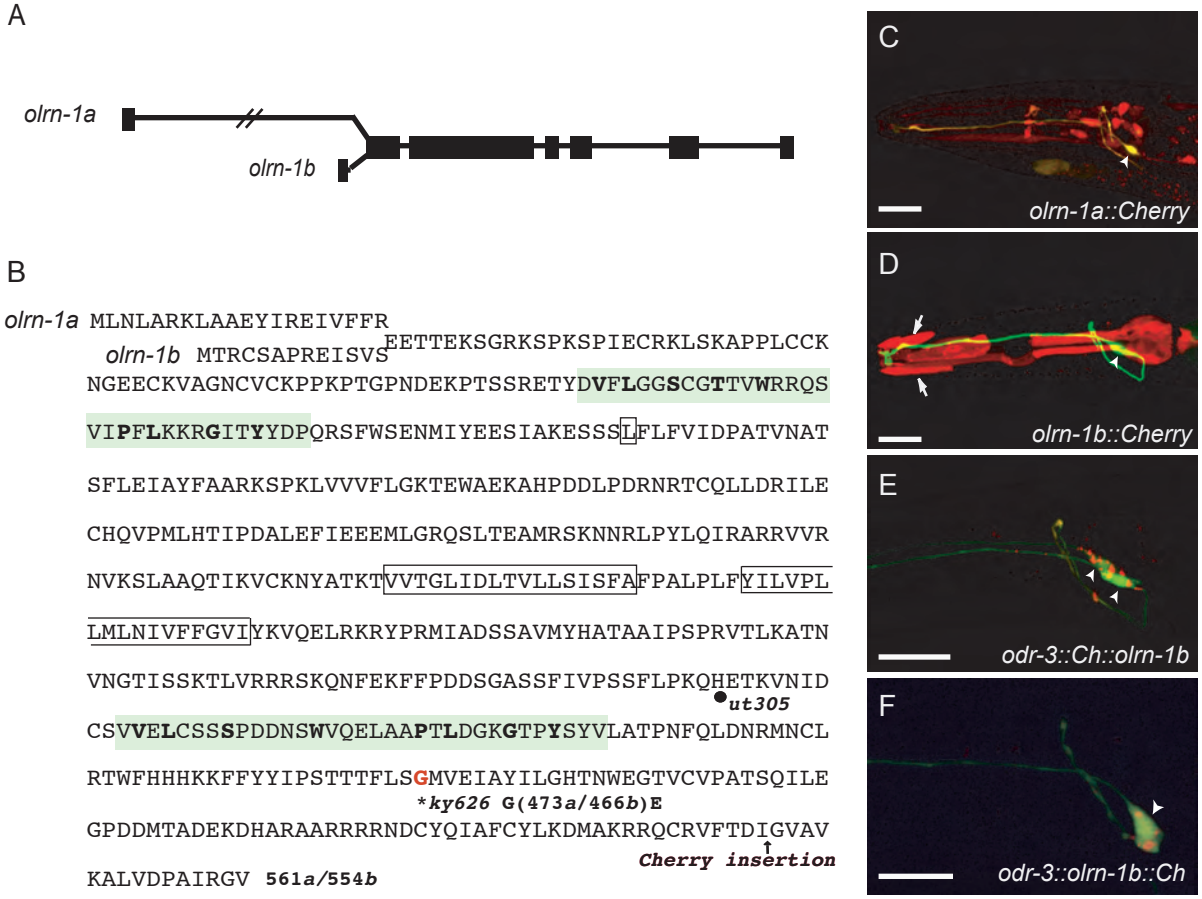

Figure 3-2. *olrn-1* encodes a protein with Raw repeats and potential transmembrane domains. (A) Genomic structure of olrn-1, showing alternative first exon for a and b isoforms, whose 5' ends are separated by 3.8 kb. (B) Translation of *olrn-1*, showing alternative first exons for *olrn-1a* and *olrn-1b* isoforms. Two short repeats shared with Drosophila Raw are highlighted in green with conserved residues in bold type; potential transmembrane domains are boxed. The location of the splice acceptor site (fourth exon) mutated in *ut305* and the residue mutated in *olrn-1(ky626)* (G 473a/466b E) are marked. Arrow marks the C-terminal insertion site of Cherry in *odr-3::olrn-1b::Ch* (panel 2F). (C) Expression of *olrn-1a::Cherry* promoter fusion. Arrowhead indicates Cherry expression in AWC neuron expressing *str-2::GFP*. (D) Expression of *olrn-1b::Cherry* promoter fusion in non-neuronal cells. Arrows, hypodermal cells. The pharynx is a prominent site of expression. Arrowhead, no Cherry expression in AWC neuron expressing *str-2::GFP*. (E) Expression of N-terminally tagged *odr-3::Cherry::olrn-1b* in an L4 *olrn-1(ky626)* animal. *odr-3::Cherry::olrn-1b* is excluded from the nucleus and is punctate in the axon and dendrite. (F) Expression of C-terminally tagged *odr-3::olrn-1b::Cherry* in an L4 *ky626* animal. *odr-3::olrn-1b::Cherry* is excluded from the nucleus, and is punctate in the axon and dendrite. Arrowheads, AWC cell bodies. Scale bars, 20µm. Images are stacked confocal images.

Table 3-3. Rescue of *olrn-1,* overexpression of *olrn-1,* and effect of mutations

Test strain	Test clone (concentration)	line	Percentage of animals (%) 2AWC^{ON}	1AWC^{ON} 1AWC^{OFF}	2AWC^{OFF}	n
olrn-1	*None*		0	1	99	1189
olrn-1	*odr-3::olrn-1b*	1	18	81	1	582
	(2.5 ng/ul)	2	1	77	22	218
olrn-1	*odr-3::olrn-1b*	1	48	51	1	639
	(5 ng/ul)	2	55	43	2	806
olrn-1	*odr-3::olrn-1b*	1	47	44	9	245
	(15 ng/ul)	2	52	41	8	293
WT	*odr-3::olrn-1b*	1	63	37	0	1528
	(15 ng/ul)	2	70	29	1	1282
WT	*odr-3::olrn-1b*	1	68	32	0	660
	(25 ng/ul)	2	70	30	0	781
olrn-1	*odr-3::olrn-1b::Ch*	line 1	81	16	3	73
	(15 ng/ul)	line 2	83	14	3	70
		line 3	76	22	2	88
olrn-1	*odr-3::olrn-1b(ΔrawR1)::Ch*	line 1	0	4	96	94
	(15 ng/ul)	line 2	0	1	99	91
		line 3	0	8	92	39
olrn-1	*odr-3::olrn-1b(ΔTM1,2)::Ch*	line 1	49	51	0	94
	(15 ng/ul)	line 2	53	46	1	96
olrn-1	*odr-3::olrn-1b(ΔrawR2)::Ch*	line 1	61	36	2	88
	(15 ng/ul)	line 2	81	19	0	83
		line 3	62	27	11	45
olrn-1	*odr-3::olrn-1b(G466E)::Ch*	line 1	6	86	7	81
	(15 ng/ul)	line 2	1	96	3	91
		line 3	5	91	5	43
olrn-1	*odr-3::olrn-1b(ΔRRRR)::Ch*	line 1	4	95	1	100
	(15 ng/ul)	line 2	20	78	2	110
		line 3	2	74	23	47
		line 4	7	88	5	152
olrn-1	*odr-3::olrn-1(ΔCterm)::Ch*	line 1	0	2	98	51
	(15 ng/ul)	line 2	0	0	100	88
		line 3	0	0	100	47

and BAG sensory neurons (Fig. 3-2C). The 3.6 kb region upstream of the *olrn-1b* start site was expressed in the marginal cells of the pharynx, anterior hypodermal cells and the rectal gland cells (Fig. 3-2D and data not shown). Although individual promoter fragments may not reproduce the entire *olrn-1* expression pattern, these results suggest that *olrn-1* may normally be expressed in AWC and in other cells.

The first Raw repeat and a C-terminal region are important for OLRN-1 function

OLRN-1 encodes a previously uncharacterized protein that is conserved along its entire length with related proteins from *Caenorhabditis remanei* and *Caenorhabditis briggsae.* It bears more distant similarity with the *Drosophila melanogaster* gene *raw* (or *cyrano).* *raw* restricts JNK signaling during dorsal closure of the fly embryo, and *raw* mutants have an embryonic dorsal-open phenotype resulting from abnormal cell migration, as well as nervous system defects [132]. The similarity between ORLN-1 and Raw is highest in two repeated domains of unknown function [132] (Fig. 3-2B). OLRN-1 has a bipartite, highly hydrophobic region of ~40 amino acids at residues 264-280 and 288-304 that is likely to mediate membrane attachment; this domain is not present in Raw. One possibility is that these two hydrophobic domains form a hairpin-like transmembrane domain, so that both the N- and C-termini of OLRN-1 face the cytoplasm.

The predicted OLRN-1B protein was tagged at its N- or C-terminus by inserting *mCherry* into the *odr-3::olrn-1* vector. Both N- and C-terminally tagged OLRN-1 rescued *olrn-1(ky626)* mutants (Table 3-3 and data not shown). The tagged OLRN-1b

proteins were localized to punctate structures in the axon, dendrite, and cell body, but largely excluded from nuclei (Fig. 3-2E, 3-2F).

Structure-function analysis of OLRN-1 was conducted to identify important domains of the protein (Fig. 3-3A). Deletions in the *odr-3::olrn-1b::Cherry* rescuing clone were made to remove the predicted Raw repeats *(ΔrawR1, ΔrawR2*), the transmembrane domains (*ΔTM1,2*) and the region C-terminal to the second Raw repeat *(ΔCterm*). A set of four adjacent arginines reminiscent of a cleavage or nuclear localization signal was deleted from the C terminus (*ΔRRRR).* Finally, the G466E *ky626* mutation was engineered into the full-length protein to examine the properties of the mutated protein. All of these Cherry-tagged mutant DNAs were cloned under the AWC-selective *odr-3* promoter and introduced into *olrn-1(ky626)* mutants at 15 ng/ul, a concentration that resulted in a $2AWC^{ON}$ phenotype in ~80% of animals carrying a wild-type *odr-3::olrn-1b::mCherry* transgene (Fig. 3-3B, Table 3-3). Deletion of the first Raw repeat (*ΔrawR1*) nearly eliminated rescue of the *olrn-1(ky626)* mutant, as did deletion of the C-terminal region *(ΔCterm*). By contrast, deletions of the transmembrane domains (*ΔTM1, 2*) or the second Raw repeat (*ΔrawR2*) did not greatly diminish rescue by *odr-3::olrn-1b::Cherry* (Fig. 3-3B, Table 3-3). Transgenes carrying the deletion of the four arginines (*ΔRRRR*) and the G466E missense mutation were intermediate in activity. Both transgenes were able to rescue *olrn-1(ky626)*, but did not cause the overexpression phenotype caused by the full-length *olrn-1* transgene (Fig. 3-3B). Their activity was similar to that of full-length *odr-3::olrn-1* injected at 6-fold lower DNA concentrations (Table 3-3). These results suggest that *ΔRRRR* and *G466E* mutations reduce the activity of the OLRN-1 protein.

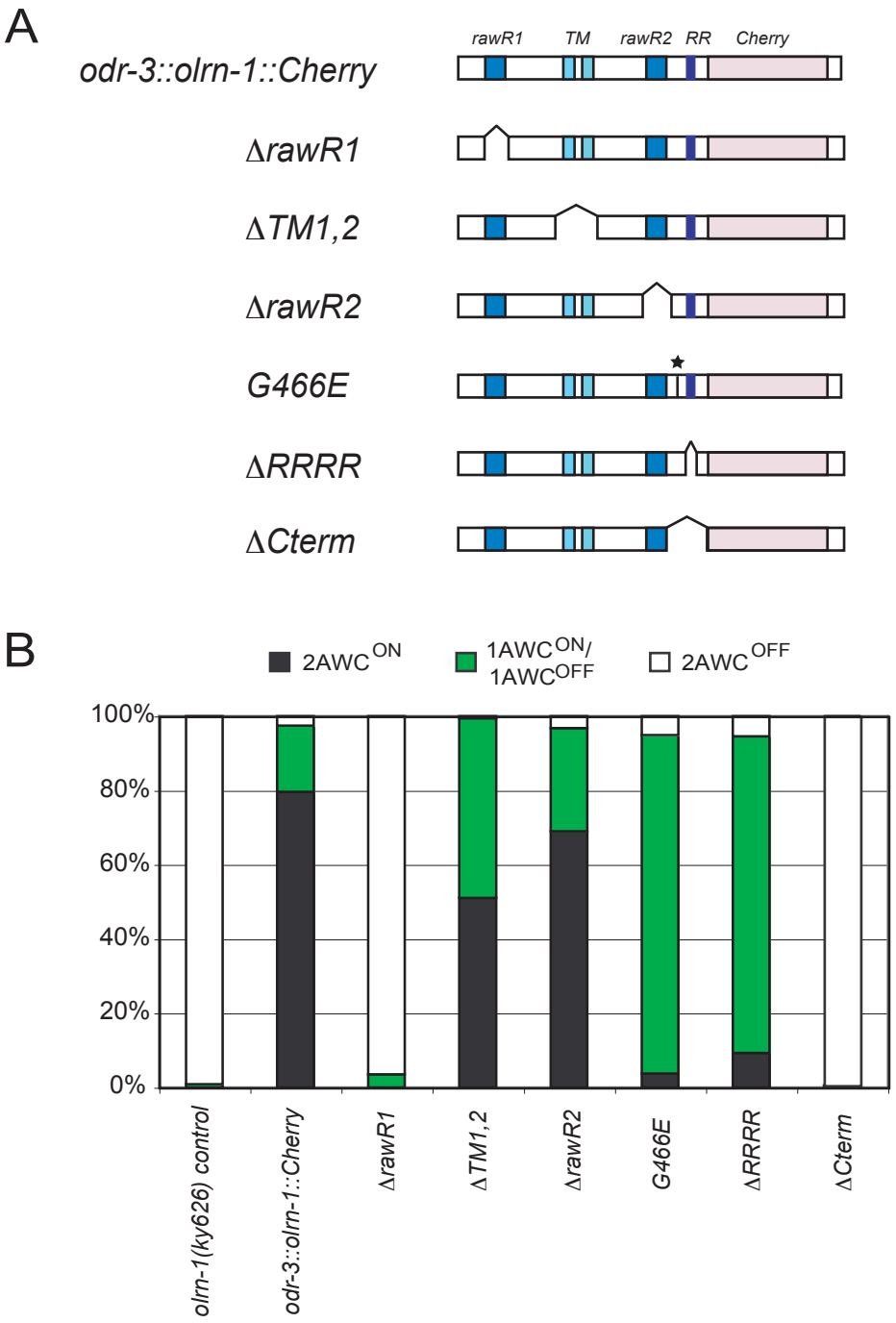

Figure 3-3. Structure-function analysis of *odr-3::olrn-1::Cherry*
(A) Mutants generated in *odr-3::olrn-1b::Cherry* affected Raw repeats (ΔrawR1, ΔrawR2), potential transmembrane domains (ΔTM1,2), the four adjacent arginines (ΔRRRR), and a C-terminal region (ΔCterm). The *ky626* mutation (G466E) was also introduced. (B) Phenotypes of *ky626* animals expressing *odr-3:olrn-1b::Cherry* transgenes. *olrn-1(ky626)* control is at left. All transgenes except ΔCterm showed significant rescue compared to nontransgenic sibling controls; all transgenes except rawR2 were significantly less active than intact *odr-3::olrn-1b::Cherry* ($P < 0.008$ by Fisher exact test or Chi square test as appropriate; 0.008 was used as the significance level based on the conservative Bonferroni correction for six comparisons; n>100 rescued animals per clone, from at least two independent transgenic lines that showed similar degrees of rescue (Table 3)).

The expression levels and localization of OLRN-1b were examined in *olrn-1(ky626)* animals bearing the mutated clones. All mutated clones produced comparable levels of OLRN-1::cherry fluorescence in AWC, suggesting that the defective mutants made dysfunctional but stable proteins (Supplementary Fig. 3-1). It was not possible to resolve the subcellular localization of OLRN-1 in embryos, but immediately after hatching the OLRN-1b::Cherry protein was present in the AWC cell body, axon and dendrite (Supplementary Fig. 3-1A). All mutant proteins had similar localization to wild-type OLRN-1b::Cherry (Supplementary Fig. 3-1B-G). Twelve hours later during the late L1 / early L2 stage, the expression of OLRN-1b::Cherry was and all mutants was similar, excepting OLRN-1b(*ΔTM1,2*), which was no longer detectable in axons (Supplementary Fig. 3-1H-N).

olrn-1 antagonizes calcium pathways in AWC signaling

The *olrn-1(ky626)* mutation and the *olrn-1(OE)* overexpressing transgene were combined with other mutations to ask how *olrn-1* interacts with AWC asymmetry genes. We first examined the upstream signaling genes, the claudin-like *nsy-4* and the innexin *nsy-5* [117, 119]. Loss-of-function mutations in *nsy-4, nsy-5* and *olrn-1* that caused $2AWC^{OFF}$ phenotypes were combined with overexpressing transgenes for *nsy-4, nsy-5* and *olrn-1* that caused $2AWC^{ON}$ phenotypes. In all combinations, the double mutants resembled the *olrn-1* parent more closely than the *nsy-4* or *nsy-5* parent (Table 3-1A), but mixed phenotypes were observed. These results suggest that *olrn-1* acts mainly at a step downstream of *nsy-4* and *nsy-5,* but the absence of definitive null alleles of *nsy-4* and *olrn-1* limits this interpretation.

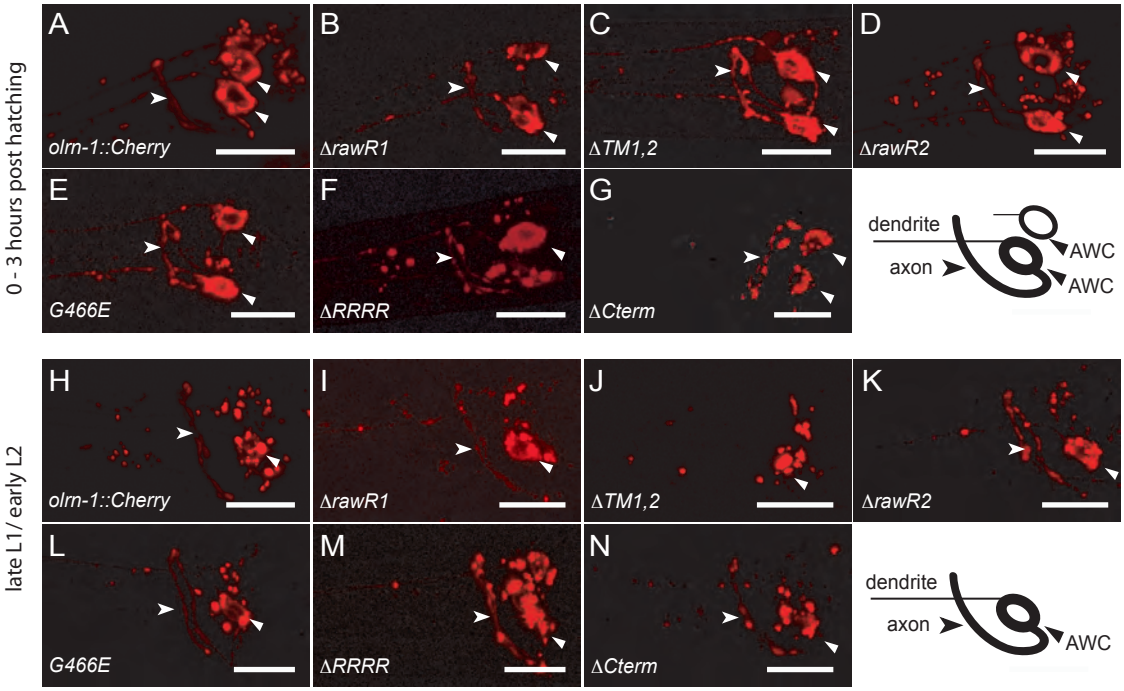

Supplementary Figure 3-1. Confocal images of *odr-3::olrn-1b::Cherry* proteins.
Confocal images of *odr-3::olrn-1b::Cherry* proteins in *olrn-1(ky626)* animals at (A-G) 0-3 hours after hatching and (H-N) L1 / L2 stage, 20 hours after hatching. Notched arrowheads indicate AWC axons, flat arrowheads indicate AWC cell bodies. The diagrams show the approximate size and disposition of AWC neurons in the images (anterior is at left). In A-G, two AWCs are visible in most images; in H-N only one AWC is visible in most images, but both AWCs have similar OLRN-1b:Cherry levels. Scale bars are 10μm.

Loss-of-function mutations in the *unc-2* α1 or *unc-36* α2δ calcium channel subunits result in a strong *(unc-36)* or mixed *(unc-2)* 2AWC^{ON} phenotype. Both *unc-36 olrn-1* double mutants and *unc-2 olrn-1* double mutants resembled *olrn-1* single mutants, with a high fraction of 2AWC^{OFF} animals (Table 3-1A). Different results were observed in double mutants between *olrn-1* and loss-of-function mutations in the CaMKII / MAP kinase cascade – the kinase genes *unc-43* (CaMKII)*, nsy-1* (MAPKKK)*,* and *sek-1* (MAPKK) [105, 126, 127]. Double mutants between *olrn-1* and the three kinases invariably resembled the kinase mutants, with a strong 2AWC^{ON} phenotype (Table 3-1A). (*tir-1 olrn-1* double mutants had a mixed, nearly wild-type phenotype (Table 3-1A), but as neither gene has definitive null alleles, the significance of these results is unclear.) These results suggest that *olrn-1* acts between the calcium channels and the CaMKII / MAP kinase cassette (see Discussion).

unc-2 CaV2 and *egl-19* CaV1 calcium channel homologs act together in AWC asymmetry

The suggestion that *olrn-1* acts at a genetic step near the voltage-activated calcium channel homolog *unc-2* prompted a more detailed examination of *unc-2* and *unc-36.* Previous studies showed that the putative CaV2 null mutant *unc-2(e55)* had a mixed AWC phenotype with 30-60% 2AWC^{ON} animals and 4-25% 2AWC^{OFF} animals [105](Table 3-1A). *unc-2(lj1),* a second strong loss-of-function mutant, shared this mixed phenotype (Table 3-1B), but null mutants for the channel-associated α2δ subunit *unc-36* had a strong 2AWC^{ON} phenotype [105] (Table 1B; see Methods for molecular analysis of *unc-36(e251)* and *unc-2(e55)*). These results could be explained if multiple α1 subunits

participate in AWC asymmetry, sharing the *unc-36* α2δ subunit. The *C. elegans* genome encodes five predicted α1 subunits, including one CaV1 subunit and one CaV2 subunit. Null mutations in the CaV1 homolog *egl-19* are embryonic lethal, and partial loss-of-function mutations have normal AWC asymmetry [87](Table 3-1B). When *egl-19* partial loss-of-function alleles were combined with null alleles of *unc-2,* the double mutants had a strong 2AWC^{ON} phenotype reminiscent of *unc-36* mutants (Table 3-1B). These results are consistent with partially redundant functions between *egl-19* and *unc-2,* with both channels contributing to AWC asymmetry.

Calcium channels can serve as scaffolding proteins in addition to their ion-conducting properties. The ion-conducting properties of EGL-19 are affected by the gain-of-function mutation *egl-19(ad695gf),* which decreases channel desensitization [87, 133]. *egl-19(ad695gf) unc-2(lf)* mutants had a strong 2AWC^{OFF} phenotype, the opposite phenotype from the *egl-19(lf) unc-2(lf)* mutants (Table 3-1B). This result suggests that the ion-conducting activity of EGL-19 contributes to its activity.

The strong 2AWC^{OFF} phenotype of *egl-19(ad695gf) unc-2(lf)* was not observed in *egl-19(ad695gf)* single mutants (Table 3-1B). At a genetic level, this result suggests that *unc-2* inhibits *egl-19* activity in AWC neurons.

olrn-1 acts in the future AWC^{ON} neuron, and *unc-2/unc-36* act in the future AWC^{OFF} neuron, to coordinate AWC signaling.

Genetic mosaic analysis is a useful approach for distinguishing between the two AWC neurons as they signal and respond to each other in development. Any gene in the asymmetry pathway could in principle function in the future AWC^{OFF} cell (the signaling

cell) or in the future AWC^{ON} cell (the responding cell). Two kinds of results have been observed in previous genetic mosaic studies. The *nsy-4* claudin and *nsy-5* innexin genes act cell-autonomously to promote induction of AWC^{ON}, and also act cell non-autonomously to prevent AWC^{ON} induction in the contralateral AWC [117, 119]. At this signaling stage, each AWC appears to monitor the activity state of the other. By contrast, the kinases *unc-43, nsy-1,* and the scaffold *tir-1* act strictly cell-autonomously: a cell with high kinase activity becomes AWC^{OFF}, and a cell with low kinase activity becomes AWC^{ON} [126, 127]. At this execution stage, the decision has been made and the AWCs are independent. To understand how the decision is made, we used genetic mosaic analysis to examine animals in which the two AWCs had different levels of *olrn-1, unc-2* and *unc-36* gene activity (Fig. 3-4, 3-5). Unstable extrachromosomal arrays containing the AWC marker *odr-1::DsRed* and either *odr-3::olrn-1, odr-3::unc-2,* or *odr-3::unc-36* test plasmids were introduced into strains with stable expression of the AWC^{ON} marker *str-2::GFP* (Fig. 3-4A, 3-4C, 3-5B, 3-5D, 3-5F, 3-5H). Random loss of the arrays from one AWC was detected using the *odr-1::DsRed* marker, and then both AWC neurons were scored for the expression of the *str-2::GFP* AWC^{ON} marker. The methods for these experiments were similar to those used in previous studies; control experiments indicate that the promoters and markers do not affect AWC asymmetry (see Methods, [119, 126, 127]).

In an *olrn-1* mutant background, most mosaic animals with a single rescued AWC had the wild-type, asymmetric phenotype: the rescued cell became AWC^{ON} and the mutant cell became AWC^{OFF} (Fig. 3-4B). This result suggests that *olrn-1* acts cell autonomously in the future AWC^{ON} (the responding cell) to induce AWC^{ON}. In wild-type animals overexpressing *odr-3::olrn-1* transgenes, most animals that lost the

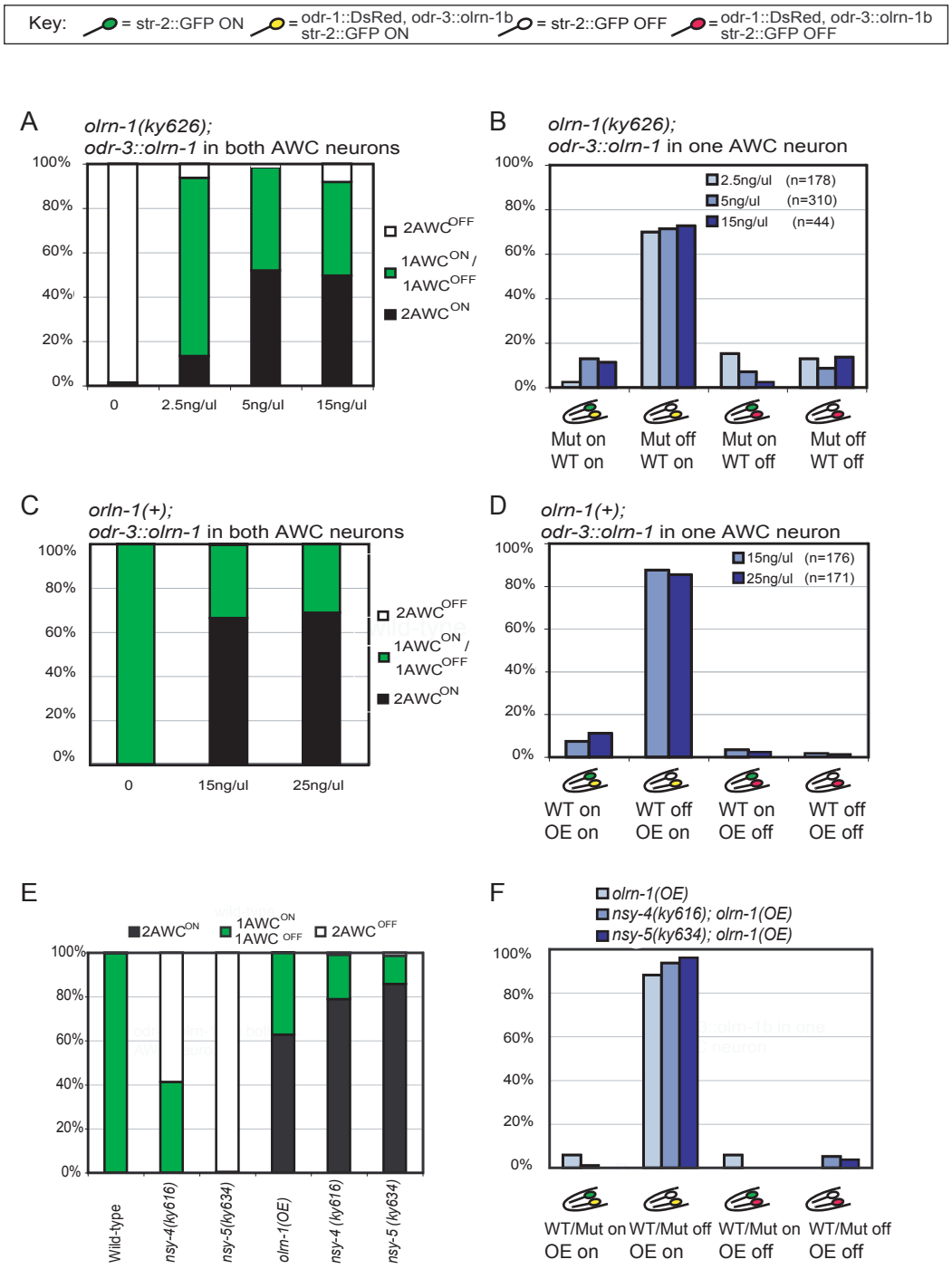

Figure 3-4. *olrn-1* mosaic analysis
(A) Rescue of *olrn-1(ky626)* by *odr-3::olrn-1b* injected at 2.5 ng/ul, 5 ng/ul, or 15 ng/ul with *odr-1::DsRed*. (B) AWC phenotypes of mosaic *olrn-1(ky626)* animals that express *odr-3::olrn-1b odr-1::dsRed* transgene in one AWC. (C) Phenotypes in wild-type animals overexpressing *odr-3::olrn-1b* injected at 15ng/ul or 25 ng/ul with *odr-1::DsRed*. (D) AWC phenotypes of wild-type mosaic animals that overexpress *odr-3::olrn-1b* in one AWC.
For statistical analysis, see Methods. (E) Phenotypes of *nsy-4 olrn-1(OE)* and *nsy-5 olrn-1(OE)* strains and controls. (F) AWC phenotypes of mosaic animals that express *odr-3::olrn-1b* in one AWC in *nsy-4* or *nsy-5* mutant backgrounds.

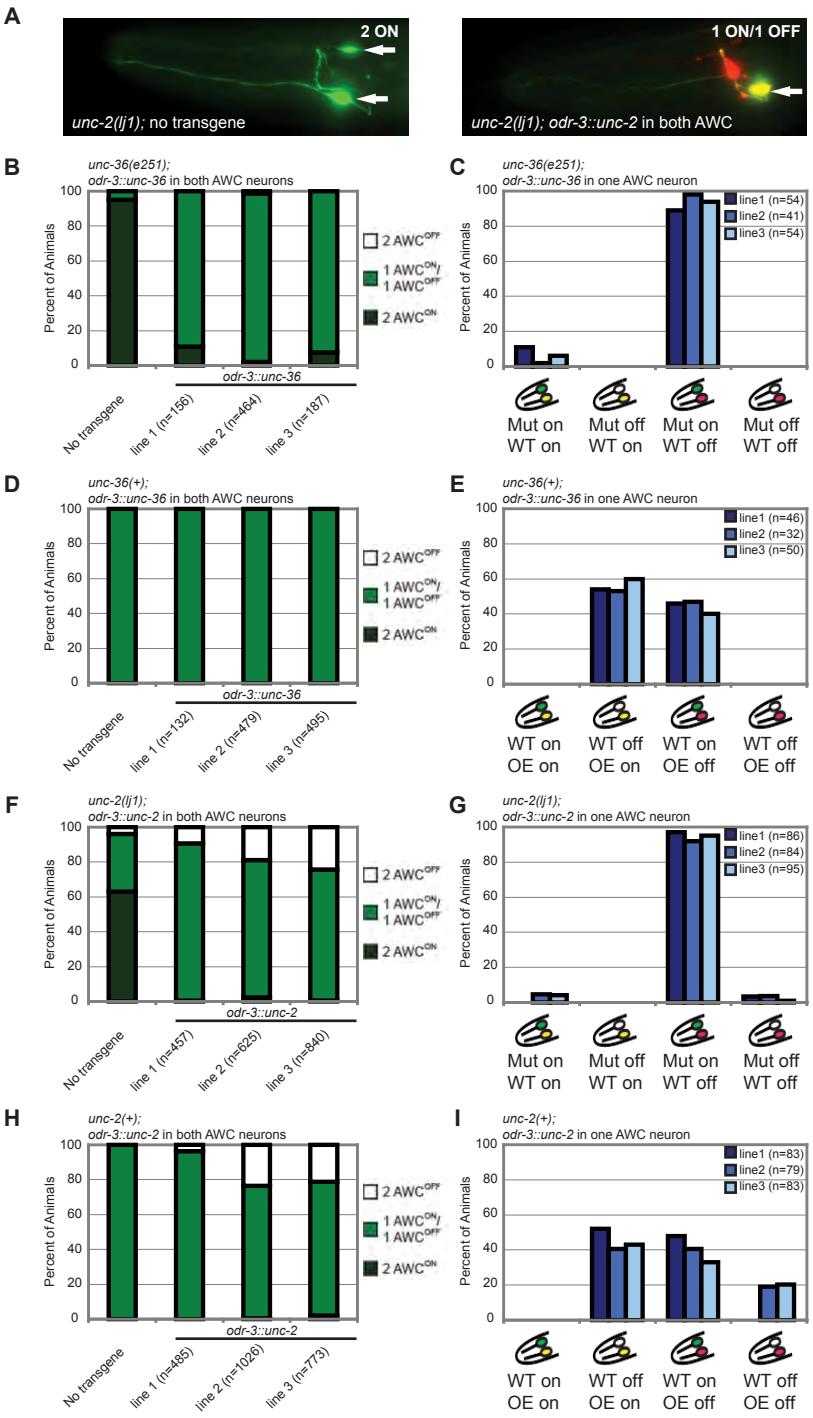

Figure 3-5. Mosaic analysis of the *unc-36/unc-2* calcium channel genes.
(A) Rescue of *unc-2(lj1)* by *[odr-3::unc-2, odr-1::dsRed*] array. Green, *str-2::GFP* expression. (B) Rescue of *unc-36(e251)* phenotypes in three *[odr-3::unc-36, odr-1::dsRed]* transgenic lines. (C) AWC phenotypes of *unc-36* mosaic animals that express *odr-3::unc-36* in one AWC. (D) The three *[odr-3::unc-36, odr-1::dsRed]* transgenes from (B) were introduced into a wild-type background. (E) AWC phenotypes of wild-type mosaic animals that overexpress *odr-3::unc-36* in one AWC. (F) Rescue of *unc-2(lj1)* phenotypes in three *Ex[odr-3::unc-2, odr-1::dsRed]* transgenic lines. (G) AWC phenotypes of *unc-2* mosaic animals that express *odr-3::unc-2* in one AWC. (H) The three *[odr-3::unc-2, odr-1::dsRed]* transgenes from (F) were introduced into a wild-type background. (I) AWC phenotypes of wild-type mosaic animals thatoverexpress *odr-3::unc-2* in one AWC.
n, number of animals scored. For statistical analysis, see Methods.

transgene in one AWC also had a wild-type asymmetric AWC phenotype. In these animals, the cell overexpressing *olrn-1* nearly always became AWC^{ON}, and the wild-type contralateral cell nearly always became AWC^{OFF} (Fig. 3-4D). This behavior is unlike the behavior of fully wild-type animals in which each cell becomes AWC^{ON} or AWC^{OFF} at equal frequencies. The wild-type mosaics suggest that a cell with higher *olrn-1* expression can prevent the contralateral cell from becoming AWC^{ON}, and therefore implicate *olrn-1* in feedback between AWCs. Very similar results were previously obtained in mosaic analysis of *nsy-4* and *nsy-5* [117, 119].

The results described above might be confounded by *nsy-4*- and *nsy-5*–dependent signaling between AWCs. To separate cell-intrinsic functions of *olrn-1* from possible network functions, we generated mosaics overexpressing OLRN-1 in one AWC in *nsy-4* and *nsy-5* mutants (Fig. 3-4E, 3-4F). In these experiments, *olrn-1(OE)* behaved exactly as it did in the wild-type background, specifically converting the *olrn-1*-expressing neuron to AWC^{ON} (Fig. 3-4F). These results suggest that *olrn-1* functions independently of, and most likely downstream of, *nsy-4* and *nsy-5* in AWC^{ON}.

Genetic mosaic experiments were then conducted with the calcium channel genes *unc-36* ($\alpha 2\delta$ subunit) and *unc-2* (CaV2 $\alpha 1$ subunit). Expression of either gene from the AWC-selective *odr-3* promoter in AWC rescued AWC asymmetry, but not coordinated movement (see Methods, Fig. 3-5A, 3-5B, 3-5F). Thus the calcium channels can function within AWC neurons. A mild gain-of-function phenotype was observed with *odr-3::unc-2,* but not with *odr-3::unc-36* (Fig. 3-5D, 3-5H).

For both *unc-36* and *unc-2*, mosaic animals with a single rescued AWC had the wild-type asymmetric phenotype: the rescued cell always became AWC^{OFF}, and the

mutant cell always became AWC^{ON} (Fig. 3-5C, 3-5G). This result was substantially different from the result with downstream kinases such as *unc-43,* where a single rescued AWC randomly became AWC^{ON} or AWC^{OFF}, and the mutant cell always became AWC^{ON} [127]. The difference suggests that *unc-36* and *unc-2* can influence the AWC^{ON} / AWC^{OFF} decision, whereas *unc-43* and other kinases act to execute a decision that has already been made. The rescue of the *unc-2* mutant cell in these mosaics is particularly informative. *unc-2* has an incompletely penetrant phenotype (63% 2AWC^{ON}), so ~18% of the *unc-2* mutant AWCs should have become AWC^{OFF} if they were not affected by the transgene. In fact, fewer than 5% of the *unc-2* mutant AWCs became AWC^{OFF}, indicating that an *unc-2* AWC neuron can sense the rescued AWC on the contralateral side.

Only a mild overexpression phenotype was observed upon introduction of *odr-3::unc-2* into wild-type animals (Fig. 3-5H), suggesting that the tightly regulated calcium channels may be relatively resistant to variations in expression levels. In mosaic animals in which only one AWC overexpressed *odr-3::unc-36* or *odr-3::unc-2* in a wild-type background, the overexpressing AWCs or the contralateral AWCs were equally likely to become AWC^{ON} or AWC^{OFF} (Fig. 3-5E, 3-5I). These results indicate that unlike *nsy-4, nsy-5,* and *olrn-1,* relative *unc-2* and *unc-36* expression levels are not critical to the AWC^{ON} / AWC^{OFF} decision.

Discussion

This analysis adds two genes to the pathway for AWC asymmetry: the new gene *olrn-1,* and the *C. elegans* CaV1 homolog *egl-19*, whose cooperation with *unc-2* explains

the weak phenotype of the *unc-2* (CaV2) mutant. These genes and other genes in the AWC asymmetry pathway have been classified in three ways (1) Double mutant analysis, which can reveal biological regulatory relationships (2) Targeted rescue and mosaic analysis to determine the essential cellular site of expression and (3) Detailed mosaic analysis to determine whether expression of the gene in one AWC affects the contralateral AWC. Together, results from these experiments suggest that the coordinated decision between AWC^{ON} and AWC^{OFF} occurs at the interface between the calcium channels (UNC-2/UNC-36/EGL-19) and OLRN-1.

In *C. elegans* AWC neurons, *olrn-1* has genetically-defined functions that are similar to those of the innexin gene *nsy-5* and the claudin/calcium channel γ subunit gene *nsy-4*. All three genes are required for the induction of AWC^{ON}, and all have similar cell-autonomous and non-autonomous effects on AWC in mosaic analysis [117, 119]. *olrn-1* overexpression induced AWC^{ON} cell-autonomously in *nsy-4* and *nsy-5* mutants, suggesting that *olrn-1* acts downstream of these two genes or independently of them in AWC^{ON}. The nature of any *olrn-1* regulation by the upstream genes is unknown. There were no obvious effects of *olrn-1* mutations on tagged NSY-4 or NSY-5 proteins in AWC, nor were there obvious effects of *nsy-4* or *nsy-5* on tagged OLRN-1 protein (data not shown). However, there could be early effects in the embryo, or effects on endogenous proteins, that were missed in these experiments.

olrn-1 mutations were epistatic to null mutations in the calcium channel genes *unc-2* and *unc-36,* whereas calcium channel null mutations are epistatic to *nsy-4* and *nsy-5* [117, 119]. The behavior of *olrn-1* in these double mutants supports the suggestion that it acts at a later step in signaling than *nsy-4* and *nsy-5*. Epistasis analysis does not provide

detailed molecular mechanisms, and some conclusions are not firm when null alleles are unavailable. However, since the *unc-2* and *unc-36* mutations are molecular nulls, the epistasis result proves that these particular channel genes are not essential for *olrn-1* activity.

The kinase mutations *unc-43 (*CaMKII), *nsy-1* (ASK1/MAPKKK), and *sek-1* (MAPKK) were fully epistatic to *olrn-1* mutations. Thus at a genetic level, *olrn-1* may prevent *unc-2* from activating the CaMKII homolog *unc-43* in the future AWC^{ON}. In molecular terms, this might mean that OLRN-1 inhibits calmodulin (which would act at this step) or that OLRN-1 prevents calcium from UNC-2 channels from activating UNC-43, perhaps by binding the channel or the kinase (Fig. 3-6). There is no evidence for direct interactions between these proteins, and many other possibilities exist. *olrn-1* is related to *Drosophila raw/cyrano,* which is required for epithelial movements that drive dorsal closure of the fly embryo, for epithelial morphogenesis, and for neuronal development [132, 134]. An *olrn-1* domain that is similar to *raw* is needed for full *olrn-1* activity, supporting the significance of the homology. The direct targets of Raw are unknown, but *raw* mutants have excessive phospho-Jnk during dorsal closure, suggesting that Raw inhibits Jnk MAP kinase pathways [132]. This biochemical analysis of Raw appears to parallel the genetic conclusion that *olrn-1* directly or indirectly inhibits the kinase pathway consisting of *unc-43* (CaMKII), *nsy-1* (ASK1, a p38/Jnk MAPKKK), and *sek-1* (MAPKK).

The analysis of *egl-19* CaV1 mutations underscores the importance of calcium channels in AWC asymmetry. *unc-2* CaV2 has a weak and mixed phenotype, raising doubt about its significance, but the highly penetrant $2AWC^{ON}$ phenotype of *egl-19 unc-*

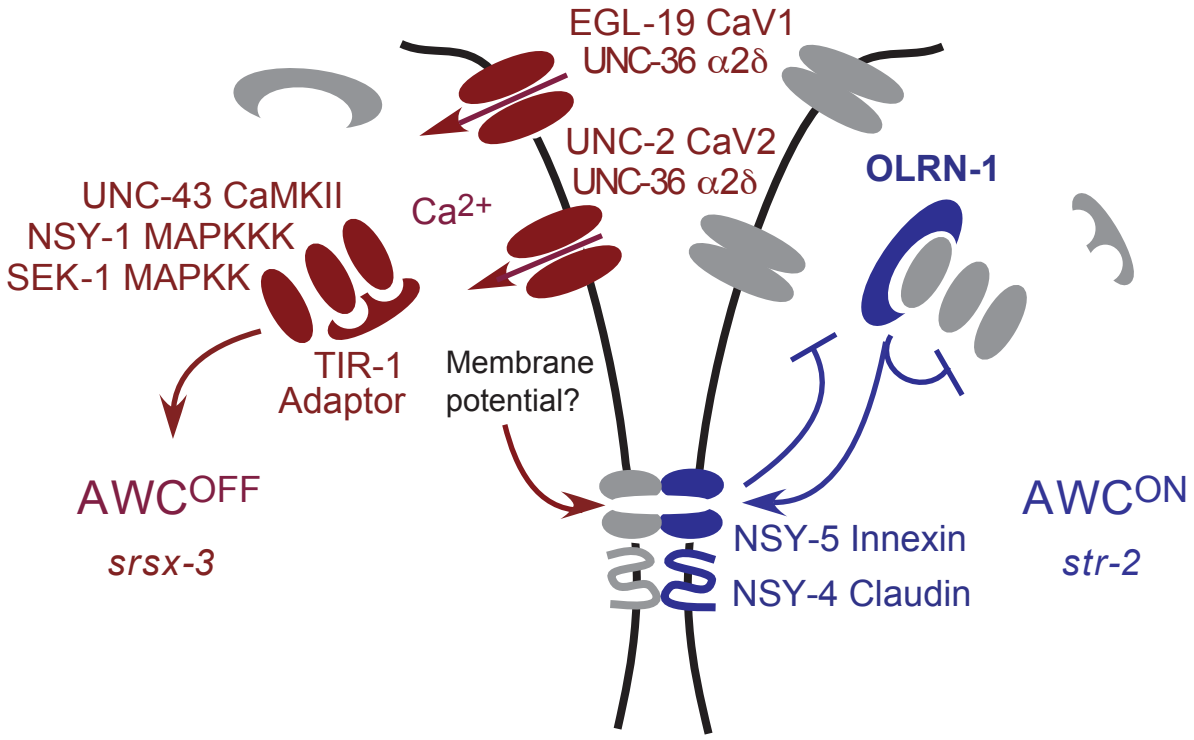

Figure 3-6. Model for calcium channel function and OLRN-1 in the AWCON / AWCOFF decision. All genes are expressed both in the left and in the right AWCs; color is used to indicate the cell in which each gene product is more active. The future AWCOFF transmits a signal to AWCON via NSY-5 gap junctions between AWC and other cells and NSY-4 claudins. This signal might be membrane potential. In AWCON, the signal suppresses the UNC-2 (CaV2) and EGL-19 (CaV1) voltage-activated calcium channels and allows high OLRN-1 activity. OLRN-1 inhibits the UNC-43 (CaMKII) / NSY-1/ SEK-1 kinase cascade cell-autonomously within AWCON. A feedback signal from the calcium channels and OLRN-1 is transmitted from AWCON back to AWCOFF.

2 double mutants suggests that calcium entry through voltage-activated calcium channels is essential for specification of AWC^{OFF}. The strong $2AWC^{OFF}$ phenotype of the *egl-19(gf) unc-2(lf)* double mutant further suggests that sufficient calcium entry through EGL-19 can act instructively to specify AWC^{OFF}. This phenotype was not observed in *egl-19(gf)* single mutants, suggesting that *unc-2* inhibits *egl-19* activity. CaV channels generate calcium and voltage signals, and are subject to calcium- and voltage-dependent activation and inactivation, so there are many levels at which cross-regulation could take place [53]. The behavior of *unc-36* suggests that it promotes the activity of both *unc-2* and *egl-19*. In previous studies, *unc-36* has been proposed to inhibit *egl-19* activity [133]; we suggest that this may be due to its positive effect on *unc-2*.

A model for the functions of *olrn-1, unc-2,* and *unc-36* in the signaling pathway, based on this work and prior work, is presented in Figure 3-6. Induction of AWC^{ON} from an AWC^{OFF}–like ground state requires cooperation between the innexin gene *nsy-5,* which assembles a multicellular gap junction network and preferentially induces AWCR to the AWC^{ON} state, and the claudin/γ-subunit like *nsy-4,* which preferentially induces AWCL to the AWC^{ON} state [117, 119]. Tight junctions (which contain claudins) and gap junctions (which are composed of innexins) potentiate one others' activity in epithelia, providing a possible analogy for the *nsy-4/nsy-5* cooperation in AWC [135]. A signal must be transmitted by this multicellular network; the strong involvement of the calcium channel homologs *unc-2, egl-19,* and *unc-36* in AWC asymmetry suggests that the signal regulates membrane potential. Voltage changes are efficiently transmitted through gap junctions, whereas calcium is poorly diffusible and is therefore transmitted inefficiently. Thus voltage signals from UNC-2, EGL-19, and possibly other channels could be

transmitted from AWC^{OFF} to AWC^{ON} via gap junctions. At least two other voltage-regulated channels, the potassium channels SLO-1 and EGL-2, also affect AWC asymmetry [105, 136]. The appeal of this model is that voltage-regulated channels such as *unc-2/unc-36* could act both to generate a signal in one AWC and to detect the signal in the contralateral AWC.

The coordinated decision to form one AWC^{ON} and one AWC^{OFF} requires a symmetry-breaking event. Like many genes in the AWC asymmetry pathway, *unc-2/unc-36* activity is predicted to be high in one AWC, and low in the other; unlike other genes, there are plausible mechanisms by which a symmetry-breaking event could differentially regulate calcium channels. An interesting example is provided by the pacemaker cells of the vertebrate heart, which are found in the sinoatrial (SA) node. Gap junctions and voltage-activated calcium channels are essential to the synchronization of SA pacemaker cells and the generation of a coherent heartbeat [137]. Isolated SA cells have rhythmic action potentials that are driven by calcium channels and other conductances. When two SA cells come into contact, they form gap junctions that lead to synchronization of the two cells, at a rhythm that is dominated by the faster, or leader, cell. Two synchronized SA cells would appear to be similar, but in fact, the result of their synchronization is a coupling of membrane potential and an uncoupling of individual conductances within the two cells [138]. During the diastolic period between heartbeats, the leader cell has an ongoing inward current, while the follower cell has an outward current [138]. In other words, the leader cell experiences inward currents both at the beginning of the calcium action potential and in the long period between action potentials; the follower cell experiences inward currents only during the action potential.

As calcium-activated signaling pathways are exquisitely sensitive to the temporal pattern of calcium signals [139, 140], different patterns of inward calcium currents in two cells have the potential to create sustained differences between them.

We suggest that in isolation, both AWCs have spontaneous activity sufficient to maintain CaMKII activity and the AWC^{OFF} state. When gap junctions form via NSY-5, the spontaneous activity of the AWCs is coupled, and by analogy to the SA node, one cell leads and the other follows. The leader cell maintains ongoing calcium entry and becomes AWC^{OFF}; gap junction coupling reduces calcium entry into the follower cell, and it becomes AWC^{ON}. In this model, the calcium channels have both an effector function (calcium entry and activation of CaMKII) and a signaling function (altering membrane potential). We speculate that similar mechanisms may operate in many developing nervous systems during the transient period that gap junctions are prominent. Since it acts at a similar step, *olrn-1* could affect either the propagation of the signal or its effectiveness in the responding cell.

Gap junctions, claudins, and membrane potential affect left-right asymmetry of the *Xenopus* body axis, suggesting a possible molecular similarity between vertebrate asymmetry and the pathways that regulate *C. elegans* AWC neurons [141-143]. Although the later nodal/Shh pathways used in vertebrate left-right patterning are different from those used in AWCs, there may be hidden similarities that remain to be discovered. The left-right asymmetry of the human brain is more variable than the human body plan; left-handedness and reversed lateralization of language areas are much more common than inversion of the internal organs [144]. Lateralized neurological disorders such as migraine headaches and Rasmussen encephalitis randomly affect one side of the brain, providing

indirect evidence of variably asymmetric brain functions [145, 146]. An asymmetric migraine syndrome in humans is caused by mutations in CaV2 calcium channels, which are orthologs of *unc-2* [146]. Further analysis of asymmetric brain function in humans may reveal unexpected connections with the asymmetric nervous system of *Caenorhabditis elegans.*

Chapter 4

Maintenance of CaV2 expression requires the nuclear protein PQN-53

Abstract

Efficient translation and folding of ion channels requires the functional integrity of the endoplasmic reticulum. Presynaptic voltage-gated calcium channels are multi-pass transmembrane proteins that provide calcium for synaptic vesicle exocytosis at nerve terminals. We show here that the expression and synaptic localization of the alpha1 subunit of the *C. elegans* CaV2 channel, UNC-2, is regulated by PQN-53, a ubiquitous polyglutamine protein that regulate the non-canonical endoplasmic reticulum stress response. In *pqn-53* mutants, UNC-2 expression is reduced in the endoplasmic reticulum but other active zone components and synaptic vesicles are expressed properly and delivered to synapses. Acute induction of *pqn-53* induces expression of UNC-2 in the endoplasmic reticulum, consistent with a role in UNC-2 biogenesis. PQN-53 is localized to the nucleus, and genome-wide transcriptome analysis revealed that PQN-53 represses expression of genes implicated in the non-canonical unfolded protein response. Consistent with the previous findings of the involvement of the unfolded protein response in pathogen resistance, *pqn-53* mutants are resistant to infection of *Salmonella enterica*. Our genetic and cell biological studies suggest that PQN-53 is a component of the endoplasmic reticulum stress sensing systems, and couples endoplasmic reticulum homeostasis, membrane protein biogenesis, and host defense against pathogenic bacteria.

Introduction

The abundance of plasma membrane transmembrane proteins including ion channels and receptors is limited by the efficacy of translation, folding, subunit assembly and functional maturation in the endoplasmic reticulum. Quality control in the endoplasmic reticulum monitors nascent proteins and prevents improperly folded or misassembled proteins from exiting the endoplasmic reticulum. Various ER-resident chaperones including Bip and lectin-based chaperones such as calnexin and calreticulin promote protein folding and assembly and assist retention of incompletely folded proteins [147]. Endoplasmic reticulum retention of the nascent proteins is mediated by the specific retention signals in the proteins or by carbohydrate residues that are attached to misfolded domains. Masking of the endoplasmic reticulum retention motifs such as dibasic residues in cytosolic domains is achieved via subunit assembly or other co-factors allowing the proteins to leave the endoplasmic reticulum [148]. Misfolded proteins are marked by the attachment of N-linked carbohydrates and subsequently recognized by lectin-based chaperones. Properly folded proteins exit from the endoplasmic reticulum upon trimming of the glucose from the N-linked core glycans. UDP-glucose:glycoproteins glucosyltransferase, on the other hands, adds glucose residue back to N-glycans near regions of disorder so that the glycoproteins re-associate with chaperones [149, 150]. The cycle of glucosylation and de-glucosylation continues until the glycoprotein either reaches its native conformation or is targeted for degradation [147]. Defects in subunit assembly or protein folding decrease total expression of the protein at the cell surface and lead to abnormal cell functions [148].

The expression of ER-resident chaperones and activation of the degradation

pathway are regulated by the load of unfolded proteins in the endoplasmic reticulum. To encounter the overload of unfolded proteins (ER stress), unfolded proteins in the endoplasmic reticulum induce the unfolded protein response (UPR) that leads to the expression of chaperone proteins and promotes degradation of the unfolded proteins via activation of ER-associated degradation (ERAD). In ERAD, the unfolded proteins are retrotranslocated to cytosol and degraded by the ubiquitin-proteasome pathway. The UPR also mediates global downregulation of translation via inhibition of translation initiation factors or degradation of messenger RNAs and reduces flux of newly synthesized proteins into the endoplasmic reticulum [151, 152]. If adaptation to ER stress is not sufficient, an apoptotic response is initiated, leading to cell death. Protein conformational disease such as cystic fibrosis is associated with the accumulation of unfolded proteins in the endoplasmic reticulum [153].

Physiological roles of the UPR are implicated in development of organisms as well as host defense against pathogens [154, 155]. *C. elegans* has been a powerful model organism to study the UPR because of dispensability of the UPR sensing genes; mutants lacking the core UPR components are viable. In the absence of IRE-1, XBP-1 or PEK-1, the major ER stress sensors of *C. elegans*, animals are highly susceptible to ER stress and develop abnormally [154]. These mutants can serve as a sensitized system for identifying sources of and responses to ER stress. For example, a non-canonical ER stress system was discovered based on its induction in *xbp-1* mutants exposed to the glycosylation inhibitor tunicamycin. The proteins in this non-canonical system are called ABU/PQN proteins. They have signal sequences and polyglutamine repeats, and are thought to reside in endoplasmic reticulum lumen inside cells. *xbp-1* mutants with RNAi

knockdown of *abu* genes are less resistant to ER stress compared to *xbp-1* mutants. Thus, the *abu* genes are likely to encode non-canonical UPR proteins, either functioning in a pathway parallel to the canonical UPR or in ERAD of misfolded proteins [156].

UPR systems are involved in a variety of cells and tissue functions in *C. elegans*. XBP-1, a transcription factor regulated by IRE-1, is required for host defense against immune activation mediated by the p38 mitogen-activated protein kinase pathway. *xbp-1* mutants are highly susceptible to *Pseudomonas aeruginosa* infection, and this susceptibility is alleviated upon disruption of the p38 kinase pathway [155]. The UPR also acts in the nervous system, and is implicated in endoplasmic reticulum exit of GLR-1 non-NMDA glutamate receptors in *C. elegans* [157] suggesting a critical role of UPR in many tissues.

Here, we studied the regulation of CaV2 channel expression in the endoplasmic reticulum, analyzing a newly identified mutant, *calf-2/pqn-53*. In addition to its role in regulating calcium channel traffic, *calf-2/pqn-53* is part of the molecular mechanism coupling the unfolded protein response with host defense against pathogenic bacteria.

Results

UNC-2 synaptic puncta are reduced in *calf-2* mutants

I conducted a genome-wide EMS screen (see methods) using the *kyis442* marker line and identified a new calcium channel localization mutant, *calf-2*. In *calf-2(ky977)* mutants, GFP::UNC-2 was barely detectable in AWC axons, but the peripheral synaptic vesicle marker RAB-3 was not affected (Fig. 4-1a-f). The total fluorescence intensity of axonal GFP::UNC-2 as well as the number of puncta per axon were greatly reduced (Fig. 4-1g,h); minimal effects were detected upon similar quantification of RAB-3 (Fig. 4-1g,h). The active zone markers ELKS-1 (Fig. 4-1i-k) and SYD-2 (Fig. 4-1l-n) appeared normal, indicating that *calf-2* has a restricted effect on UNC-2 and not all synaptic proteins.

calf-2 also affected GFP::UNC-2 localization in motor neurons. The dorsal nerve cord of *calf-2* mutants had reduced levels of GFP::UNC-2 fluorescence and few GFP::UNC-2 puncta, but near-normal RAB-3 puncta, suggesting a loss of UNC-2 from DD synapses (Fig. 4-2a-h). Expression of the single-pass transmembrane synaptic vesicle marker SNB-1::GFP was normal in DD neurons (Fig. 4-2i-l), underscoring the selectivity of the *calf-2* defect in UNC-2 localization.

The overall defect in GFP::UNC-2 localization in *calf-2* mutants was weaker than that in *calf-1* or *unc-36*, as substantial fluorescent signal was still detectable at the synapses in *calf-2* mutants. Accordingly, *calf-2* mutants had a normal sinusoidal posture with apparently normal locomotory behavior (data not shown).

calf-2 mutants were characterized further by examining expression of other neuronal transmembrane proteins. Interestingly, the expression of the G-protein coupled odorant receptor ODR-10::GFP was reduced in AWA sensory neurons of *calf-2* mutants

Figure 4-1. Presynaptic GFP::UNC-2 puncta are reduced in AWC sensory neurons of *calf-2(ky977)* mutants.
(a-c) Representative images of GFP::UNC-2 and RAB-3::mCherry in the AWC cell body (white arrowhead) and axon (yellow arrowheads). The more dorsal cell body is AWB (asterisk). (d-f) Representative images of GFP::UNC-2 and RAB-3::mCherry in AWC neuron of a *calf-2(ky977)* mutant. (g, h) Quantification of GFP::UNC-2 and RAB-3::mCherry in AWC; (g) Normalized total fluorescence intensity and (h) number of fluorescent clusters. (i-k) Representative images of GFP::UNC-2 and ELKS-1::mCherry in AWC neurons of a *calf-2(ky977)* mutant. (l-n) Representative images of GFP::UNC-2 and SYD-2::mCherry in AWC neurons of a *calf-2(ky977)* mutant. All error bars indicate s.e.m. In g,h, asterisks indicate results different from wild-type controls by unpaired t-test at $P<0.01$ (**). In all Figures, the AWC promoter is *odr-3,* which is also expressed weakly in AWB, ASH, AWA, and ADF sensory neurons, and all data are taken from adult animals, unless otherwise noted. Head is to the left and dorsal is up in all images unless otherwise noted. Scale bar, 10 μm.

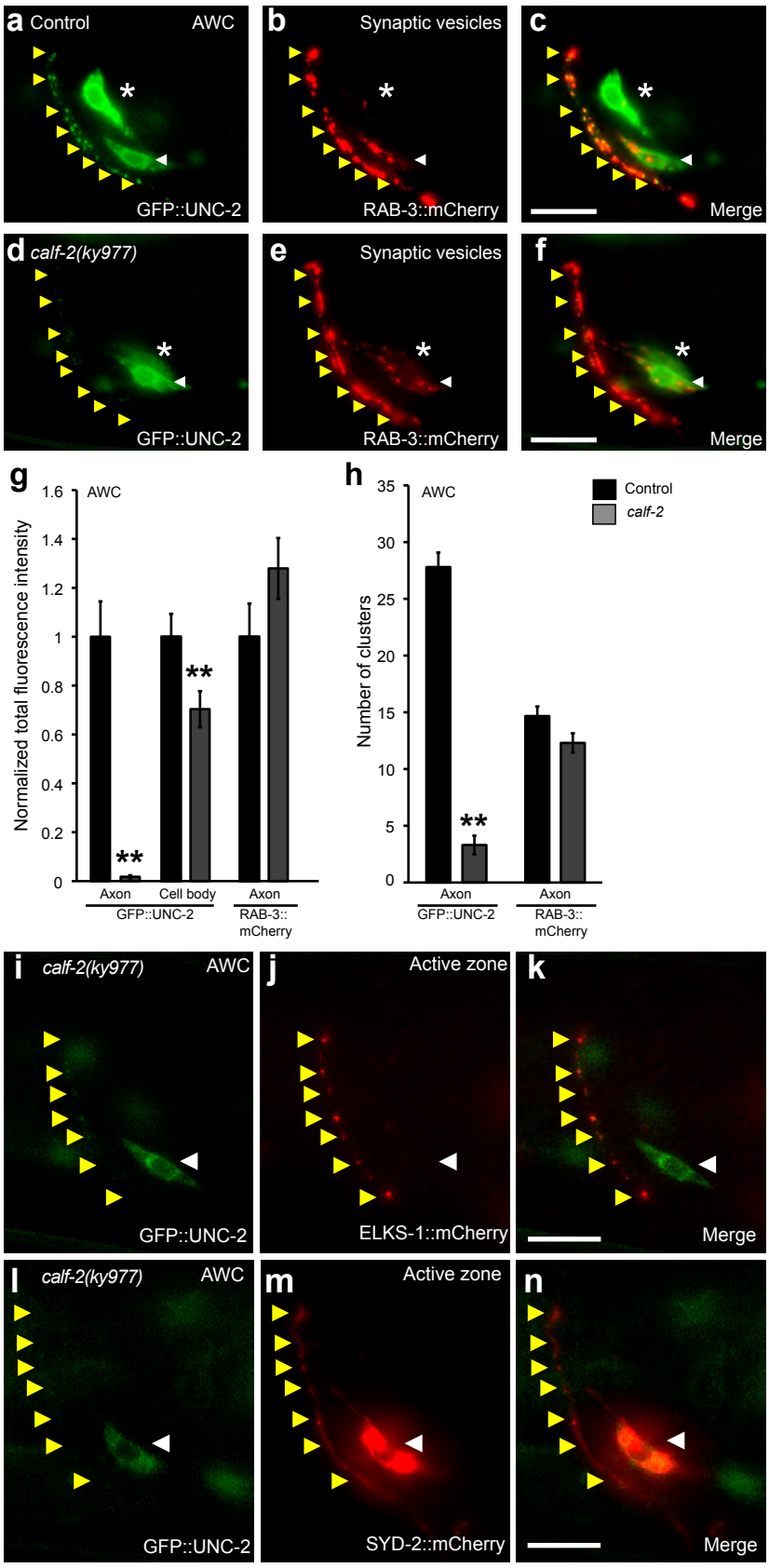
a Control AWC
GFP::UNC-2
b Synaptic vesicles
RAB-3::mCherry
c
Merge
d calf-2(ky977)
GFP::UNC-2
e Synaptic vesicles
RAB-3::mCherry
f
Merge
g AWC
Normalized total fluorescence intensity
1.6
1.4
1.2
1
0.8
0.6
0.4
0.2
0
**
**
Axon
Cell body
Axon
GFP::UNC-2
RAB-3::
mCherry
h AWC
Control
calf-2
Number of clusters
35
30
25
20
15
10
5
0
**
Axon
Axon
GFP::UNC-2
RAB-3::
mCherry
i calf-2(ky977) AWC
GFP::UNC-2
j Active zone
ELKS-1::mCherry
k
Merge
l calf-2(ky977) AWC
GFP::UNC-2
m Active zone
SYD-2::mCherry
n
Merge

Figure 4-1

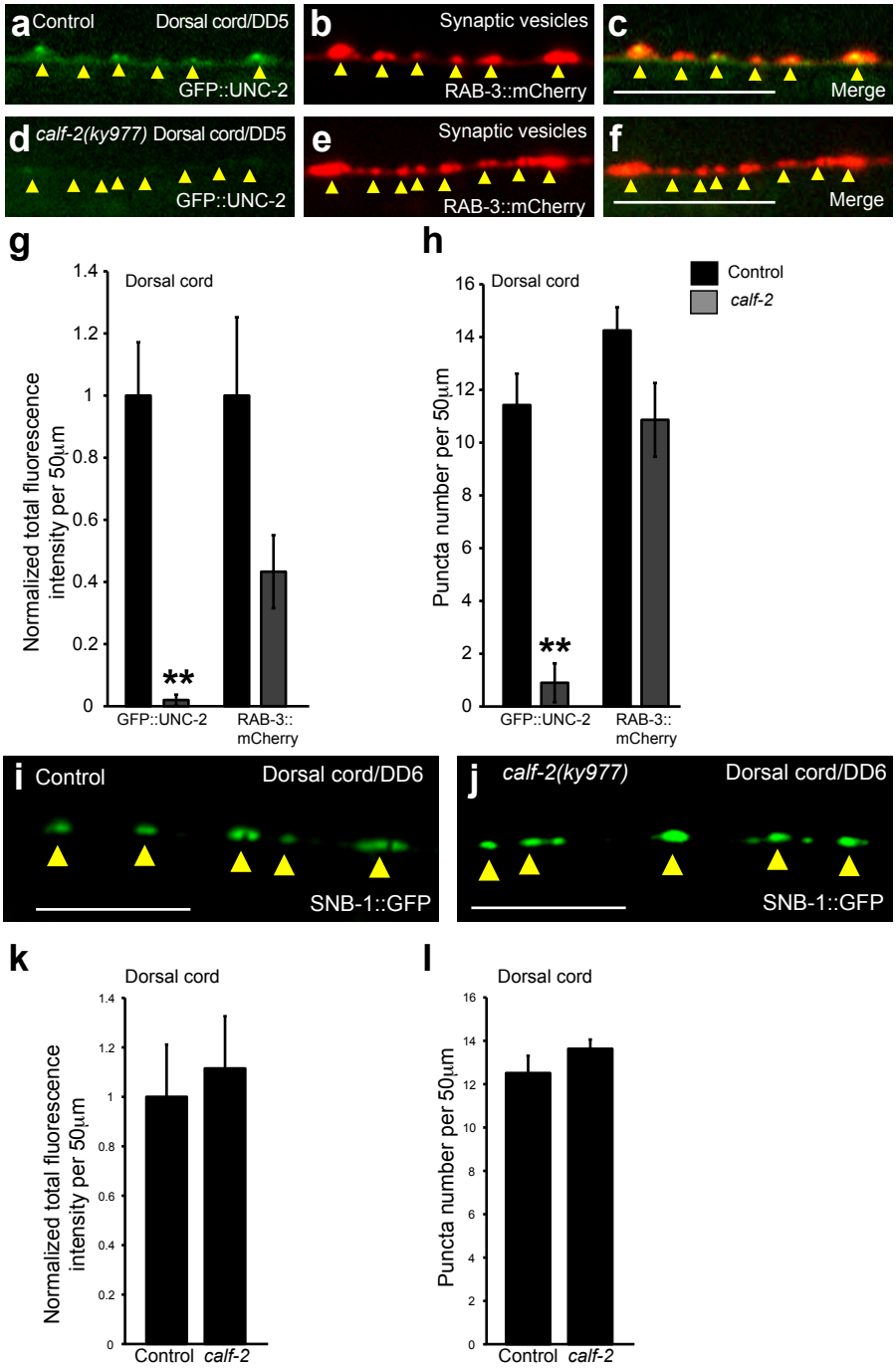

Figure 4-2. GFP::UNC-2 puncta are reduced in VD/DD GABAergic motor neurons of *calf-2(ky977)* mutants.

(a-c) Representative images of GFP::UNC-2 and RAB-3::mCherry in DD axons (dorsal nerve cord) of GABAergic motor neurons. (d-f) Representative images of GFP::UNC-2 and RAB-3::mCherry in DD neurons of a *calf-2(ky977)* mutant. (g,h) Quantification of GFP::UNC-2 and RAB-3::mCherry in 50 µm covering DD5 and DD6 axons in the dorsal nerve cord; (g) Normalized total fluorescence intensity and (h) number of fluorescent puncta. Asterisks indicate results different from wild-type controls by unpaired t-test at $P<0.01$ (**). (i,j) Representative images of SNB-1::GFP in DD neurons; (i) A wild type control animal and (j) a *calf-2(ky977)* mutant. (k) Quantification of SNB-1::GFP in 50 µm covering DD5 and DD6 axons in the dorsal nerve cord; (k) Normalized total fluorescence intensity and (l) number of fluorescent puncta. The VD/DD promoter is *unc-25*; and all data are taken from adult animals. Scale bar, 10 µm.

(Fig. 4-3a-d). ODR-10::GFP is normally localized to sensory cilia, not to synapses, and the *calf-2* defect was most evident as a reduction in ciliary ODR-10. These results indicate that *calf-2* defects are not restricted to calcium channels or synapses, but can affect multipass transmembrane proteins in other neuronal compartments.

calf-2 encodes a ubiquitously expressed nuclear protein

Genetic mapping and transgenic rescue identified *calf-2* as the previously uncharacterized gene *pqn-53* (Fig. 4-4a). Sequencing of *calf-2(ky977)* DNA revealed a G to A mutation at a splice donor site (Fig. 4-4a). The effect of the mutation was examined by RT-PCR analysis of *pqn-53* cDNA from wild type animals and *calf-2* mutants. Wild type animals expressed both spliced and unspliced *pqn-53* mRNA, consistent with previous transcript analysis (Wormbase: www.wormbase.org). In contrast, *calf-2* mutants only expressed unspliced mRNA (Fig. 4-4b). This splicing defect results in an early stop codon in the *pqn-53* open reading frame (Fig. 4-4c).

The *calf-2* mutant is recessive, and a *pqn-53* gene with the *ky977* mutation did not affect GFP::UNC-2 localization when injected into wild-type animals (data not shown). These results suggest that *ky977* is a reduction or loss of function allele of *pqn-53*.

The spliced *pqn-53* cDNA encodes a predicted 361 amino acid long glutamine/asparagine (Q/N)-rich domain containing protein (Fig. 4-4c). The *pqn* genes constitute a 79-member nematode gene family characterized by prion-like Q/N-rich amino acid sequences [158]. Homologs of *pqn-53* have been identified in *Caenorhabditis* nematodes (Fig. 4-4c) and possibly in other nematode species including *Brugia malayi*. Among *Caenorhabditis* nematodes, conservation of PQN-53 extended across the entire

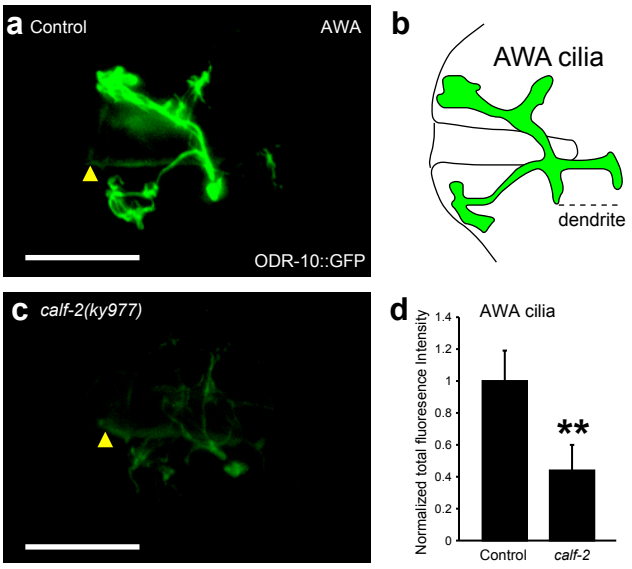

Figure 4-3. ODR-10::GFP cilia expression is affected in *calf-2* animals.
(a) A representative image of ODR-10::GFP in AWA sensory cilia. Yellow arrowhead marks nose. (b) Schematic of AWA sensory cilia, with cilia in green. (c) A representative image of ODR-10::GFP in AWA sensory cilia of a *calf-2(ky977)* mutant. (d) Quantification of ODR-10::GFP in AWA cilia. Asterisks indicate results different from wild-type controls by unpaired t-test at $P<0.01$ (**). Scale bar, 10 μm.

Figure 4-4. *calf-2* encodes a glutamine/asparagine (Q/N)-rich domain containing protein. (a) Mapping and cloning of *calf-2*. A PCR fragment containing the operon CEOP5320 rescued the *calf-2* mutant phenotype. The *ky977* allele has a G to A transition at the splice donor site in the third intron of *pqn-53* gene. (b) RT-PCR analysis of the splicing of *pqn-53*. The *ky977* mutation disrupts splicing of the third intron, leaving only a non-spliced isoform; a mature full spliced isoform of *pqn-53* is not detectable in *calf-2(ky977)* mutants. (c) Alignment of *Caenorhabditis* PQN-53 proteins. *ky977* mutation leaves only a non-spliced isoform, which adds extra 10 amino acids at the position 134 and creates 144 amino acids protein. Small (small+ hydrophobic (including aromatic -Y)) residues, acidic residues, basic residues and hydroxyl + amine + basic residues are marked in red, blue, purple and green respectively. (d) Schematic of a *pqn-53* cDNA rescuing construct. Fully spliced *pqn-53* cDNA was expressed under the *tag-168* promoter for rescue experiments.

a

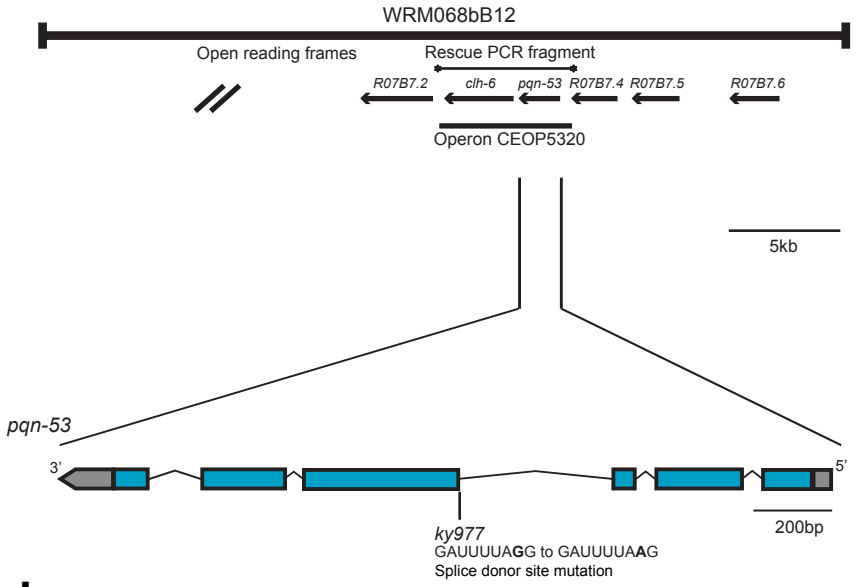

b

c

```
C.briggsae  MAEKINMTLDDIIKNGQKKIKAEKVVDANN-ANKTANDNKARSGGKTGGQ---GAKNNRK 56
C.elegans   MAEKINMSLDEIIKHGQKKVKSERVSAPAG-ASTS---NKAGNKPTRPGN---AGRNNRR 53
C.remaneri  MTDKLTMSLDDIIKNNKKNAKTDKPGTSNGNKNDNNKSNNAGNNKSRPGVKLGAGRNNRR 60
C.japonica  MADKINMSLDEIIKLKNPKKEVNQNQKPGP-RNKNAGANNKGERAGAKGA---RLGAGRR 56
            *::*:.*:**:***  : : : ::   .    . .   *:  .     *        .*:

C.briggsae  GPPAKNAKIALANKVLKRSRAIAAR---GVGAKRQALGSRG-KPMAAAGLSAVATKKLVN 112
C.elegans   VPPRKSAQVVLANKVLKKSKAIAARR--AAGGQKRVFGARG-KPAAAAGLSAVATKKLVN 110
C.remaneri  PPPAKNARVALANKVLKRSKAIAARKAAGAGAQRRVFGARGGKPVAAVGLSTVATKKLVN 120
C.japonica  APPAKNARVALANKVLKKSQAIARRA--GAGPQRRALGARS---VAATGLNAVATKKLVN 111
             ** *.*::.*******:*:*** *   ..* :::.:*:*.    **.**.:********

C.briggsae  KLVKNAIRKRINITTNLGIRKRGGVAAFTLAARRTAAIRRNVAAARGIVQPV----QQRP 168
C.elegans   KLVKNALRKRTNITTVPVVRKRGGVAASTLAARRNFALKRNVTAAQ-VIQPVRTIIQQRP 169
C.remaneri  KLVKNALRKRTNITTTQVVRKRGGVAASTLAARRNLTIKRNVAAARGVIQPVRTVVQHVP 180
C.japonica  KLVKNALRKRTNITTAQVVRKRGGVAASTIAARRNFAVRRNFAATRAALQPTRSVIQRPS 171
            ******:*** ****   :********* *:****. :::**.:*::  :**.    *: .
                                VRFYQILFYS Stop
C.briggsae  KAP---RTIIQHVQPAPVRVVRQIITAPPTETHVIRRAPPQQ-VRRAPPQQVRRVQQQQQ 224
C.elegans   ITAP-VRTIVQHVRQAPVKVVRQIITAP-VQSQVIRRAPQQQ-VRQNRPQ---------Q 217
C.remaneri  VAP--VRTIVQHVQPAPVRVVRQVISAPQMETQVIRRGPPQQQGRRNRPQP-----QQQQ 233
C.japonica  VVRAPVRTVVQHVQPAPVRVVRQVITAP--PADVIRRVPAQQ-ARRNRPQQ--------Q 220
             .    **::***: ***:****:*:**   :.**** * **  *:  **         *

C.briggsae  RRVVVVQPVQQGRRFRPGNN---NSRR-NNTVIRRQV------------PQYEQVVQRVI 268
C.elegans   RRNVIIQ-SQQSRRFRPTNN---NNNN-RPTVIRRQVVQQVPRRAQVQRPQYEQVVQRVI 272
C.remaneri  RRSVVVQQVQQGRRFRQNNN---NRRNDRPTVIRRQVVQQAPRR----VPQYEQVVQRVI 286
C.japonica  QRTVVVQQVQGGRRFRPNNNQRRNVVNERPTVIRRQVVQQPRR------VQYQEVVQRVV 274
             * *::*  * .****  **   *  . . *******              **::*****:

C.briggsae  QVPVPQQRFQQQ----QQQSRRFQQQNQ-RFQRPQQSG-----GNVRYVNGGGRQVQRKT 318
C.elegans   QTPVAQQRFQRQPQRFQQQQPRFQQQPP-RFQRQQQPQQQQVVRSVRYVN-ARPPVQRNN 330
C.remaneri  QAPVPQQRFQQQ-----QSPRRFQQQQQQRFQRPQQNG-----GNVRYVNAGPRQVQRNT 336
C.japonica  RR-APQQ-------------RQFQ-------QRPQSAGR----NNVRYVNPRPVQQQRRT 309
              .:**              :**       ** *.      .*****      **..

C.briggsae  VVR-----QVQ-PVQYRPVQYVSDQAVTSRGRGFRA- 348
C.elegans   VVR-----QVQ-PVQYRPVQYVTDQVVNSRGRGFRAF 361
C.remaneri  VVR-----QVQQPVQYRPVQYVTDQVVTSRGRGFRAY 368
C.japonica  VVQQAVDLQVQ-PVRYQPVQYVTERVVTNRGRGFRGY 345
            **:     *** **:*:*****:::.*..******.
```

* Identical residues
: Strongly similar groups
. Weakly similar groups

d

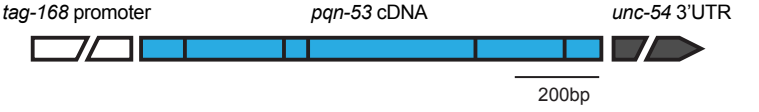

3 lines rescued / 3 lines tested

Figure 4-4

361 amino acid coding region (Fig. 4-4c). PQN-53 has additional notable sequence features that are not typical of other PQN proteins, including a preponderance of arginine and lysine residues and a highly basic predicted pKa of 13.09. The splicing defect in *calf-2(ky977)* results in a predicted protein of 144 amino acids lacking much of the conserved *pqn-53* sequence (Fig. 4-4c).

The defective GFP::UNC-2 localization in *pqn-53* mutants was rescued by a 1.1 kb spliced *pqn-53* cDNA expressed under the *tag-168* pan-neuronal promoter (Fig. 4-4d). However, a PCR product consisting of the *pqn-53* gene with 0.8kb of promoter sequence, the distance to the next coding region, did not rescue the mutant phenotype (data not shown). *pqn-53* is a upstream gene in an operon that contains another gene, *clh-6* [159](Fig. 4-4a). We hypothesized that regulatory elements required for proper *pqn-53* expression could be distributed throughout the operon. Thus, we amplified the entire 7kb operon covering both the *pqn-53* gene and the *clh-6* gene; this 7kb PCR product was ligated into the *pSM* vector (CEOP5320 in the Fig. 4-5e,f), and it was able to rescue defective GFP::UNC-2 localization (Fig. 4-4a, 4-5e,f). *clh-6* alone did not rescue, and a *clh-6* null mutants did not show the *calf-2* defect in GFP::UNC-2 expression, excluding *clh-6* as the coding region affected by the *calf-2* mutation (data not shown).

To characterize the expression pattern of *pqn-53*, we fused GFP internally to the *pqn-53* gene in-frame in the 7kb genomic fragment that rescued UNC-2 localization (CEOP5320::GFP). GFP tagged PQN-53 (PQN-53::GFP) fluorescence was detected ubiquitously in the nuclei of many cell types, including many or all neurons (Fig. 4-5a). Coexpression with an *odr-1::mCherry* transgene confirmed that *pqn-53* is expressed in AWC neurons, which were used for the initial genetic screen (Fig. 4-5b-d).

Figure 4-5. PQN-53 acts cell autonomously in neurons and localizes to the nucleus. (a) Expression of PQN-53 detected by an operon CEOP5320::GFP fusion (see methods); PQN-53::GFP translational fusion localizes in the nucleus. Scale bar, 50 μm. (b-d) AWC expresses *odr-1::mCherry* and *PQN-53::GFP*. Scale bar, 10 μm. (e,f) Rescue of *calf-2(ky977)* mutants with *pSM::CEOP5320* or *pqn-53* cDNA under the pan-neuronal *tag-168* promoter, muscle-specific *myo-3* promoter or AWC specific *odr-3* promoter. (e) GFP::UNC-2 clusters and (f) Normalized fluorescence intensity of GFP::UNC-2 in AWC axons. Asterisks denote strains different from *calf-2(ky977)* control by Bonferroni t-test, **= $P<0.01$.

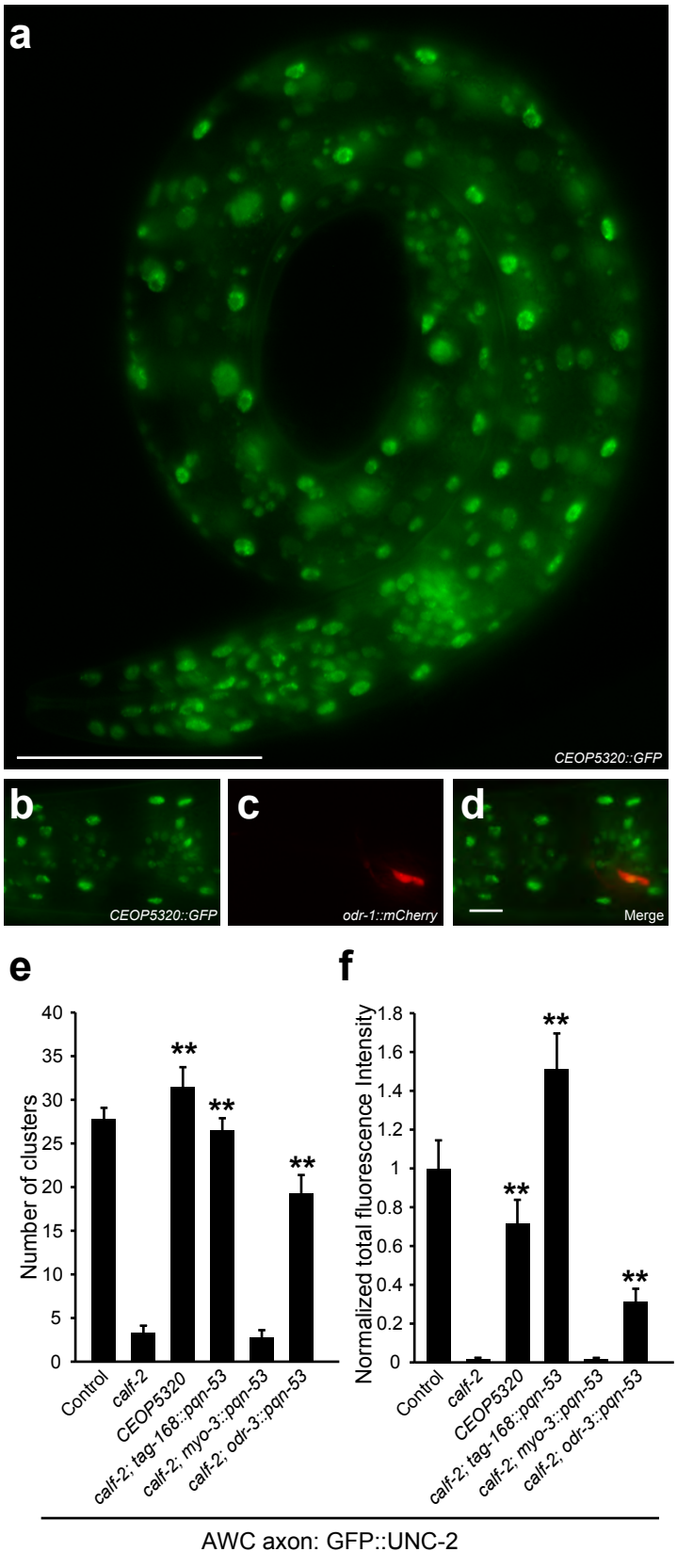
a
CEOP5320::GFP
b
CEOP5320::GFP
c
odr-1::mCherry
d
Merge
e
Number of clusters
40
35
30
25
20
15
10
5
0
**
**
**
Control
calf-2
CEOP5320
calf-2; tag-168::pqn-53
calf-2; myo-3::pqn-53
calf-2; odr-3::pqn-53
f
Normalized total fluorescence Intensity
1.8
1.6
1.4
1.2
1
0.8
0.6
0.4
0.2
0
**
**
**
Control
calf-2
CEOP5320
calf-2; tag-168::pqn-53
calf-2; myo-3::pqn-53
calf-2; odr-3::pqn-53
AWC axon: GFP::UNC-2

Figure 4-5

Expression of the *calf-2* cDNA under the control of the pan-neuronal *tag-168* promoter rescued the GFP::UNC-2 localization phenotypes (see above), but expression from the muscle-specific *myo-3* promoter did not (Figs. 4-5e,f). Expression of *pqn-53* under the AWC-selective *odr-3* promoter partially rescued GFP::UNC-2 synaptic puncta in AWC neurons (Fig. 4-5e,f). These results suggest that *pqn-53* acts cell autonomously in AWC to affect GFP::UNC-2 localization.

To determine the subcellular localization of PQN-53, we tagged *pqn-53* cDNA with GFP. We did not obtain full rescue of the defective GFP::UNC-2 localization in *calf-2* mutants with three GFP-fusions tested (N-terminal fusion, C-terminal fusion, and internal fusion), but they were all exclusively localized to the nucleus (internal fusion: Fig. 4-5a-d). Although they are still biologically active (Supplementary Fig. 4-1a,b and data not shown), with the caveat that *pqn-53* activity is reduced in the tagged proteins, these results suggest that PQN-53 is a nuclear protein.

The expression of *pqn-53* under the VD/DD motor neuron promoter *unc-25* did not rescue GFP::UNC-2 puncta; and in addition, it suppressed dorsal RAB-3::mCherry signals in DD neurons, but have not been pursued further. These results suggest a broader effect of *pqn-53* on DD neurons development or survival.

PQN-53 acts acutely to increase UNC-2 levels in the endoplasmic reticulum

GFP::UNC-2 fluorescence in the perinuclear endoplasmic reticulum region of AWC was reduced in *pqn-53* mutants compared to wild type animals, although not as strongly reduced as synaptic fluorescence (Fig. 4-6a). These results contrast with the GFP::UNC-

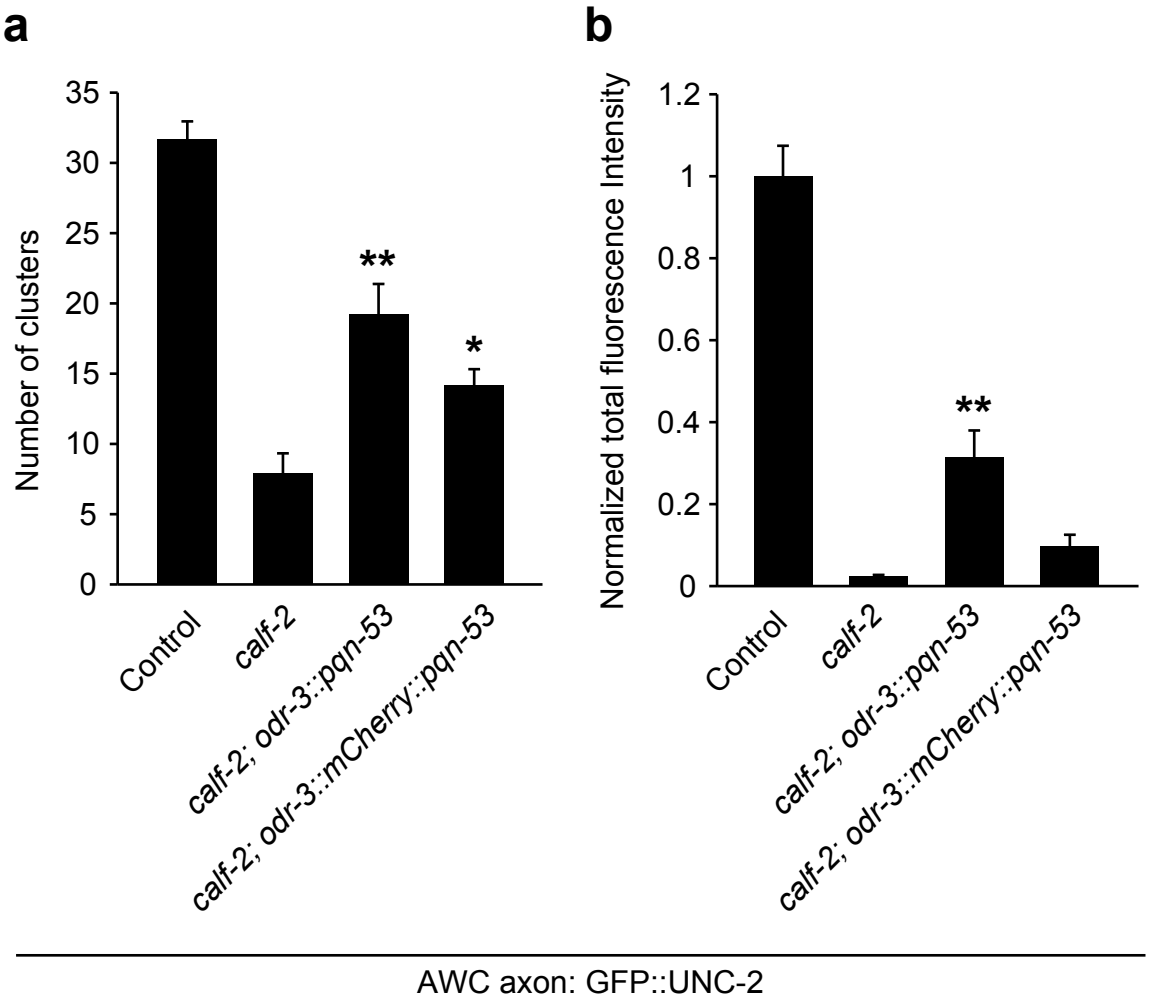

Supplementary Figure 4-1. N-terminally tagged *odr-3::mCherry::pqn-53* partially rescues *calf-2(ky977)* mutants.
(a,b) Rescue of *calf-2(ky977)* mutants with *pqn-53* cDNA and *mCherry::pqn-53* cDNA under the AWC specific *odr-3* promoter. (a) GFP::UNC-2 clusters and (b) Normalized fluorescence intensity of GFP::UNC-2 in AWC axons. Asterisks denote strains different from *calf-2(ky977)* control by Bonferroni t-test, **= P<0.01, *=P<0.05

Figure 4-6. PQN-53 is required for expression of GFP::UNC-2 in the endoplasmic reticulum.
(a) Quantification of GFP::UNC-2 fluorescence in the AWC perinuclear regions of *calf-2(ky977)* and *calf-1(ky867)*. Asterisks indicate results different from wild type controls or *calf-1* mutants by unpaired t-test at P<0.01 (**). (b,c) Heat shock induction of *pqn-53* rescues GFP::UNC-2 localization defects and increases expression of GFP::UNC-2 in the endoplasmic reticulum. (b) GFP::UNC-2 puncta in AWC axons and (c) GFP::UNC-2 fluorescence in the AWC perinuclear region of heat-shocked and non-heat-shocked *calf-2; hsp16.2::pqn-53* animals. Asterisks indicate results different from non-heat shocked controls by unpaired t-test at P<0.01 (**). (d,e) Representative images of GFP::UNC-2 in the head region; (d) A wild type control animal and (e) a *calf-2(ky977)* mutant. Asterisks indicate punctate localization of GFP::UNC-2 in axons at the nerve ring; white arrowheads mark neuronal cell bodies. (f) Quantification of GFP::UNC-2 in the nerve ring. (g) Schematic illustration of 2xmEos2::UNC-2 pulse-chase experiment; converted region circled in purple. Images from the regions indicated by square boxes were obtained and compared. (h,i) A Representative images before and after photoconversion of 2xmEos2::UNC-2 in the head region. Area of nerve ring axons is marked by asterisks. (j,k) Quantification of photoconverted 2xmEos2::UNC-2 in the nerve ring of wild type control and *calf-2(ky977)* mutants. (j) Normalized fluorescence intensity and (k) turn over rate of 2xmEos2::UNC-2 obtained by dividing the total fluorescence intensity of 6 hour time point by original fluorescence signals. All error bars indicate s.e.m. Scale bar, 10 μm.

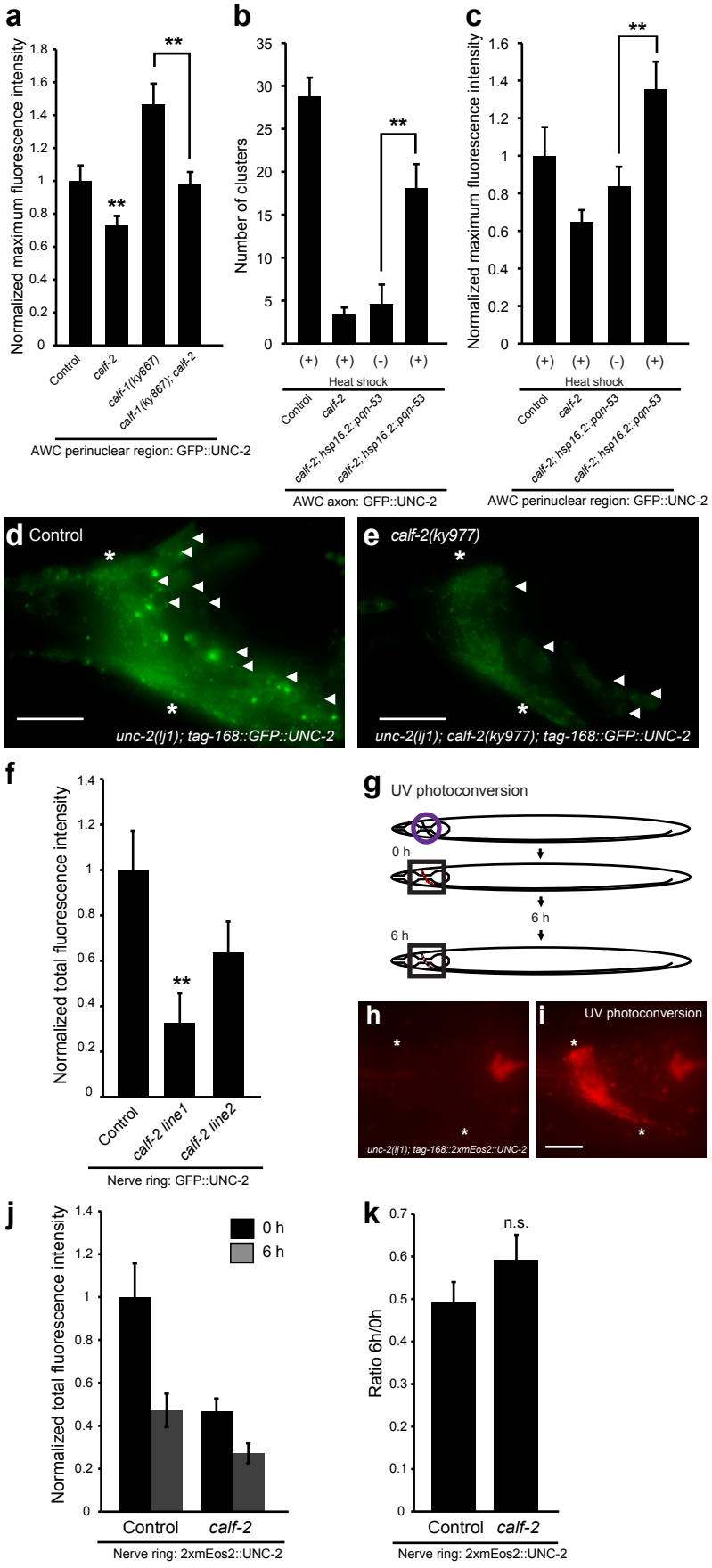
a
Normalized maximum fluorescence intensity
Control
calf-2
calf-1(ky867)
calf-1(ky867); calf-2
AWC perinuclear region: GFP::UNC-2
b
Number of clusters
Heat shock
Control
calf-2
calf-2; hsp16.2::pqn-53
calf-2; hsp16.2::pqn-53
AWC axon: GFP::UNC-2
c
Normalized maximum fluorescence intensity
Heat shock
AWC perinuclear region: GFP::UNC-2
d Control
unc-2(lj1); tag-168::GFP::UNC-2
e calf-2(ky977)
unc-2(lj1); calf-2(ky977); tag-168::GFP::UNC-2
f
Normalized total fluorescence intensity
Control
calf-2 line1
calf-2 line2
Nerve ring: GFP::UNC-2
g UV photoconversion
0 h
6 h
6 h
h
i UV photoconversion
unc-2(lj1); tag-168::2xmEos2::UNC-2
j
Normalized total fluorescence intensity
0 h
6 h
Control
calf-2
Nerve ring: 2xmEos2::UNC-2
k
n.s.
Ratio 6h/0h
Control
calf-2
Nerve ring: 2xmEos2::UNC-2

Figure 4-6

2 pattern in *calf-1* mutants, where reduced expression in synapses is accompanied by higher expression of GFP::UNC-2 in the endoplasmic reticulum [160]. To assess the contribution of *pqn-53* to protein levels in the endoplasmic reticulum, we examined GFP::UNC-2 phenotypes and genetic interactions in *calf-1; pqn-53* double mutants. In *calf-1; pqn-53* double mutants, GFP::UNC-2 fluorescence was present in the endoplasmic reticulum at a reduced level compared to a *calf-1* mutants (Fig. 4-6a). These results suggest that PQN-53 acts upstream of CALF-1 to regulate the amount of UNC-2 protein in the endoplasmic reticulum.

To examine the acute effects of *pqn-53*, we used the heat shock promoter *hsp16.2* [106] to drive expression of *pqn-53* under temperature control. A three hour heat pulse in L4 animals was sufficient to rescue synaptic GFP::UNC-2 localization and endoplasmic reticulum expression of GFP::UNC-2 in AWC neurons (Fig. 4-6b,c). Heat shock induction of *pqn-53* increased the expression of perinuclear GFP::UNC-2 to a level above that of the wild type control, indicating an active role of PQN-53 in UNC-2 accumulation in the endoplasmic reticulum (Fig. 4-6c). We also examined the overall effects of *pqn-53* by assessing the pan-neuronally expressed GFP::UNC-2 at nerve ring synapses and cell bodies in the head region (Fig. 4-6d,e). The expression levels of GFP::UNC-2 were reduced both at synapses and cell bodies, indicating that *pqn-53* acts in multiple neurons for UNC-2 expression (Fig. 4-6f). The double mutant analysis and heat-shock rescue of *pqn-53* suggest that *pqn-53* affects GFP::UNC-2 translation or stability in the endoplasmic reticulum, and argue against an essential role for *pqn-53* that is specific to synapses or early development.

If *pqn-53* affects overall GFP::UNC-2 stability, it might also affect GFP::UNC-2 stability at the synapses. To examine the rate of synaptic UNC-2 turnover, we tagged UNC-2 at its N terminus with two copies of the photoconvertible protein mEos2, which irreversibly changes from green to red emission upon UV irradiation [161]. 2xmEos2::UNC-2 protein behaved similarly to GFP::UNC-2, both before and after photoconversion; it had a synaptic location in wild-type animals, and expression was reduced in *pqn-53* mutants (see below).

A pool of 2xmEos2::UNC-2 protein at the nerve ring was photoconverted to red in *pqn-53* animals (Fig. 4-6g-i), and after photoconversion, fluorescence intensity was measured at the nerve ring after 0 hour and after 6 hours (Fig. 4-6j). Although the original fluorescence intensity of 2xmEos2::UNC-2 in wild type animals was higher than that in *pqn-53* mutant animals, the rate of reduction in fluorescence over time was comparable (Fig. 4-6k). These results demonstrate that UNC-2 turnover in the nerve ring is similar in wild type and *pqn-53* mutant animals, arguing against a direct role of PQN-53 in stabilizing UNC-2 at synapses.

PQN-53 regulates expression of *pqn/abu* non-canonical unfolded protein response genes

The nuclear localization of PQN-53 suggested that PQN-53 might regulate transcription, mRNA splicing or mRNA export of *unc-2* itself or of other factors involved in UNC-2 maintenance in the endoplasmic reticulum. The GFP::UNC-2 plasmid used for these studies had a heterologous promoter and a fully spliced *unc-2* cDNA, excluding *unc-2* as a likely target of gene regulation or splicing by *pqn-53*, therefore we initially focused on

expression of two known regulators of *unc-2* trafficking, *unc-36* and *calf-1*. GFP was expressed under *calf-1* or *unc-36* promoters in *pqn-53* mutants background to assess expression of these two genes. The expression levels of *calf-1* and *unc-36* GFP fusions in *calf-2* mutants were comparable to those of wild type animals (Fig. 4-7a-d). In a second experiment, rescuing cDNA fragments were used to ask if *pqn-53* might regulate *calf-1* or *unc-36* splicing. Overexpression of spliced cDNAs of *calf-1* or *unc-36* did not rescue the GFP::UNC-2 defects of *pqn-53* mutants (Fig. 4-7e). These experiments failed to find evidence that *calf-1* or *unc-36* transcription or splicing were the direct targets of regulation by *pqn-53*.

To seek a broader role of PQN-53 in gene regulation, we compared the mRNA transcriptome of stage-matched *pqn-53* mutants and wild type animals using Illumina/Solexa Paired-end mRNA sequencing technology (mRNAseq, see methods). mRNAseq data can be used to infer quantitative information about expression levels and also qualitative information on splicing and other sequence variations of individual gene at a genome-wide scale [162, 163]. No major changes in splicing patterns were detected in *pqn-53* mutants, suggesting that the primary function of *pqn-53* is not related to mRNA splicing (data not shown). In particular, no major qualitative or quantitative differences in *unc-2*, *calf-1* or *unc-36* mRNA expression levels or transcript structures were observed between wild type animals and *pqn-53* mutants. *pqn-53* itself was identified as incompletely spliced in *pqn-53(ky977)* mutants, a positive control indicating that the technique succeeded (Fig. 4-8a)

Direct comparison of expression levels in Cufflink program were used to identify genes that were differentially expressed in *pqn-53* mutants compared to wild type animals

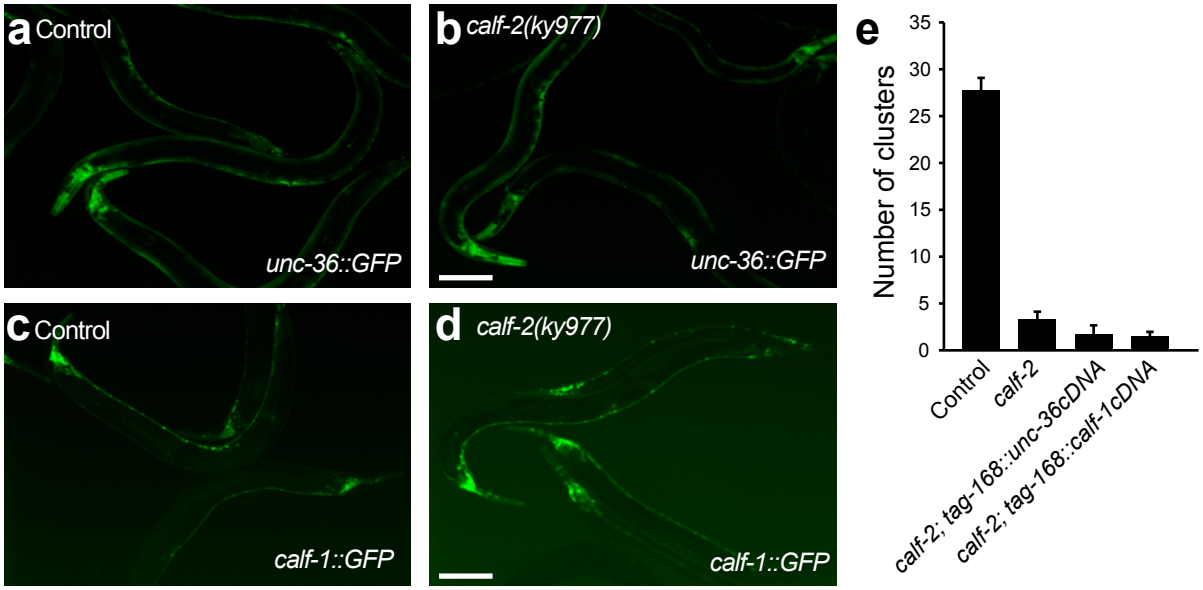

Figure 4-7. *calf-1* and *unc-36* are not direct targets of *pqn-53*.
(a-d) Representative images of GFP expression under (a,b) the *unc-36* promoter and (c,d) the *calf-1* promoter in wild type control animals and *calf-2(ky977)* mutants. (e) Overexpression of functional cDNAs of *unc-36* and *calf-1* under the pan-neuronal *tag-168* promoter in *calf-2* mutants; analysis of GFP::UNC-2 clusters in AWC axons. Error bars indicate s.e.m.
Scale bar, 100 μm.

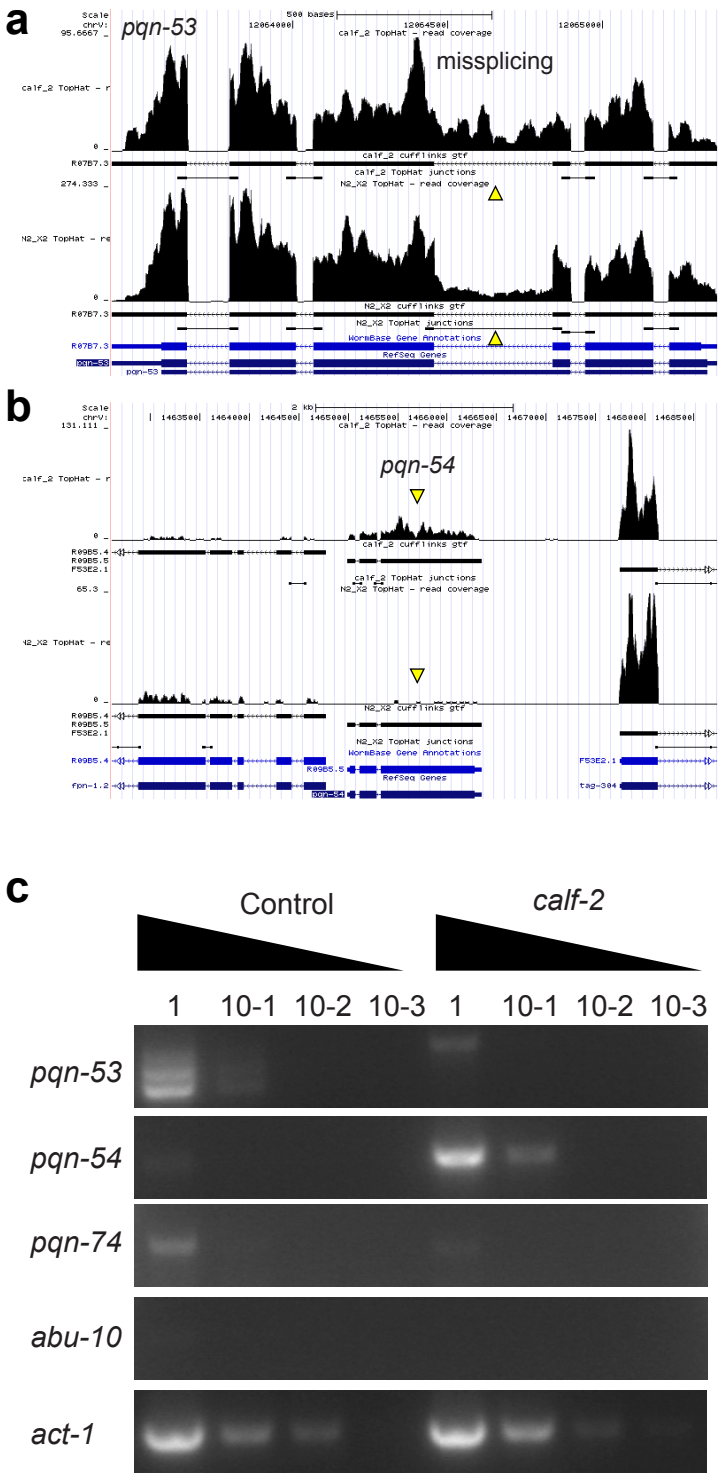

Figure 4-8. pqn/abu gene expression are regulated by PQN-53.
(a,b) Representative images of mRNAseq data visualized by UCSC genome browser. Reads coverage, predicted gene models and splicing junctions are shown for (a) *pqn-53* and (b) *pqn-54*. Missplicing of *pqn-53* and upregulation of *pqn-54* are marked by yellow arrowheads.
(c) RT-PCR analysis of mRNA abundance of *pqn-53*, *pqn-54*, *pqn-74*, *abu-10*. cDNA samples were 10-fold serially diluted three times. *act-1* was used as an internal control.

(Table 4-1,4-2) (http://cufflinks.cbcb.umd.edu/). The DAVID bioinformatics tool was used to obtain functional annotation clusters of genes that were co-regulated in the mRNAseq datasets [164]. The highly upregulated genes in *pqn-53* mutants included a significant enrichment of *pqn* and *abu* genes ($p<0.01$) (Table 4-1). Out of 79 *pqn* family genes, eleven genes have been further classified as *abu* (activated in blocked unfolded protein response)[156]. 5 *pqn* genes (non *abu*) and 4 *abu* genes were included in the top 30 genes that were upregulated in *pqn-53* mRNAseq data (Table 4-1).

The mRNAseq data were confirmed by RT-PCR using primers targeting *pqn-53, pqn-54, pqn-74* and *abu-10* (Fig. 4-8c). *pqn-53* was downregulated, and *pqn-54* was upregulated in *pqn-53(ky977)* mutants, but changes in *pqn-74* and *abu-10* were not detected. The reason for this discrepancy is currently unclear.

Among genes that were downregulated in *calf-2* mutants, enriched gene sets included genes encoding major sperm proteins and genes encoding germline differentiation proteins (Table 4-2). These results have not yet been retested by RT-PCR.

These data suggest that PQN-53 regulates global gene transcription. They also suggest that the GFP::UNC-2 defects in the *pqn-53* mutants might originate from misregulation of UPR. We focused on *pqn* and *abu* genes for further analysis because their proposed function in ER stress-sensing pathway and UPR matched the genetic results suggesting an alteration in GFP::UNC-2 levels in the endoplasmic reticulum.

pqn-53 mutants are resistant to pathogenic *Salmonella enterica* bacteria

Previous microarray analysis showed that some *pqn/abu* genes implicated in the non-canonical UPR pathway are upregulated upon *Salmonella enterica* infection in a CED-1-

Table 4-1. Top 30 genes upregulated in *calf-2* mutants

Sequence name	Gene name	N2 (RPKM)	*calf-2* (RPKM)	Fold change
AC3.4	*pqn-2*	0.0272	3.9481	145.2465
T20F7.7	*acs-9*	0.0005	0.0300	66.3666
R09B5.5	*pqn-54*	0.1462	4.7931	32.7777
AC3.3	*abu-1*	0.0248	0.8000	32.3116
R03C1.1		0.0961	2.4110	25.0819
T01D1.6	*abu-11*	0.2006	4.7604	23.7316
T06E4.12		0.2621	5.9580	22.7279
T06E4.11	*pqn-63*	0.1110	2.1006	18.9245
F35A5.3	*abu-10*	0.1461	2.6508	18.1418
C03A7.14	*abu-8*	0.3989	7.1227	17.8552
F17E9.12	*his-31*	0.0459	0.7695	16.7606
C54D2.1		0.0597	0.9107	15.2602
C34E11.2		0.0329	0.4721	14.3673
R12A1.3		0.1569	1.7188	10.9581
F20B10.3		0.0929	0.9949	10.7146
E01G6.1		0.0703	0.7384	10.5059
F07C6.4		1.2830	13.0387	10.1625
B0228.5	*trx-1*	0.0652	0.6409	9.8339
W02A2.3	*pqn-74*	1.0045	9.6598	9.6169
ZK1067.7	*pqn-95*	1.6639	14.6340	8.7948
C18A3.8	*hlh-14*	0.0523	0.4589	8.7665
Y49C4A.9	*cyp-33C11*	0.0312	0.2583	8.2795
ZK662.2		0.2961	2.4227	8.1821
ZK622.t2	*rte-4*	1.9345	15.7027	8.1171
K04A8.10		0.0286	0.2228	7.7986
M03E7.4		0.0278	0.2169	7.7924
T25E4.1		0.3798	2.9363	7.7314
C04G6.10		0.1415	1.0833	7.6556

Table 4-2. Bottom 100 genes downregulated in *calf-2* mutants

Sequence Name	Gene name	N2 (RPKM)	*calf-2* (RPKM)	Fold change
H12I13.5		0.031	0.000	0.000
T06D8.2		0.053	0.000	0.000
R102.4		98.046	0.072	0.001
C16C10.13		0.059	0.000	0.005
C25A1.2	*fkh-10*	0.050	0.001	0.020
K06H6.2		2.196	0.052	0.024
C14C6.6		0.903	0.042	0.046
T10C6.14	*his-1*	0.774	0.036	0.047
H31G24.4	*cyb-2.2*	0.585	0.034	0.058
Y48G1C.5		0.218	0.013	0.059
ZK858.2		1.451	0.088	0.061
K06H6.1		1.383	0.084	0.061
T25F10.1		0.578	0.040	0.069
C48E7.8	*oac-9*	0.249	0.018	0.072
F57C9.7		0.487	0.037	0.075
F15E11.15		95.056	7.395	0.078
F55A12.10		0.859	0.067	0.078
R148.4		0.741	0.066	0.089
W09D6.4		0.805	0.076	0.094
K02B9.1	*meg-1*	0.403	0.038	0.095
F09D12.2		0.659	0.066	0.100
Y39B6A.9		4.154	0.424	0.102
F15E11.12		52.756	5.497	0.104
F47H4.4	*fbxa-185*	0.125	0.014	0.108
Y47D3A.11	*wht-8*	0.508	0.055	0.108
T28C12.3	*fbxa-202*	0.323	0.035	0.108
C04E6.5		0.264	0.029	0.108
K02F6.2		0.385	0.042	0.108
F36A4.4		1.514	0.164	0.108
T23B3.5		0.724	0.078	0.108
C53D6.10		1.539	0.171	0.111
Y39C12A.8	*dnj-26*	0.359	0.041	0.115
B0513.6		0.206	0.024	0.115
F56H9.4	*gpa-9*	0.317	0.039	0.122
ZK39.6	*clec-97*	0.584	0.071	0.122
F49C12.14		0.497	0.061	0.123
Y57A10A.6		0.150	0.019	0.125
ZK970.8		1.666	0.209	0.126
F58B4.4		1.738	0.218	0.126
R03D7.2		0.144	0.018	0.127
ZK617.3	*spe-17*	0.799	0.104	0.130
F55C10.4		0.629	0.082	0.130
Y9C9A.16		0.321	0.042	0.130
F42F12.9	*nspc-10*	0.543	0.071	0.130

F18A1.1		0.158	0.021	0.133
W03F11.3	*dct-9*	1.100	0.148	0.134
C06A5.5		0.405	0.056	0.139
Y71G12B.22		0.523	0.073	0.139
T10B9.4	*cyp-13A8*	0.212	0.030	0.139
H27M09.5		0.317	0.044	0.139
C47D12.3	*sfxn-1.4*	0.639	0.092	0.144
C46G7.5		0.790	0.115	0.146
Y47D7A.6		0.692	0.101	0.146
F07C6.4		12.661	1.857	0.147
C08F8.3		1.721	0.256	0.148
F15E11.13		384.610	57.599	0.150
F43D2.2		0.205	0.031	0.150
C31H1.2		0.281	0.042	0.150
T05B4.11	*phat-5*	0.328	0.049	0.150
H20J04.1		0.235	0.035	0.150
T01G6.3	*str-196*	0.281	0.042	0.150
6R55.2		0.680	0.102	0.150
Y73F8A.14		0.774	0.116	0.150
T04A8.3	*clec-155*	0.271	0.041	0.150
F10D11.5		0.263	0.040	0.154
C34D4.10		0.405	0.062	0.154
ZK792.3	*inx-9*	0.889	0.138	0.155
F45D11.2		0.762	0.122	0.161
Y71H2AM.7		0.778	0.125	0.161
Y71H2B.1		1.135	0.184	0.162
Y48B6A.10		0.169	0.027	0.162
Y37H2A.9	*fbxc-46*	0.308	0.050	0.162
ZK488.1	*nhr-250*	0.487	0.079	0.162
F22B5.3	*cut-3*	0.438	0.071	0.162
Y42H9AR.2		0.338	0.055	0.162
F30A10.14		0.640	0.104	0.162
F21F8.10	*str-135*	0.268	0.044	0.162
C45G9.4		2.759	0.450	0.163
Y19D10B.7		54.673	8.954	0.164
R01H2.3	*egg-2*	1.378	0.228	0.165
C14A6.6		0.247	0.041	0.168
B0393.6		1.658	0.278	0.168
K02B12.6		2.981	0.502	0.169
W03D8.3		1.359	0.230	0.169
ZK1098.9		0.893	0.153	0.172
AH6.3		0.569	0.098	0.172
F54H12.5		0.336	0.058	0.172
Y55F3BR.7		0.621	0.107	0.172
W03D8.5		0.745	0.128	0.172
W09C3.7		2.739	0.474	0.173
D1081.9		0.767	0.133	0.174

W01B6.6		0.594	0.103	0.174
F45D11.1		0.911	0.159	0.175
T23F11.2		0.460	0.081	0.176
W02A2.8		0.650	0.115	0.177
R11H6.6		0.243	0.043	0.177
W05F2.5	*fbxa-203*	0.260	0.046	0.177
B0524.5		0.415	0.074	0.177
C47E8.1		0.455	0.081	0.177
K12B6.2		0.118	0.021	0.177

dependent manner [165]. *ced-1 (cell death-abnormality 1)* mutants are hyper-susceptible to *Salmonella enterica* infection, indicating that CED-1 and the *pqn/abu* response are involved in host defense against the pathogen [165]. CED-1 is a single pass transmembrane receptor originally identified based on its involvement in engulfment of apoptotic cells in *C. elegans* [166]. Based on the results of Haskins et al, we hypothesized that *pqn/abu* genes that are upregulated in *pqn-53* mutants might also have beneficial effects against pathogens through constitutive activation of the non-canonical UPR.

To test this hypothesis, *pqn-53* mutants were tested for susceptibility to *Salmonella enterica*-mediated killing by comparing *Salmonella enterica* killing of wild-type animals to that of *pqn-53* mutants. Indeed, *pqn-53* mutants were resistant to the pathogen and lived longer than wild-type animals when fed on *Salmonella enterica* strain 1344 (Fig. 4-9a). The time for 50% of the nematode to die (TD50) when fed at 25°C on live *Salmonella enterica* was 5 days for wild-type animals and 6.5 days for *pqn-53* mutants, which represents an increase of 30%. *pqn-53* mutants did not exhibit extended lifespan on the *E. coli* strain OP50, suggesting that the *pqn-53* longevity effect is specific to the pathogenic bacteria (Fig. 4-9b,c).

Discussion

Communication between the endoplasmic reticulum and the nucleus is prominent in the UPR. The rough endoplasmic reticulum is a center of translation, folding, and transport of transmembrane proteins and secretory proteins. Thus, the rough endoplasmic reticulum must constantly translate thousands of proteins and monitor their proper folding by housekeeping molecules such as chaperones. An imbalance between the load

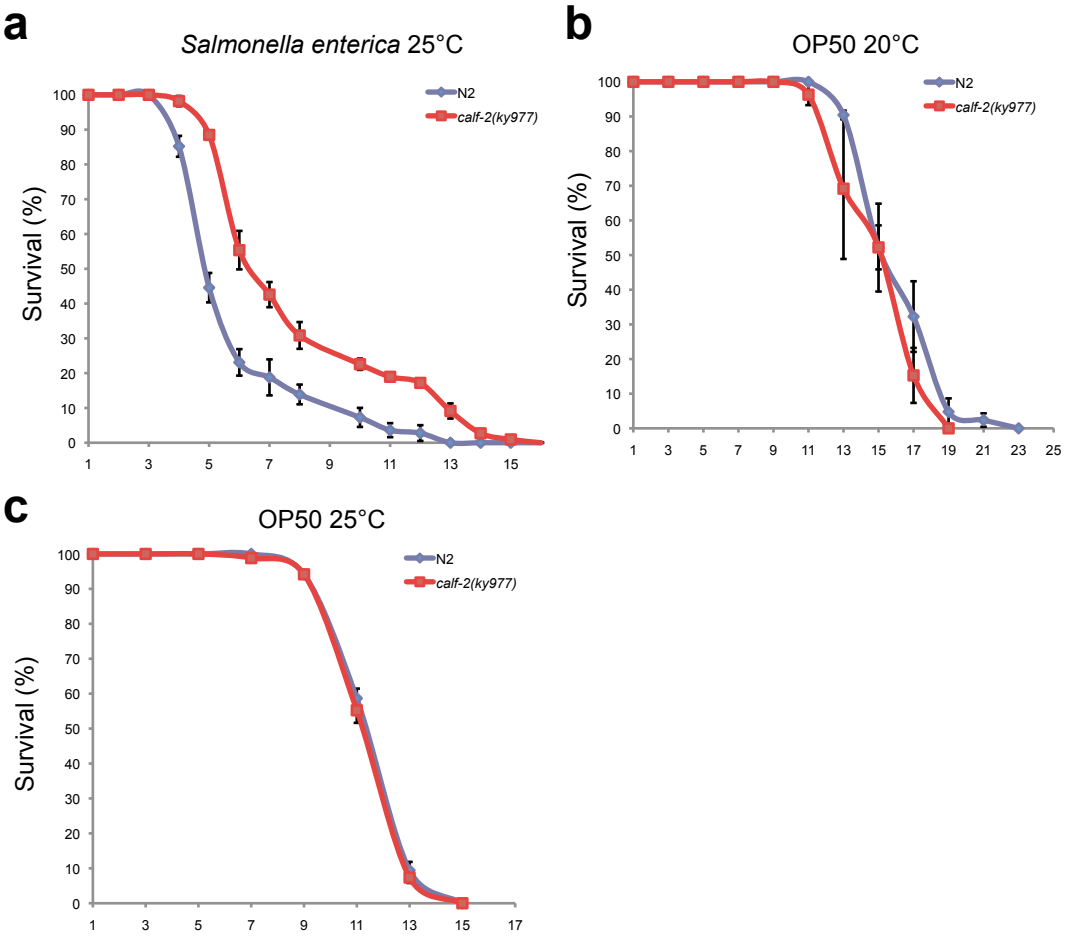

Figure 4-9. *calf-2* mutants are resistant to Salmonella infection.
(a) Salmonella enterica killing assay of *calf-2* mutants. Wild type and *calf-2(ky977)* animals were exposed to Salmonella enterica. *calf-2* mutants are highly resistant to Salmonella enterica infection. (b,c) Life-span analysis of *calf-2* mutants on *E. coli* OP50. Wild type and *calf-2* animals were exposed to OP50 and grown at (b) 20C° and (c) 25C°. Error bars indicate s.e.m.

of unfolded proteins that enter the endoplasmic reticulum and the endoplasmic reticulum capacity creates ER stress, which induces the UPR to cope with a burden of translation and folding. For example, tunicamycin, an inhibitor of protein glycosylation, causes an accumulation of unfolded proteins in the endoplasmic reticulum and induces the UPR [154]. Infection with the pathogen *Pseudomonas aeruginosa* or assault with bacterial pore-forming toxins also induce the UPR, suggesting its broad involvement in innate immunity and host defense [155, 167, 168]. So far, three different classes of ER stress transducers have been identified (IRE1, ATF6 and PERK). Each class defines a distinct arm of the UPR. In each case, an integral membrane protein senses the protein folding state in the endoplasmic reticulum lumen and transmits information to the cytosol through its cytosolic domain. IRE1 is an endoplasmic reticulum resident transmembrane protein that senses unfolded proteins in the endoplasmic reticulum with its luminal domain. When IRE1 detects unfolded proteins in the endoplasmic reticulum, IRE1 mediates splicing of cytoplasmic XBP1 mRNA with its cytosolic nuclease domain and allows translation of XBP1 and its import into the nucleus [169]. The nuclear XBP1 protein induces expression of a wide variety of proteins including chaperones and ERAD proteins [151, 170]. ATF6 and PERK are also activated by ER stress and induce transcriptional activation of UPR genes. PERK is phylogenetically related to IRE1, but in addition to its function in transcriptional regulation of UPR genes, PERK phosphorylates the alpha-subunit of eukaryotic translation initiaion factor-2 (eIF2alpha) and lower the levels of active eIF2 to result in global reduction in the load of newly synthesized proteins [154]. IRE1-XBP1 is a conserved UPR pathway between yeast and metazoan, and ATF6 and PERK are specifically evolved in metazoans, suggesting that the IRE-1-XBP-1 is the ancient UPR pathway.

Therefore, the endoplasmic reticulum is able to communicate with the nucleus to maintain its functional integrity against ER stress using these unfolded protein sensors.

We found that efficient expression of a GFP-tagged UNC-2 in the endoplasmic reticulum requires the nuclear protein PQN-53. PQN-53 is expressed ubiquitously in many tissues, but it acts cell autonomously in neurons for GFP::UNC-2 expression. Acute expression in late stage animals rescued the defective GFP::UNC-2 expression, suggesting that PQN-53 can act acutely on a relatively short time scale. Either directly or indirectly, PQN-53 regulates GFP::UNC-2 expression in the endoplasmic reticulum. It is not yet clear whether PQN-53 affects translation of GFP::UNC-2 at the level of endoplasmic reticulum, or processing or mRNA export of the GFP::UNC-2 mRNA from the nucleus. We prefer the first possibility since the mRNA level of endogenous UNC-2 as well as that of other mRNA export factors was not affected in *pqn-53* mutants. However, the susceptibility of transgenes to the transgene silencing phenomenon suggests that future studies should be done to verify the precise effect of *pqn-53* on GFP::UNC-2 abundance in the endoplasmic reticulum. Turnover of GFP::UNC-2 in nerve ring axons is normal in *pqn-53* mutants, suggesting that PQN-53 does not have a role in UNC-2 stability at synapses.

PQN-53 is a member of the *pqn* gene family. *pqn* genes were identified bioinformatically based on their composition bias towards glutamine and asparagine [158]. 79 genes are assigned as *pqn* family genes, most of which have unknown biological functions. One clue to the function of PQN-53 was obtained by the mRNAseq analysis. In *pqn-53* mutants, we observed a global transcriptional activation of other *pqn* genes that are involved in the non-canonical UPR pathway (also known as *abu* genes [156]). Thus,

PQN-53 seems to act as a repressor of these *pqn/abu* genes. Urano et al. showed that *pqn/abu* genes are upregulated upon ER stress in animals lacking functional XBP1; *xbp-1* mutants become less resistant to ER stress when expression of these *abu* genes was reduced with RNAi. Based on these findings, they proposed that *abu* genes are involved in a non-canonical UPR pathway that acts in parallel to the IRE1-XBP1 pathway [156]. Interestingly, some of these genes are involved in longevity and immunity against pathogenic bacteria. Resveratol inhibits SIR-2.1, a homolog of yeast SIR2 NAD^+-dependent deacetylases, and induces transcriptional activation of *pqn/abu* genes to increase life span [171]. Knockdown of *abu-11* confers a reduction in life-span, whereas overexpression increases longevity [171]. This effect is apparently independent of the well-characterized insulin/IGF signaling longevity pathway, which includes the DAF-2 transmembrane receptor, a series of intracellular kinases, and the DAF-16 forkhead-transcription factor.

The CED-1 phagocytic receptor is required for activation of *pqn/abu* genes in response to infection by *Salmonella enterica* [165]. *ced-1* mutants or animals with RNAi knockdown of *pqn/abu* genes (*abu-11, abu-8, abu-7, abu-1, pqn-54, pqn-5*) are more susceptible to infection by *Salmonella enterica,* and overexpression of *abu-11* or *abu-1* make animals more resistant to the bacteria, indicating that *pqn/abu* genes are involved in innate immunity and host defense [165]. Therefore, some *pqn* genes are involved in an ER stress-sensing pathway that is physiologically important for normal survival and host defense against pathogenic bacteria in *C. elegans*.

pqn-53 mutants are also resistant to *Salmonella enterica*. This is probably due to the constitutive activation of *pqn/abu* genes in the mutants. Innate immunity in *C.*

elegans has been characterized using a wide variety of pathogenic bacteria such as *Pseudomonas aeruginosa* and *Salmonella enterica* [172]. *C. elegans* possess a single gene encoding Toll-like receptor, *tol-1,* but lacks MYD88 and NF-kB homologs that are required for activation of Toll/Toll-like receptor signaling in insects and mammals [173]. Instead, a Toll/IL-1R (TIR) protein-protein interaction domain containing scaffold protein TIR-1, the SARM1 homolog, acts independently from TOL-1 and activates p38 mitogen-activated protein kinase pathways (TIR-1-NSY-1-SEK-1-PMK-1) to mediate the core immune response in *C. elegans* [174, 175]. Other innate immunity components include the DAF-2-DAF-16 insulin-like signaling pathway, BAR-1, a Beta-catenin and a component of the *C. elegans* canonical WNT signaling pathway, and FSHR-1, a homolog of the mammalian follicle-stimulating hormone receptor 1 [176]. The necessity of each pathway depends on which pathogens are involved in infection, and each component differentially regulates activation of immune response genes upon infection [173]. PQN-53 may interact with some of these pathways to control transcription of *pqn/abu* genes. We intend to study the relationship between CED-1 and PQN-53. CED-1 is required for engulfment of apoptotic somatic cells and of germ-cell corpses by phagocytic cells such as ventral hypodermal cells and gonadal sheath cells [165]. CED-1, however, is expressed not only in these phagocytic cells but also in many non-phagocytic cells including neurons. This broad expression pattern indicates that CED-1 has other roles besides phagocytosis of apoptotic cells. SCARF1, a mammalian CED-1 homolog, is implicated as a receptor of pathogens in macrophages required for recognition of *Cryptococcus neoformans* to activate immune responses [177]. It will be interesting to determine in which cell types CED-1 functions and how it activates *pqn/abu* genes in response to *Salmonella*

infection. PQN-53 is a good candidate to be the downstream effecter of CED-1, based on its ubiquitous expression and its implicated function in the expression of *pqn/abu* genes. The relationship between CED-1 and PQN-53 in neurons as well as other tissues is a subject to examine, considering the observation that *pqn-53* mutants have defective GFP::UNC-2 expression in neurons. I am planning to conduct rescue experiments to identify the tissue responsible for the *Salmonella* susceptible (*ced-1* mutants) and resistant (*pqn-53* mutants) phenotype and analyze double mutants between *pqn-53* and *ced-1* to determine genetic epistasis in the pathogen infection. We may identify mechanistic linkage between these two systems.

PQN-53 is conserved in nematodes, but homologs were not identified in other organisms. Yeast Swi1 protein, however, might have a related function. The Snf/Swi nucleosome remodeling complex is involved in repression and activation of -6% of yeast genes [178]. Swi1 is very rich in glutamine and asparagine, and it acts as a prion forming protein [179]. The prion form of the Swi1 protein is inactive, and it quenches the function of the non-prion form of the Swi1 allowing global transcriptional change. Environmental stress is known to increase the frequency of prion formation, thus prion-forming proteins such as Swi1 might act as stress sensors to modulate global gene expression depending on the stress levels in the environment [180]. It needs to be determined whether the Q/N rich domain of PQN-53 can act as a prion-forming module. Q/N rich domains are also suggested to act as protein-protein interaction domains. Using the Q/N rich domain, PQN-53 may interact with other transcription factors or act as a Swi-like molecule to regulate global transcription to cope with environment stress.

We propose that PQN-53 suppress the induction of non-canonical UPR under non-stressed condition. Upon ER stress or infection of pathogens, the activity of PQN-53 is reduced, leading to activation of *pqn/abu* genes (non-canonical UPR induction). The non-canonical UPR may reduce protein translation burden in the endoplasmic reticulum through activation of pathways such as ERAD. When the non-canonical UPR is active at high levels, inhibited translation or enhanced degradation may lead to reduced levels of some transmembrane proteins including UNC-2 and ODR-10, and perhaps increased translation of proteins required for counteracting the harmful stimulus. Therefore, PQN-53 may act in a defensive system that protect against environmental stress. Longevity and innate immunity genes are also implicated in stress sensing. It will be interesting to characterize the interaction between PQN-53, longevity factors and innate immunity genes in the future.

Chapter 5

Conclusions and Future Directions

Summary

Neurotransmitter release for presynaptic nerve terminals is triggered by depolarization that is sensed by presynaptic voltage-gated calcium channels. Many physiological studies have addressed the opening kinetics of calcium channels and their modulation by auxiliary subunits. However, how the biogenesis of calcium channels is achieved in neurons *in vivo* has been elusive, partly due to a difficulty in visualizing the channels in live samples. My thesis work focused on elucidating the mechanism that regulates CaV2 presynaptic voltage-gated calcium channel expression and localization through genetics and cell biological approaches. Although synaptic localization was the goal, the conclusions are more general cell biology.

My thesis work involved the establishment of *in vivo* system allowing visualization of the UNC-2 alpha1 subunit of the *C. elegans* CaV2 channel, the identification of mutants that are defective in UNC-2 localization through a forward genetic screen, phenotypic analysis of the mutants, and the mapping and functional analysis of three genes, *calf-1*, *unc-36* and *pqn-53/calf-2*, that affect UNC-2 expression and localization *in vivo*. In the first study, I showed that *calf-1* and *unc-36* act in the endoplasmic reticulum to regulated endoplasmic reticulum exit of UNC-2. In the second study, I showed that nuclear protein PQN-53 is involved in the inhibition of non-canonical UPR pathway, and activation of this pathway in *pqn-53* mutants leads to the

reduced expression of GFP::UNC-2 and other transmembrane proteins. Furthermore, I showed that *pqn-53* mutants confer resistance to pathogenic bacteria, potentially by constitutive activation of the non-canonical UPR.

Screen

I conducted a direct clonal screen of 1594 mutagenized genomes, but the GFP::UNC-2 localization screen is obviously not saturated. The steps that could affect UNC-2 localization and expression include translation, folding, or post-translational modification of UNC-2, endoplasmic reticulum to Golgi transport, targeting at the Golgi, axonal transport by motor proteins, fusion of targeting vesicles to active zones, proper tethering, and internalization and turnover of UNC-2 (Fig. 5-1). We are still missing molecular components that act in many of these steps. Our identification of UNC-36 and CALF-1 as regulators of ER exit of UNC-2 gave a clue as to how the UNC-2 maturation occurs in the endoplasmic reticulum, but we do not yet know the precise molecular mechanisms of UNC-2 delivery to synapses. These may include unknown motor proteins, Golgi proteins or endosomal proteins such as Rab GTPases. Cell-biological evidence suggests that specific vesicles contain active zone components including Piccolo, Bassoon, Pre-VGCC and other exocytosis machinery components, and that these vesicles deliver their cargo to synapses to form active zones. The vesicles are large and reminiscent of dense-core vesicles (DCVs), which have a role in neuropeptide secretion [181, 182]. Exo- and endo-cytosis proteins are also implicated in membrane insertion and recycling of active zone components. None of the candidate mutants I examined, however, showed defect in GFP::UNC-2 localization in AWC. The modification of UNC-2 via posttranslational

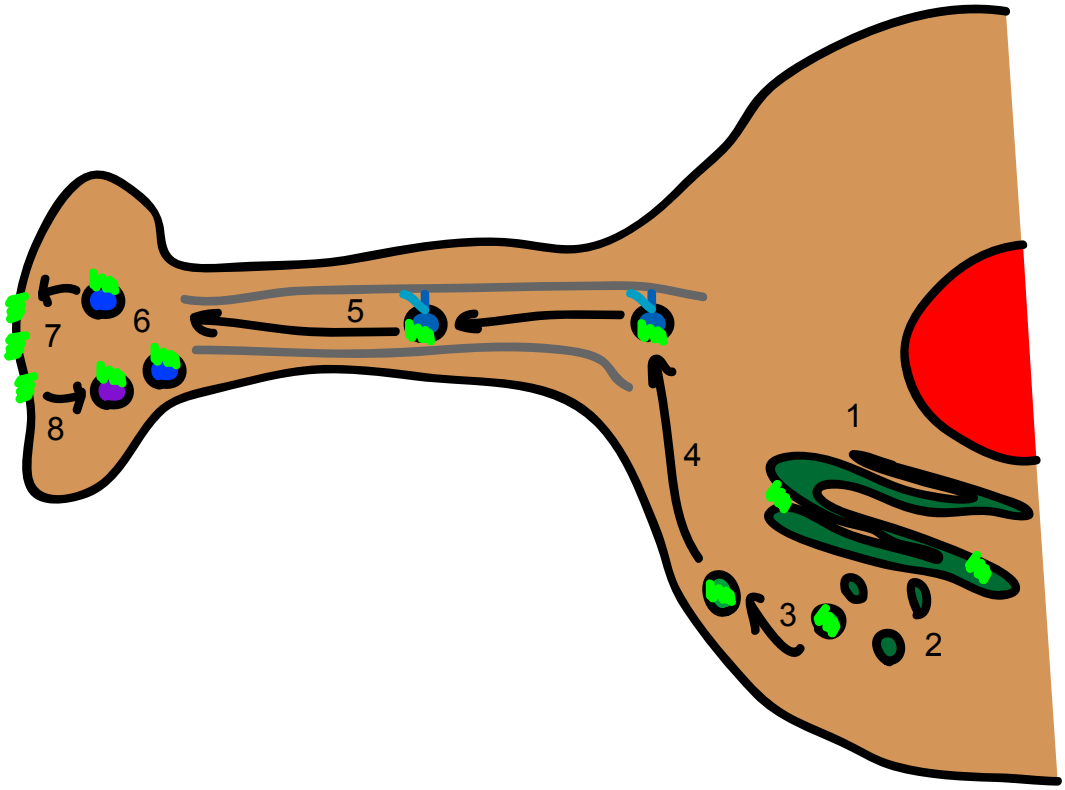

Figure 5-1.The steps that could affect UNC-2 localization and expression.
1) translation, folding, or post-translational modification of UNC-2,
2) endoplasmic reticulum to Golgi transport,
3) incorporation into targeting vesicles,
4) targeting to axonal segments,
5) axonal transport by motor proteins,
6) exocytosis/fusion of targeting vesicles to active zones,
7) proper tethering,
8) internalization and turnover of UNC-2.

modification such as glycosylation or phosphorylation might also be involved in its proper trafficking or stability of at the synapses.

There appears to be a high degree of genetic redundancy in synaptogenenic pathways. Elimination of a single synaptogenic protein may not affect synaptogenesis if another protein has a redundant or overlapping role. This issue might apply to UNC-2 trafficking, clustering and maintenance. Thus, if there are parallel mechanisms, eliminating single proteins may not cause a major defect in GFP::UNC-2 localization. More refined second-generation screens using sensitized backgrounds could yield additional genetic insights into the pathway. Alternatively, since I focused only on AWC neurons, screens with other neuronal cell types may facilitate mutant identification. In the synaptogenesis screens performed by the Jin, Nonet, and Bargmann labs, some mutations had larger effects than others on synaptic vesicle clustering depending on the neuronal cell types examined (e.g. VD/DD motor neurons v.s. ASI sensory neurons). Thus, it may be worthwhile to use other cell types such as VD/DD or DA9 for the next screen.

More quantitative approaches

So far, our work has focused on identification of genes that are required for absolute UNC-2 abundance at the AWC synapses; the visual screen identified three mutants that showed dramatic reduction in the GFP::UNC-2 signals. Because of the limitation in detection of fluorescence signals by eye, we could not identify mutants that changed synaptic puncta density or size. Thus, the screen was biased toward identification of qualitative rather than quantitative changes of the synaptic puncta signals (either absent

or present). With this in mind, a systematic approach could be used to study the roles of other presynaptic proteins in the stability or clustering of UNC-2 at presynapses.

Motor neuron synapses onto muscles are evenly spaced, and the synapses are large in size, so that individual synaptic puncta are easily quantifiable [26]. It would be more practical to quantitatively analyze the GFP::UNC-2 puncta in motor neurons such as VD/DD and DA9 than it would be in AWC neurons. There are many presynaptic molecules that are implicated in scaffolding functions at the nerve terminals. Proposed scaffolding proteins such as Neurexin, CASK, Mint and Veli may regulate local stability of presynaptic molecules including Pre-VGCC rather than their absolute clustering. With quantitative microscopic analysis, it should be possible to determine their precise contributions in regulating cluster size or density of GFP::UNC-2. To detect turnover rate of Pre-VGCC, the photoconvertible fluorescent tagged UNC-2 (e.g. Dendra2::UNC-2, 2xmEos2::UNC-2) represents a useful tool, as I showed in previous chapters. Therefore, we are now equipped with tools to test the hypotheses generated by previous *in vitro* studies quantitatively *in vivo*. For example, the role of individual exo- and endocytosis genes in the membrane insertion and recycling of Pre-VGCC *in vivo* is unclear. Examining exo- and endocytosis genes systematically, it should be possible to determine the contribution of each component in local insertion and recycling of Pre-VGCC at presynapses.

Concluding remarks

In my graduate research, I have used molecular biology, genetic methods, calcium imaging and cell biological analysis to answer fundamental questions in neuroscience.

Since I was a medical student, I have kept my interest in pathological conditions that are currently untreatable. After spending years in basic research, I still believe that the treatment of medical conditions will be achieved through detailed studies of basic biological phenomenon. In future experiences, I would like to elucidate fundamental biological questions from the viewpoints of medicine, genetics, and cell biology.

Materials and Methods

Materials and Methods for Chapter 2

Strains

Wild-type worms were Bristol variety N2. Strains were maintained using standard methods at 21-23°C. Some strains were provided by the *Caenorhabditis* Genetics Center and the National Bioresource Project. Mutants used were *calf-1(ky867), unc-2(lj1), unc-36(e251), syd-2(ju37), sad-1(ky289), rpm-1(js410), syd-1(ju82), elks-1(tm1233), nrx-1(ds1), lin-2(n1610), lin-7(n308cs), lin-10(e1439), unc-13(e51), unc-10(e102), dpy-23(e840), unc-101(m1), unc-11(ky280), unc-31(e928), unc-104(e1265), unc-116(e2310)*.

Germline transformation was carried out as described [106]. *odr-3::GFP::unc-2*, *tag-168::Dendra2::unc-2* and *unc-25::GFP::unc-2* were injected at 100 ng/µl. For rescue, overexpression and structure-function analysis, all *calf-1* plasmids were injected at 20 ng/µl except *hsp16.2::calf-1* at 10 ng/µl. Relatively high levels of GFP::UNC-2 and Dendra2::UNC-2 were needed for reliable visualization, and these overexpressed, tagged proteins might distort endogenous traffic. However, GFP::UNC-2 and Dendra2::UNC-2 were able to rescue *unc-2*-dependent locomotion, and were reliably trafficked to synapses in heat-shocked *calf-1* animals carrying *hsp16.2::calf-1,* indicating that the proteins in transgenic animals can interact effectively with the trafficking machinery.

For localization experiments, *calf-1::GFP* fusion plasmids were injected at 10 ng/µl. *unc-36::GFP* fusion plasmids were injected at 50ng/µl. All cell compartment markers including *odr-3::mCherry::rab-3* and *odr-3::CP450::mCherry* were injected at 0.5 to 5ng/µl. *ofm-1::GFP, ofm-1::DsRed, elt-2::mCherry, odr-1::mCherry, odr-*

1::DsRed, odr-1::GFP and flp-17::mCherry were used as coinjection marker and injected at 6-20 ng/µl.

Isolation and characterization of *calf-1(ky867)*

A strain expressing GFP::UNC-2 in AWC *(kyIs442)* was mutagenized with EMS according to standard protocols [183]. 209 F1s were cloned into different plates, and 30 to 50 F2 animals from individual F1 animals were subjected to a direct visual screen under a compound microscope. The mutants were isolated based on the loss of GFP::UNC-2 puncta from the AWC axon as observed with a Plan Apochromat 63x objective on a Zeiss Axioplan2 microscope.

Mapping and cloning of *calf-1*

calf-1(ky867) was mapped to the far right end of LGV using SNP polymorphisms in the CB4856 strain [184]. A genomic fragment containing only the B0250.2 reading frame with 0.8 kb of 5′ sequence and 1.2 kb of 3′ sequence was generated by PCR and injected at 1 ng/µl into *calf-1(ky867)* mutants. The PCR fragment rescued both uncoordinated movements and GFP::UNC-2 localization in AWC axons. To identify the *calf-1* mutation, the *calf-1* genomic coding region in *ky867* was amplified by PCR, and PCR products were sequenced.

Fluorescence microscopy and quantification

Animals were mounted on 4% agarose pads containing 400 mM tetramisole. Multiple transgenic lines of each transgene were examined for fluorescent expression and

localization patterns. Wide-field fluorescence images were obtained on Zeiss Axioplan2 imaging system (Fig. 2-1a-f, h,i, k-m; Fig. 2-2a-f, i,j; Fig. 2-4c,d; Fig. 2-6a-f, k; Fig. 2-7e,f; Supplementary Fig. 2-1a-f; Supplementary Fig. 2-2a-r; Supplementary Fig. 2-3a-i). Confocal images were obtained on Zeiss LSM 510 META laser scanning confocal imaging system (Fig. 2-4e-g, j-r; Fig. 2-5b bottom panels; Fig. 2-6g; Supplementary Fig. 2-5a-r; Supplementary Fig. 2-7a-c, e-v).

To quantify fluorescence intensities and number of fluorescent clusters, images were captured under consistent detector settings with a Hamamatsu Photonics C2400 CCD camera on a Zeiss Axioplan2 Imaging System with a 63x Plan-Apochromat objective and Metamorph software. ImageJ (NIH) was used to quantify fluorescence in AWC axons and cell bodies and DD dorsal axons. Images of AWC nerve rings and cell bodies were projected into a single plane by maximum projection; for DD, a single image of best focus was chosen for the quantification. Background intensity was subtracted and fluorescent clusters containing signals above an arbitrary threshold were measured for the total fluorescence intensity and the number of fluorescent clusters. The same thresholds were used for all images in each quantification. Normalized fluorescence intensity was obtained by dividing individual values with mean total fluorescence intensity of wild-type control animals. For the perinuclear region of AWC, a single image of best focus was chosen for the quantification and maximum fluorescence intensity was measured after background subtraction (Supplementary Fig. 2-7d). 6-10 animals were scored for each experiment.

Calcium imaging

Calcium imaging was performed as described [102]. For AWC^{ON} imaging, the strain CX10536 expressing the calcium indicator G-CaMP2.2b [185] in AWC^{ON} under the *str-2* promoter was crossed to *unc-2(lj1)* and *calf-1(ky867)* to generate the strains CX11391 and CX11386. For AIB imaging, the strain CX7469 expressing G-CaMP1.0 in AIB neurons [102] was crossed with *unc-2(lj1)* and *calf-1(ky867)* to generate CX11394 and CX11383. Animals were washed in buffer without food for ~20 minutes prior to imaging, a protocol designed to mimic the washes before chemotaxis assays, and imaging was conducted in a polydimethylsiloxane (PDMS) chamber in which an animal's nose was exposed to a stream of buffer that could be switched between odor-containing and odor-free solutions using an electronically gated valve. The standard stimulus protocol consisted of a 5-minute step pulse of the 10^{-4} dilution of odor in S-basal (without cholesterol) followed by odor removal. G-CaMP fluorescence intensity was measured for 10 seconds before and 50 seconds after the onset or offset of the odor stimulus; the same animals were imaged for odor onset and offset. 100% values were set by taking the average response from 1-4s in the trace. Controls and mutants were interleaved during imaging.

Subcellular localization in neurons and intestinal epithelial cells

For endoplasmic reticulum markers, cDNAs of *C. elegans* homologs of mammalian cytochrome P450, RAMP4 and cytochrome b5 (abbreviated as CP450 and cb5) were obtained using primers flanking the open reading frame C49C8.4, F59F4.2 and C31E10.7 [101]. For the Golgi marker, a cDNA fragment of *C. elegans* alpha-mannosidase II (ManII

in the text, the first 82 amino acids sequences including signal sequence/TM-anchor domain) was amplified from F58H1.1 [101, 186]. cDNAs were fused to mCherry at their C termini.

Individual regions of CALF-1 were tested for endoplasmic reticulum localization by expressing GFP-tagged CALF-1 mutants in intestinal epithelial cells, which are larger than neurons and easier to examine for subcellular protein localization. Full-length GFP-tagged CALF-1 colocalized with the endoplasmic reticulum marker CP450::mCherry in intestinal epithelial cells.

Heat shock experiments

Experiments with *hsp16.2::calf-1* were performed on young adult hermaphrodites. A 30°C heat shock was given for 3 hours. The plates were then incubated at 20°C for 2 hours for recovery before scoring GFP::UNC-2 localization and swimming behavior.

Photoconversion experiments

Dendra2::UNC-2 was expressed under *tag-168* pan-neuronal promoter in *calf-1(ky867);unc-2(lj1)* double mutant background; transgenic animals carrying *hsp16.2::calf-1* were crossed into the Dendra2::UNC-2 expressing animals. Prior to photoconversion, L4 larvae expressing Dendra2::UNC-2 were mounted on an agar pad. The tail regions of individual animals were illuminated with UV light with a 63x Plan-Apochromat objective to achieve local photoconversion. Animals were recovered on agar plates with OP50, and a 30°C heat shock was given for 1 hour. The plates were then incubated at 20°C for 3 hours before scoring Dendra2::UNC-2 localization in the head

region. The maximum fluorescence intensity of the photoconverted Dendra2::UNC-2 was quantified at the perinuclear region of a single image of best focus after background fluorescent intensity subtraction. Individual animals were mounted on agar pads in the same orientation before and after heat shock to allow the comparison of the same tail neurons.

Swimming assay

Individual young adult worms were transferred into a drop of M9 buffer on top of agar plate. After a 30 second recovery period, body bends were counted for 2 minutes.

Statistical Analysis

For fluorescent images and swimming assay, statistical analysis was performed using Student's unpaired t-test, Bonferroni t-test or Dunnett's test as appropriate. For AIB calcium imaging experiments, responses with an average value of zero were counted as failures, and the fraction of failures was compared for each genotype by Chi-squared test (a nonparametric method appropriate for non- normally distributed data). Consistent results were obtained in two independent blocks of experiments.

List of Strains and Transgenes

UNC-2 localization analysis

CX9272 kyIs439 and CX9275 kyIs442 [odr-3::GFP::unc-2, odr-3::mCherry::rab-3, ofm-1::GFP], CX10416 kyIs479 [unc-25::GFP::UNC-2, unc-25::mCherry::rab-3, odr-1::mCherry], CX11643 kyEx3049 [unc-25::GFP::unc-2, unc-25::CP450::mCherry],

CX10338 kyEx2448 [itr-1b::GFP::unc-2, itr-1b::mCherry::rab-3, odr-1::DsRed], CX9963 kyEx2242 [odr-3::GFP::unc-2, odr-3::CP450::mCherry, ofm-1::DsRed], CX10156 kyEx2328 [odr-3::GFP::unc-2, odr-3::syd-2::mCherry, ofm-1::DsRed], CX10157 kyEx2329 [odr-3::GFP::unc-2, odr-3::elks-1::mCherry, ofm-1::DsRed], CX10823 calf-1(ky867); unc-2(lj1); kyEx2785 [tag-168::Dendra2::unc-2, ofm-1::DsRed], CX10408 calf-1(ky867); unc-2(lj1); kyEx2785 [tag-168::Dendra2::unc-2, ofm-1::DsRed]; kyEx2787 [hsp16.2::calf-1, ofm-1::GFP].

calf-1 rescue and overexpression experiments

CX10918 kyIs442; calf-1(ky867); kyEx2830 [calf-1::calf-1, ofm-1::GFP], CX10922 kyIs442; calf-1(ky867); kyEx2833 [tag-168::calf-1, ofm-1::GFP], CX10923 kyIs442; calf-1(ky867); kyEx2834 [myo-3::calf-1, ofm-1::GFP], CX10925 kyIs442; calf-1(ky867); kyEx2836 [odr-3::calf-1, ofm-1::GFP], CX10520 kyIs479; calf-1(ky867); kyEx2578 [unc-25::calf-1, flp-17::mCherry], CX10167 kyIs442; calf-1(ky867); kyEx2339 [hsp16.2::calf-1, ofm-1::GFP], CX10614 kyIs442; calf-1(ky867); kyEx2662 [tag-168::unc-36, ofm-1::GFP], CX10704 kyIs442; unc-36(e251); kyEx2730 [tag-168::calf-1, ofm-1::GFP], CX10706 kyIs479; calf-1(ky867); kyEx2732 [tag-168::unc-36, odr-1::GFP], CX10524 kyIs479; unc-36(e251); kyEx2582 [tag-168::calf-1, flp-17::mCherry], CX8811 unc-2(lj1); kyEx1625 [tag-168::unc-2, ofm-1::GFP], CX11423 calf-1(ky867); kyEx1625 [tag-168::unc-2, ofm-1::GFP] Line1, CX11424 calf-1(ky867); kyEx1625 [tag-168::unc-2, ofm-1::GFP] Line2, CX11426 unc-36(e251); kyEx1625 [tag-168::unc-2, ofm-1::GFP] Line1, CX11425 unc-36(e251); kyEx1625 [tag-168::unc-2, ofm-1::GFP] Line2.

CALF-1 structure-function analysis

CX10515 kyIs442; calf-1(ky867); kyEx2573 [calf-1::calf-1 Deletion I, ofm-1::GFP], CX10178 kyIs442; calf-1(ky867); kyEx2344 [calf-1::calf-1 Deletion II, ofm-1::GFP], CX10513 kyIs442; calf-1(ky867); kyEx2571 [calf-1::calf-1 Deletion III, ofm-1::GFP], CX10270 kyIs442; calf-1(ky867); kyEx2399 [calf-1::calf-1 Deletion IV, ofm-1::GFP], CX10698 kyIs442; calf-1(ky867); kyEx2724 [calf-1::calf-1 Deletion V, ofm-1::GFP], CX10268 kyIs442; calf-1(ky867); kyEx2397 [calf-1::calf-1 Deletion VI, ofm-1::GFP], CX10180 kyIs442; calf-1(ky867); kyEx2346 [calf-1::calf-1 TM Deletion, ofm-1::GFP], CX10342 kyIs442; calf-1(ky867); kyEx2452 [calf-1::calf-1 TM Replacement, ofm-1::GFP], CX10318 kyIs442; calf-1(ky867); kyEx2429 [calf-1::calf-1 RAR Deletion, ofm-1::GFP], CX10321 kyIs442; calf-1(ky867); kyEx2432 [calf-1::calf-1 RR Deletion, ofm-1::GFP], CX10360 kyIs442; calf-1(ky867); kyEx2470 [calf-1::calf-1 RKR Deletion, ofm-1::GFP], CX10362 kyIs442; calf-1(ky867); kyEx2472 [calf-1::calf-1 RLRE Deletion, ofm-1::GFP], CX10565 kyIs442; calf-1(ky867); kyEx2624 [calf-1::calf-1 C-terminus KDEL, ofm-1::GFP], CX10568 kyIs442; calf-1(ky867); kyEx2627 [calf-1::calf-1 C-terminus KKYL, ofm-1::GFP], CX10574 kyIs442; calf-1(ky867); kyEx2633 [calf-1::calf-1 Adrenergic a2 C-terminus, ofm-1::GFP], CX10570 kyIs442; calf-1(ky867); kyEx2629 [calf-1::calf-1 NMDAR C1 domain, ofm-1::GFP].

CALF-1 Endoplasmic reticulum retention motif search

CX10503 kyEx2564 [odr-3::calf-1TM::GFP, odr-3::CP450::mCherry, ofm-1::DsRed], CX10511 kyEx2569 [odr-3::PAT-3TM::GFP, odr-3::CP450::mCherry, ofm-1::DsRed],

CX10457 kyEx2520 [odr-3::PAT-3TM::calf-1(entire cytosolic region)::GFP, odr-3::CP450::mCherry, ofm-1::DsRed], CX10537 kyEx2596 [odr-3::PAT-3TM::calf-1(basic & proline rich region)::GFP, odr-3::CP450::mCherry, ofm-1::DsRed], CX10514 kyEx2572 [odr-3::PAT-3TM::calf-1(basic region)::GFP, odr-3::CP450::mCherry, ofm-1::DsRed], CX10540 kyEx2599 [odr-3::PAT-3TM::calf-1(proline rich region)::GFP, odr-3::CP450::mCherry, ofm-1::DsRed], CX10526 kyEx2584 [odr-3::PAT-3TM::calf-1(basic region & C-terminus)::GFP, odr-3::CP450::mCherry, ofm-1::DsRed], CX10543 kyEx2602 [odr-3::PAT-3TM::calf-1(C-terminus)::GFP, odr-3::CP450::mCherry, ofm-1::DsRed], CX11072 kyEx2915 [odr-3::PAT-3TM::calf-1(proline rich region & C-terminus)::GFP, odr-3::CP450::mCherry, ofm-1::DsRed].

CALF-1 localization and expression and UNC-36 localization analysis

CX10273 kyEx2401 [odr-3::calf-1::GFP, odr-3::mCherry::rab-3, ofm-1::DsRed], CX10345 kyEx2455 [odr-3::calf-1::GFP, odr-3::CP450::mCherry, ofm-1::DsRed], CX10351 kyEx2461 [odr-3::calf-1::GFP, odr-3::cb5::mCherry, ofm-1::DsRed], CX11689 kyEx3150 [odr-3::calf-1::GFP, odr-3::RAMP4::mCherry, ofm-1::DsRed], CX10350 kyEx2460 [odr-3::calf-1::GFP, odr-3::ManII::mCherry, ofm-1::DsRed], CX10262 kyEx2394 [unc-25::calf-1::GFP, unc-25::mCherry::rab-3, odr-1::DsRed], CX10344 kyEx2454 [unc-25::calf-1::GFP, unc-25::CP450::mCherry, odr-1::DsRed], CX10356 kyEx2466 [unc-25::calf-1::GFP, unc-25::ManII::mCherry, odr-1::DsRed], CX10916 kyEx2828 [calf-1::GFP, odr-1::DsRed], CX11478 kyEx3050 [odr-3::unc-

36::GFP, odr-3::CP450::mCherry, elt-2::mCherry], CX11025 kyEx2887 [unc-36::unc-36::GFP, ofm-1::DsRed].

Calcium imaging

CX10536 kyEx2595 [str-2::G-CaMP2.2b, ofm-1::GFP], CX11391 kyEx2595; unc-2(lj1), CX11386 kyEx2595; calf-1(ky867), CX7469 kyEx903 [odr-2b::G-CaMP1.0, ofm-1::GFP], CX11394 kyEx903; unc-2(lj1), CX11383 kyEx903; calf-1(ky867).

Molecular Biology

odr-3::unc-2 and odr-3::GFP::unc-2

The *odr-3::GFP::unc-2* was constructed by insertion of GFP into the N-terminus of *unc-2* at an artificially created NotI site in a previously described *odr-3::unc-2* plasmid [92]. To construct the *unc-2* mini-gene, a full-length *unc-2* cDNA was first assembled from three PCR fragments generated from a *C. elegans* cDNA library, flanked by the 5' and 3' primers:

5' unc-2C Frag1:

GAGCTAGCCCCGGGGATGATACCAATCGCCGCATCGGAAATTATAC

3' unc-2C Frag3:

GTCATCATGCATCTCGAGCTAAACAATTGCCCATCGAGGATCATCTTC

The full-length cDNA in a pBluescript SK(-) vector was highly toxic to bacteria, and suffered from frequent rearrangements. To overcome this issue, bacteria were grown at 30°C, and a small synthetic intron was inserted at exon 6 of the *unc-2* cDNA by site-directed mutagenesis to create the mini-gene.

The synthetic intron sequence was,

GTAAGTTTAAACTATTCGTTACTAACTAACTTTAAACATTTAAATTTTCAG

Flanking sequences were,

CTAGGTTCTTTTTTCATGCTCAATC – TCGTTCTCGGAGTATTGTCTGGAGA

Promoter and 3' UTR ligation:

The *odr-3* promoter was amplified from an existing pSM vector and ligated into the NheI site of the *unc-2* mini-gene. Primers were:

5' NheI odr-3P: GAATCGTAGCTAGCGGCCGGCCATCTCAACATAGTAGATTTTT

3' pSM (Orig) new: CTGATGACAGCGGCCGATGCGGAGCTCAG

The *unc-54* 3' UTR was isolated from a pSM vector and ligated between XhoI and ApaI sites in the mini-gene construct.

For N-terminal GFP tagging, a NotI site was added in front of the initial ATG of the *unc-2* mini-gene by mutagenesis, and GFP was inserted, using the following primers:

unc-2 c QC NotI up:

CATAACATAGAACATTTTCAGGAGgcggccgcgctagcATGATACCAATCGCCGCAT

C

unc-2 c QC NotI down:

GATGCGGCGATTGGTATCATgctagcgcggccgcCTCCTGAAAATGTTCTATGTTATG

5' NotI GFP pSM:

GAATCGTAgcggccgcATGAGTAAAGGAGAAGAACTTTTCACTG

3' NotI GFP pSM: GATTGGAAgcggccgcTTTTGTATAGTTCATCCATGCCATGTG

The full-length *unc-2* cDNA and all junctions were verified by sequencing. When the *odr-3* promoter was replaced by pan-neuronal *tag-168* promoter, both the *tag-168::unc-2* and the *tag-168::GFP::unc*-2 rescued the locomotion defects of *unc-2(lj1)*.

Dendra2 cDNA synthesis and tag-168::Dendra2::unc-2

Dendra2 cDNA was synthesized from -50-mer oligonucleotides according to the GeneDesign protocol [187] with the substitution of PfuTurbo polymerase (Stratagene, La Jolla, CA) for ExTaq polymerase. Dendra2 transgene expression was increased by codon-optimizing the Dendra2 sequence for *C. elegans* and adding synthetic intron sequences. The *tag-168::Dendra2::unc-2* was constructed by insertion of the Dendra2 cDNA into the N-terminus of *unc-2* at the NotI site in the *tag-168::unc-2* construct. *tag-168::GFP::Dendra2::unc*-2 rescued the locomotory defect of *unc-2(lj1)* (data not shown).

odr-3::unc-36 and odr-3::unc-36::GFP

unc-36 cDNA was obtained by PCR from a *C. elegans* cDNA library using primers flanking the ORF C50C3.9a. Primers used were,

5’ unc-36C:

GAATCGTAGCTAGCCCCGGGGATGCGAGTGGTTCATCTGCTCGTCGTG

3’ unc-36C: GATTGGAAGGTACCCCGCGGTTAAAATATGCAAAAATGAAGGAA

The PCR product was cloned into the pCR4Blunt-TOPO. The *unc-36* cDNA was excised and ligated between NheI and Asp718 in the pSM vector. The *odr-3* promoter was amplified by PCR and ligated between FseI and AscI to create *odr-3::unc-36*.

For C-terminal GFP tagging, the *unc-36* cDNA was amplified by using the following primers:

5'NheI unc-36: GAATCGTAGCTAGCATGCGAGTGGTTCATCTGCTCGTCGTG

3'Asp718 unc-36:

GA TTGGAAGGTACCGTAAATATGCAAAAATGAAGGAAAACACCGAAAAG

The PCR product was ligated between NheI and Asp718 in the C-terminal GFP pSM vector containing the *odr-3* promoter to create *odr-3::unc-36::GFP*.

The full-length *unc-36* cDNA and all junctions were verified by sequencing. When the *odr-3* promoter was replaced by the endogenous *unc-36* promoter, both the *unc-36P::unc-36* and *unc-36P::unc-36::GFP* rescued the locomotion defect of *unc-36(e251)*.

odr-3::mCherry::rab-3

odr-3::mCherry::rab-3 was constructed by replacing the promoter in a plasmid containing *mCherry::rab-3* (a gift from K. Shen) using FseI and AscI sites.

Promoters

Promoters were obtained by PCR from N2 genomic DNA using the following primers. Genomic sequences are shown in lower case.

calf-1 promoter

5' FseI calf-1P: GAATCGTAGGCCGGCCctgcggaaaagaggtaaacactacaaaaatag

3' AscI calf-1P: GATTGGAAGGCGCGCCtttagtggaaaatattagctaaaaattgag

odr-3 promoter

5' FseI odr-3P: GAATCGTAGGCCGGCCatctcaacatagtagatttttaaaaatag

3' AscI odr-3P: GATTGGAAGGCGCGCCatctaaaaaaacaatgatctatgagtaattg

unc-25 promoter:

5’ FseI unc-25P: GAATCGTAGGCCGGCCcaaaaaacacccacttttgatctcaaatttg

3’ AscI unc-25P: GATTGGAAGGCGCGCCttttggcggtgaactgagcttttccctattc

itr-1B promoter

5' FseI itr-1Pb: GAATCGTAGGCCGGCCatctattccagagttcgttcccgag

3' AscI itr-1Pb: GATTGGAAGGCGCGCCcaattcgtgtgcttccaccaccac

unc-36 promoter

5’ FseI unc-36P: GAATCGTAGGCCGGCCgcagtaattagtgtccgttattcc

3’ AscI unc-36P: GATTGGAAGGCGCGCCtctcgttttactctttgaaatccg

myo-3 promoter

5’ FseI myo-3P: GAATCGTAGGCCGGCCgggctgcaggtcggctataataag

3’ AscI myo-3P: GATTGGAAGGCGCGCCtggatctagtggtcgtgggtttgatgg

tag-168 promoter

5’ FseI tag-168P: GAATCGTAGGCCGGCCtctccttgaagctcatccagacgtcgctg

3’ AscI tag-168P: GATTGGAAGGCGCGCCacacgggccagagctgcagctggatggca

Active zone and endoplasmic reticulum markers

cDNAs were obtained by PCR from a *C. elegans* cDNA library using the following primers. cDNA sequences are shown in lower case.

elks-1 cDNA

5' SalI elks-1C: GAATCGTAGTCGACatggcacctggtcccgcaccatacagcagccgaac

3' AgeI elks-1C: GATTGGAAACCGGTGGggcccaaattccgtcagcatcgtcgtgatc

syd-2 cDNA

5' NheI syd-2C: GAATCGTAGCTAGCatgagctacagcaatggaaacataaattgtgatat

3' Asp718 syd-2C: GATTGGAAGGTACCGTggtatataaatgaaactcgtaggattttgctatg

CP450 cDNA

5' NheI CP450: GAATCGTAGCTAGCatgattttacttattctcacttcg

3' Asp718 CP450: GATTGGAAGGTACCGTatatctttccttcattgaaactctg

RAMP4 cDNA

5' NheI RAMP4: GAATCGTAGCTAGCatggccccaaagcaacgtatgacac

3' Asp718 RAMP4: GATTGGAAGGTACCGTccatcccatcttgacgtagcggatg

Cb5 cDNA

5' NheI Cb5: GAATCGTAGCTAGCatggccgatcttaagcaaatcaccc

3' Asp718 Cb5: GATTGGAAGGTACCGTcgcagcgataagataataaacaag

ManII cDNA

5' NheI ManII: CAGAATGCTAGCatgggaaaacgcaatttctatattat

3' Asp718 ManII: TTGTTCGGTACCACttctttttcttcatcaaaatctaccg

These cDNAs were ligated between NheI and Asp718 except SalI and AgeI for *elks-1* cDNA in the C-terminal mCherry pSM vector, and appropriate promoters were ligated between FseI and AscI.

calf-1 cDNA cloning and GFP tagging

calf-1 cDNA was obtained by PCR from *C. elegans* cDNA library using the following primers. cDNA sequences are shown in lower case.

5' NheI calf-1C: GAATCGTAGCTAGCatgtcatctccacaacaattcacaattccgg

3' NcoI calf-1C w/ Stop: GATTGGAACCATGGctacacaatatggatcgatcctcgaggttg

The PCR product was ligated between NheI and NcoI in the pSM vector, and appropriate promoters were ligated between FseI and AscI. The *hsp16.2::calf-1* plasmid was created by ligating *calf-1* cDNA between NheI and NcoI in pPD49.78.

For GFP internal tagging, GFP was amplified by PCR from pSM::GFP using the following primers:

5' EcoRI GFP:

GAATCGTAGAATTCATGAGTAAAGGAGAAGAACTTTTCACTGGAG

3' EcoRI GFP:

GATTGGAAGAATTCTTTGTATAGTTCATCCATGCCATGTGTAATC

The PCR product was ligated at the EcoRI site in the *calf-1cDNA*, which precedes the proline-rich region. When expressed from the endogenous *calf-1* promoter, *calf-1::GFP* rescued the uncoordinated phenotype of *calf-1(ky867)* (data not shown).

calf-1::calf-1 TM deletion and calf-1::calf-1 TM replacement

calf-1(entire cytosolic region) was amplified by PCR from *calf-1* cDNA using the following primers.

5' NheI calf-1 TMdel: GAATCGTAGCTAGCATGaataaatgcaagcagtgggagctggacaagg

3' NcoI calf-1C w/Stop: GATTGGAACCATGGctacacaatatggatcgatcctcgaggttg

The PCR product was ligated between NheI and NcoI in the pSM vector containing *calf-1* promoter to create *calf-1::calf-1 TM deletion.*

pat-3 membrane sequence was amplified from pPD133.51 using the following primers.

5' NheI_PAT-3 MLS: GAATCGTAGCTAGCatgccaccttcaacatcattgctgctcctcg

3' NheI_PAT-3 MLS: GATTGGAAGCTAGCtacctcggatctatcatgaagtactgtgagc

The *pat-3* transmembrane PCR product was ligated into the NheI site of the *calf-1::calf-1 TM deletion* to create *calf-1::calf-1 TM replacement*.

calf-1 deletion analysis and endoplasmic reticulum retention

For deletion analysis of CALF-1, primers flanking target regions were created and individual cDNAs were amplified either directly or by using fusion PCR methods from *calf-1* cDNA [188]. These cDNAs were inserted between NheI and NcoI in the pSM vector containing the endogenous *calf-1* promoter.

For the endoplasmic reticulum retention search of CALF-1, primers flanking target regions were created and individual cDNAs were amplified either directly or by using fusion PCR methods from the *calf-1::calf-1 TM replacement* plasmid. These cDNA were inserted between NheI and AgeI in the C-terminal GFP pSM vector containing the *odr-3* promoter.

calf-1::calf-1 Adrenergic a2 C-terminus and calf-1::calf-1 NMDAR c1 domain

calf-1 Adrenergic a2 C-terminus and *calf-1 NMDAR c1 domain* were synthesized from ~50-mer oligonucleotides by adding NheI and NcoI sites according to the GeneDesign protocol with the substitution of PfuTurbo polymerase for ExTaq polymerase. These fragments were ligated between NheI and NcoI in the pSM vector containing *calf-1* promoter to create *calf-1::calf-1 Adrenergic a2 C-terminus* and *calf-1:: calf-1 NMDAR c1 domain* respectively.

calf-1::calf-1 C-terminus KDEL and calf-1::calf-1 C-terminus KKYL

calf-1::calf-1 C-terminus was mutagenized by the following oligos to create *calf-1::calf-1 C-terminus KDEL* and *calf-1::calf-1 C-terminus KKYL* respectively.

C-term KDEL mut UP:

GGCTGTCATCAACCTCGAGGATCGAAAGATGAGCTTTAGCCATGGTATTGAT

ATCTGAGC

C-term KDEL mut DOWN:

GCTCAGATATCAATACCATGGCTAAAGCTCATCTTTCGATCCTCGAGGTTGAT

GACAGCC

C-term KKYL mut UP:

GGCTGTCATCAACCTCGAGGATCGAAAAAGTACCTTTAGCCATGGTATTGAT

ATCTGAGC

C-term KKYL mut DOWN:

GCTCAGATATCAATACCATGGCTAAAGGTACTTTTTCGATCCTCGAGGTTGAT

GACAGCC

Materials and Methods for Chapter 3

Strains

Wild-type strains were *C. elegans* variety Bristol, strain N2. The CB4856 strain was used for *mapping olrn-1* [184]. Strains were maintained by standard methods [189]. Germline transformation was carried out as previously described [190]. Co-injection markers were *ofm-1::GFP, ofm-1::RFP* or *elt-2::GFP*. Integrated transgenes used in this study include *kyIs140 I [str-2::GFP, lin-15(+)]*, *kyIs323 II [str-2::GFP, ofm-1::GFP],*

zdIs5 [mec-4::GFP]. Mutations used in this study included *olrn-1(ky626) X*, *olrn-1(ut305) X, egl-19 (n582) IV, egl-19(ad695gf) IV, nsy-4(ky616)IV*, *nsy-5(ky634) I*, *unc-36(e251) III*, *unc-2 (lj1) X, unc-2(e55) X*, *unc-43(n1186) IV, unc-43(n408) IV, unc-43(n498gf) IV, tir-1(tm1111) III*, *nsy-1(ky542) II*, *nsy-1(ag3) II, nsy-1(ok593) II, sek-1(km4) X*.

Transgenes maintained as extrachromosomal arrays included the following lines used for mosaic analysis: *kyEx914 (line 1) & kyEx918 (line 2) [odr-3::olrn-1b 15ng/ul, odr-1::dsRed 7.5ng/ul, ofm-1::gfp 20ng/ul]*, *kyEx1072 (line 1) & kyEx1074 (line 2) [odr-3::olrn-1b 5ng/ul, odr-1::dsRed 7.5ng/ul, ofm-1::gfp 20ng/ul]*, *kyEx1097 (line 1) & kyEx1098 (line 2) [odr-3::olrn-1b 2.5ng/ul, odr-1::dsRed 7.5ng/ul, elt-2::GFP 10ng/ul], kyEx1102 (line 1) & kyEx1103 (line 2) [odr-3::olrn-1b 25ng/ul, odr-1::dsRed 7.5ng/ul, elt-2::GFP 5ng/ul]*. For *unc-2* and *unc-36* mosaics, the same extrachromosomal arrays were examined in wild-type and mutant backgrounds: *kyEx1628 (line 1) kyEx1629(line 2) & kyEx1630(line 3) [odr-3::unc-2 20ng/ul, odr-1::RFP 2.5ng/ul, ofm-1::GFP 10ng/ul]; kyEx1229(line 1) kyEx1387(line 2) & kyEx1388(line 3) [odr-3::unc-36 20ng/ul, odr-1::RFP 2.5ng/ul, elt-2::GFP 10ng/ul]*.

Additional transgenic arrays were *kyEx822 [odr-3::nsy-4a 75ng/ul, ofm-1::GFP 20ng/ul], kyEx996 [18.5kb nsy-5 PCR fragment 13ng/ul, odr-1::DsRed 12.5ng/ul, ofm-1::GFP 25ng/ul]*, *kyEx1075 [srsx-3::GFP 10ng/ul, str-2::DsRed 50ng/ul, elt-2::gfp 10ng/ul]*, *kyEx1096 [odr-1::dsRed 7.5ng/ul, elt-2::GFP 10ng/ul]*, *kyEx1182 [odr-3::olrn-1b::Ch 5ng/ul, ofm-1::GFP 15ng/ul], kyEx1320 [olrn-1a::Ch 25ng/ul, ofm-1::GFP 15ng/ul], kyEx1315 [olrn-1b::Ch 50ng/ul, elt-2::GFP 10ng/ul], kyEx1310 [odr-3::Ch::olrn-1b 25ng/ul, elt-2::GFP 10ng/ul]*.

The following arrays were used in the deletion analysis: (A) *odr-3::olrn-1b::Ch* = *kyEx1318* (line 1) , *kyEx1319* (line 2), *kyEx1317* (line 3); (B) *odr-3::olrn-1bΔrawR1::Ch* = *kyEx1337* (line 1), *kyEx1345* (line 2), *kyEx1344* (line 3); (C) *odr-3::olrn-1bΔTM1,2::Ch = kyEx1297* (line 1), *kyEx1298* (line2); (D) *odr-3::olrn-1bΔrawR2::Ch* = *kyEx1338* (line 1), *kyEx1339* (line 2), *kyEx1340* (line 3); (E) *odr-3::olrn-1b(G466E)::Ch* = *kyEx1358* (line1), *kyEx1357* (line 2), *kyEx1359* (line 3); (F) *odr-3::olrn-1b(ΔRRRR)::Ch = kyEx1332* (line 1); *kyEx1296* (line 2), *kyEx1300* (line 3), *kyEx1299* (line 4); (G) *odr-3::olrn-1bΔCterm::Ch = kyEx1382* (line 1), *kyEx1352* (line 2), *kyEx1351* (line 3). These transgenes were injected at 15ng/ul with 10-15 ng/ul of *ofm-1::GFP* co-injection marker.

Isolation and characterization of *olrn-1(ky626)*

kyIs140 I animals were subjected to EMS mutagenesis according to standard procedures [183]. A chemotaxis enrichment was used to isolate F2 animals that sensed 2,3 pentanedione (an AWC^{OFF}-sensed odorant) but failed to sense butanone (an AWC^{ON}-sensed odorant) [119]. F2 mutants that failed to migrate to butanone were screened for the AWC^{OFF} *str-2::GFP* phenotype using a fluorescence dissecting microscope. The failure to express *str-2::GFP* was confirmed using 400X magnification under a compound microscope. Additional rounds of screening were done without the behavioral enrichment.

olrn-1(ky626) was mapped on LGX between single nucleotides polymorphisms pkP6166 (physical position: X: 14678988) and pkP6172 (physical position X:17707311) using the CB4856 strain [184]. A complementation test between *ky626* and *ut305* resulted

in a failure to complement: 93.5% of *ky626/ut305* (n=138) animals at 25° were 2AWC^{OFF}. *olrn-1(ut305)* has previously been shown to correspond to C02C6.2 (X:15539330-15546729) [124]. To identify the *olrn-1(ky626)* mutation, genomic coding regions of C02C6.2 were amplified by PCR and sequenced on both strands. The *olrn-1(ky626)* mutation was a G→A transition, resulting in a G→E missense mutation at residue 473 in the *olrn-1a* isoform, and position 466 in the *olrn-1b* isoform.

Molecular biology

Identification of unc-2(e55) and unc-36(e251) mutations

Resequencing *unc-2(e55)* revealed that the stop mutation originally assigned to residue 458 was actually present at reside 511 of T02C5.5b gene model (Q>stop nonsense mutation), but supported the identification of *e55* as a strong loss-of-function mutation. Sequencing of *unc-36(e251)* revealed that the *unc-36(e251)* mutation was G>A transition, resulting in a Trp>stop nonsense mutation at residue 496 in the C50C3.9a gene model. This mutation should truncate the UNC-36 protein immediately after the vWA domain.

odr-3::unc-2

unc-2 cDNAs were obtained by PCR from a *C. elegans* cDNA library using primers flanking the ORF T02C5.5b. Due to toxicity of the full-length cDNAs in bacteria, they were maintained as minigenes with a synthetic intron interrupting their coding regions. When expressed from the pan-neuronal *H20* promoter, the *unc-2* minigene rescued the uncoordinated phenotype of *unc-2(lj1)*. The minigene was subcloned behind the *odr-3* promoter for mosaic analysis.

odr-3::unc-36

unc-36 cDNAs were obtained by PCR from a *C. elegans* cDNA library using primers flanking the ORF C50C3.9a. Expression of the cDNA under 2 kb of *unc-36* upstream region rescued the uncoordinated phenotype of *unc-36(e251).* The cDNA was subcloned behind the *odr-3* promoter for mosaic analysis.

odr-3::olrn-1b

odr-3::olrn-1b was constructed by inserting a KpnI-C02C6.2b-SmaI fragment into the pPD49.26 vector at the KpnI and EcoRV sites. A KpnI-C02C6.2b-ApaI fragment from this clone was then inserted downstream of the *odr-3* promoter in the *odr-3::GFP* vector [191] removing the GFP.

odr-3::mCherry::orln-1b & odr-3::olrn-1b::mCherry

The mCherry coding sequence was amplified using primers with linkers on each side of mCherry, and subcloned into either the 5' NheI site upstream of the *olrn-1b* start site or an internal EcoRV site in the C-terminus in the *odr-3::olrn-1b* vector. This insertion site was C-terminal to the second Raw repeat domain (*rawR2*).

***odr-3::olrn-1b* deletions**

To make the domain deletions described in Figure 3, the *odr-3::olrn-1b::Cherry* vector was deleted at residues 77-108 *(ΔrawR1*), 265-304 *(ΔTM1/2*), 396-428 *(ΔrawR2*), 510-513 *(ΔRRRR*), and 429-539 *(ΔC-term*) by PCR overlap extension with suitable primers [78, 192]. The same technique was used to introduce the G466bE mutation.

olrn-1a::mCherry and olrn-1b::mCherry

3.8 kb 5' to the *olrn-1a* start site and 3.6 kb 5' to the *olrn-1b* start site were subcloned into the pSM-mCherry vector. The second clone represented the entire intron between the alternative first exons of the OLRN-1 isoforms.

Genetic mosaic analysis.

Loss of function mosaic analysis was performed on six independent lines with unstable extrachromosomal transgenic arrays *[odr-3:olrn-1b, odr-1::dsRed]* in a *kyIs140 I, olrn-1(ky626) X* mutant. Gain-of-function mosaic analysis was performed on four independent lines in a *kyIs140 I* wild type strain. Each data point in Figure 4 represents combined data from two independent lines injected with the same concentration of DNA. The presence or absence of the transgene in mosaics was inferred by the presence of *odr-1::dsRed*, which is expressed in AWC and AWB neurons. The *str-2::GFP* expression phenotype in mosaic cells was examined under a compound scope at 100-400X. Previous experiments have used a similar strategy [117, 119, 126, 127]. Statistical analysis was performed for mutant mosaics rescued at 2.5 or 5 ng/ul of *odr-3:olrn-1b*, and for wild-type mosaics injected with 15 or 25 ng/ul of *odr-3:olrn-1b*, to test (1) the null hypothesis that both AWC neurons behaved as independent units, purely as predicted by the proportions in the non-mosaic controls (2) the null hypothesis that the DsRed-positive (rescued) AWC behaved purely as predicted by the rescued controls (3) the null hypothesis that the DsRed-negative (non-rescued) AWC behaved purely as predicted by the non-rescued controls. In all cases, results were different from the null hypothesis at $P < 0.001$ by Chi square test or Fisher exact test as appropriate, using the calculator at www.graphpad.com. Both the rescued AWC and the non-rescued AWC in *olrn-1; odr-3::olrn-1b* mosaics became AWC^{ON} more often than predicted by the null hypothesis. Thus there is both autonomous and non-autonomous rescue of *olrn-1*. In wild-type mosaics overexpressing *olrn-1*, the overexpressing AWC became AWC^{ON} more often

than predicted by the null hypothesis, and the wild-type AWC became AWC^{OFF} more often than predicted.

In rare *olrn-1* mosaic animals, the transgene was lost in both AWC neurons but retained in either or both AWB neurons. These animals did not express *str-2::GFP* (n=5 animals), suggesting that *olrn-1* expression in AWC accounts for its major role in AWC asymmetry.

Mosaic analysis of *olrn-1* in *nsy-4* or *nsy-5* mutants was performed a single line per genetic background. A single unstable extrachromosomal array was examined in wild type, *nsy-4(ky616)* or *nsy-5(ky634)* backgrounds bearing stable integrated *str-2::GFP* transgenes.

Loss-of-function mosaic analysis for *unc-2* was performed on three independent lines with unstable extrachromosomal transgenic arrays *[odr-3::unc-2, odr-1::dsRed]* in a *kyIs140 [str-2::GFP] I; unc-2(lj1) X* mutant. Gain-of-function mosaic analysis for *unc-2* was performed on three independent lines in the *kyIs140 I* strain. Loss-of-function mosaic analysis for *unc-36* was performed on three independent lines with unstable extrachromosomal transgenic arrays *[odr-3::unc-36-SL2-CFP, odr-1::dsRed]* in a *kyIs140 I; unc-36(e251) III* mutant. Gain-of-function mosaic analysis for *unc-36* was performed on three independent lines in the *kyIs140* strain. Loss of the transgene was inferred by loss of the coinjection marker *odr-1::dsRed* in AWC neurons. Results from all lines were combined for statistical analysis, which was performed as described above for *olrn-1*. In all cases the null hypothesis that the two AWCs behaved as independent units could be excluded at $P < 0.001$. Both the rescued AWC and the non-rescued AWC in *unc-2; odr-3::unc-2* mosaics were strongly affected by the contralateral cell -- the

rescued AWC became AWC^{OFF} more often than predicted by the null hypothesis, and the non-rescued AWC became AWC^{ON} more often than predicted ($P < 0.001$ in both cases). Thus a single *unc-2(+)* AWC can bias both AWC neurons. In wild-type mosaics overexpressing *unc-2,* the wild-type AWC became AWC^{OFF} more often than predicted by the null hypothesis ($P = 0.003$), but the overexpressing AWC was not affected by the wild-type AWC ($P = 0.1943$). In *unc-36; odr-3::unc-36* mosaics, the wild-type AWC became AWC^{OFF} more often than predicted by the null hypothesis ($P < 0.001$), but the mutant AWC was not significantly affected ($P = 0.075$). There was no significant effect of *unc-36* overexpression in a wild-type background.

Microscopy

50-100 gravid adults were picked and allowed to lay eggs overnight. Adults were washed off the plate with M9, and eggs were allowed to hatch for three hours. L1 larvae were examined on a compound microscope at 400-630X magnification or used for confocal microscopy. To obtain late L1/early L2 animals, ~50-60 gravid adults were picked to a plate and allowed to lay eggs for 3 hours, after which the adults were removed from the plate. Progeny were examined 30 hours later under the confocal microscope.

Materials and Methods for Chapter 4

Strains

Wild-type worms were Bristol variety N2. Strains were maintained using standard methods at 21-23°C. Some strains were provided by the *Caenorhabditis* Genetics Center

and the National Bioresource Project. Mutants used were *calf-2(ky977), calf-1(ky867), unc-2(lj1), unc-36(e251), odr-4(n2144), ced-1(e1735).*

Germline transformation was carried out as described [106]. For rescue and heat-shock analysis, all *pqn-53* plasmids were injected at 20 ng/µl except *hsp16.2::pqn-53* at 10 ng/µl and *pSM::CEOP5320* injected at 5 ng/µl. *tag-168::GFP::UNC-2* and *tag-168::2xmEos2::UNC-2* were injected at 50ng/µl and 100 ng/µl, respectively. Relatively high levels of 2xmEos2::UNC-2 were needed for reliable visualization, and these overexpressed, tagged proteins might distort endogenous traffic. However, 2xmEos2::UNC-2 were able to rescue *unc-2*-dependent locomotion, and were reliably trafficked to synapses, indicating that the proteins in transgenic animals can interact effectively with the trafficking machinery.

For expression and localization experiments, *CEOP5320::GFP* fusion plasmids were injected at 5 ng/µl. *elt-2::mCherry, odr-1::mCherry* were used as a coinjection marker and injected at 6-20 ng/µl.

Isolation and characterization of *calf-2(ky977)*

A strain expressing GFP::UNC-2 in AWC *(kyIs442)* was mutagenized with EMS according to standard protocols [183]. 5 F1 animals were plated into each plate, and 30 to 50 F2 animals from the F1 animals were subjected to a direct visual screen under a compound microscope (F1 semi-clonal screen, total 1385 F1s were screened). The mutants were isolated based on the loss of GFP::UNC-2 puncta from the AWC axon as observed with a Plan Apochromat 63x objective on a Zeiss Axioplan2 microscope.

Mapping and cloning of *calf-2*

calf-2(ky977) was mapped to the middle of LGV using SNP polymorphisms in the CB4856 strain [184]. A genomic fragment containing the R07B7.3 and R07B7.1 reading frames with 1.4 kb of 5′ sequence and 0.8 kb of 3′ sequence (operon CEOP5320) was generated by PCR and cloned into pSM vector (see below for details). The plasmid was injected at 5 ng/µl into *calf-2(ky977)* mutants. The plasmid rescued both uncoordinated movements and GFP::UNC-2 localization in AWC axons. *calf-2(ky977)* and *clh-6(tm617)* null mutants complemented each other for the GFP::UNC-2 localization defect, suggesting that the *clh-6* is not involved in the UNC-2 phenotype. In addition, there was no detectable change in the mRNA expression level of *clh-6* in calf-2 mutants (mRNAseq, data not shown). To identify the *calf-2* mutation, the *pqn-53* genomic coding region in *ky977* was amplified by PCR, and PCR products were sequenced.

Fluorescence microscopy and quantification

Animals were mounted on 4% agarose pads containing 400 mM tetramisole. Multiple transgenic lines of each transgene were examined for fluorescent expression and localization patterns. Wide-field fluorescence images were obtained on Zeiss Axioplan2 imaging system (Fig. 4-1a-f, i-n; Fig. 4-2a-f, i,j; Fig. 4-3a,c; Fig. 4-5a-d; Fig. 4-6e,f; Fig. 4-7a-d).

To quantify fluorescence intensities and number of fluorescent clusters, images were captured under consistent detector settings with a Hamamatsu Photonics C2400 CCD camera on a Zeiss Axioplan2 Imaging System with a 63x Plan-Apochromat objective and Metamorph software. ImageJ (NIH) was used to quantify fluorescence in

AWC axons and cell bodies, DD dorsal axons, and AWA cilia. Images of AWC nerve rings and cell bodies and AWA cilia were projected into a single plane by maximum projection; for DD, a single image of best focus was chosen for the quantification. Background intensity was subtracted and fluorescent clusters containing signals above an arbitrary threshold were measured for the total fluorescence intensity and the number of fluorescent clusters. The same thresholds were used for all images in each quantification. Normalized fluorescence intensity was obtained by dividing individual values with mean total fluorescence intensity of wild-type control animals. For the perinuclear region of AWC, a single image of best focus was chosen for the quantification and maximum fluorescence intensity was measured after background subtraction. 6-10 animals were scored for each experiment.

Heat shock experiments

Experiments with *hsp16.2::pqn-53* were performed on L4 animals. A 30°C heat shock was given for 3 hours. The plates were then incubated at 20°C for 3 hours for recovery before scoring GFP::UNC-2 localization.

Photoconversion experiments

2xmEos2::UNC-2 was expressed under *tag-168* pan-neuronal promoter in *unc-2(lj1)* mutant background (extrachromosomal array *kyEx3522*), and *unc-2(lj1); kyEx3522* animals were crossed into *calf-2(ky977)* mutants to create *unc-2(lj1); calf-2(ky977); kyEx3522*. L4 larvae expressing 2xmEos2::UNC-2 were mounted on an agar pad. The head regions of individual animals were illuminated with UV light with a 63x Plan-

Apochromat objective to achieve local photoconversion (green to red conversion). We imaged the photoconverted 2xmEos2::UNC-2 at the nerve rings to estimate the turnover rate of UNC-2 at the synapses. After taking images from individual animals, animals were recovered on agar plates with OP50 for 6 hours and imaged again. Images of the nerve rings were projected into a single plane by maximum projection, and the total fluorescence intensity of the photoconverted 2xmEos2::UNC-2 was quantified after background fluorescence intensity subtraction. Individual animals were mounted on agar pads in the same orientation before and after heat shock to allow the comparison of the same nerve rings.

List of Strains and Transgenes

UNC-2 localization analysis

CX9275 kyIs442 [odr-3::GFP::unc-2, odr-3::mCherry::rab-3, ofm-1::GFP], CX10416 kyIs479 [unc-25::GFP::UNC-2, unc-25::mCherry::rab-3, odr-1::mCherry], CX10156 kyEx2328 [odr-3::GFP::unc-2, odr-3::syd-2::mCherry, ofm-1::DsRed], CX10157 kyEx2329 [odr-3::GFP::unc-2, odr-3::elks-1::mCherry, ofm-1::DsRed], CX12623 unc-2(lj1); kyEx3522 [tag-168::2xmEos2::unc-2], CX12670 calf-2(ky977); unc-2(lj1); kyEx3522 [tag-168::2xmEos2::unc-2], CX12620 kyEx3521 [hsp16.2::pqn-53, elt-2::mcherry], CX8874 unc-2(lj1); kyEx1671 [tag-168::GFP::UNC-2], CX12621 unc-2(lj1); calf-2(ky977); kyEx1671 line-1, CX12622 unc-2(lj1); calf-2(ky977); kyEx1671 line-2

ODR-10, SNB-1 localization analysis

CX3344 kyIs53 [AWA::odr-10::GFP], CX4010 juIs1 [unc-25::SNB-1::GFP]

pqn-53 rescue and overexpression experiments

CX11954 kyIs442; calf-2(ky977); kyEx3261 [tag-168::pqn-53, elt-2::mcherry], CX12442 kyIs442; calf-2(ky977); kyEx3460 [myo-3::pqn-53, elt-2::mcherry], CX12411 kyIs442; calf-2(ky977); kyEx3453 [odr-3::pqn-53, elt-2::mCherry], CX12270 kyIs442; calf-2(ky977); kyEx3401 [tag-168::unc-36, elt-2::mCherry], CX12411 kyIs442; calf-2(ky977); kyEx3459 [tag-168::calf-1, elt-2::mCherry], CX12113 calf-2(ky977); kyEx2828 [calf-1::GFP, odr-1::DsRed], CX12115 calf-2(ky977); kyEx1258 [unc-36::GFP, odr-1::DsRed], CX12743 kyIs442; calf-2(ky977); kyEx3580 [pSM::CEOP5320, elt-2::mCherry], CX12757 kyIs442; calf-2(ky977); kyEx3583 [odr-3::mCherry::pqn-53, elt-2::mCherry]

PQN-53 localization and expression

CX12811 kyEx3601 [CEOP5320::GFP, odr-1::mCherry]

Molecular Biology

mEos2 cDNA synthesis and tag-168::2xmEos2::unc-2

mEos cDNA was synthesized from ~50-mer oligonucleotides according to the GeneDesign protocol [187] with the substitution of PfuTurbo polymerase (Stratagene, La Jolla, CA) for ExTaq polymerase. mEos plasmid was sent to Loren Looger's lab for further mutagenesis to create mEos2. mEos2 transgene expression was increased by codon-optimizing the mEos2 sequence for *C. elegans* and adding synthetic intron sequences. The *tag-168::2xmEos2::unc-2* was constructed by insertion of the mEos2

cDNA into the N-terminus of *unc-2* at the NotI site in the *tag-168::unc-2* construct. *tag-168::2xmEos2::unc*-2 rescued the locomotory defect of *unc-2(lj1)* (data not shown).

pqn-53 cDNA cloning and GFP tagging

pqn-53 cDNA was obtained by PCR from *C. elegans* cDNA library using the following primers. cDNA sequences are shown in lower case.

5' NheI pqn-53c: GAATCGTAGCTAGCatggctgaaaaaatcaacatg

3' KpnI pqn-53c w/ Stop: GATTGGAAGGTACCttagaaggcacggaatccacg

The PCR product was ligated between NheI and KpnI in the pSM vector, and appropriate promoters were ligated between FseI and AscI. The *hsp16.2::pqn-53* plasmid was created by ligating *pqn-53* cDNA between NheI and KpnI in pPD49.78.

Operon CEOP5320 was amplified by PCR from *C. elegans* genomic DNA using the following primers:

5' NheI Pro, GAATCGTAGCTAGCccattcaatggtcaaggtgtcaattg

3' KpnI Pro1, GATTGGAAGGTACCctgaagcgttataatgattattaatt

The PCR product was ligated between NheI and KpnI in the pSM vector to create *pSM::CEOP5320*. *pSM::CEOP5320* rescued the GFP::UNC-2 expression defect phenotype of *calf-2(ky977).*

For GFP internal tagging, GFP was amplified by PCR from pSM::GFP using the following primers:

5' MluI GFP:

GAATCGTAacgcgtcATGAGTAAAGGAGAAGAACTTTTCACTGGA

3' MluI NoStop GFP:

GATTGGAAacgcgtTTGTATAGTTCATCCATGCCATGTGTAATCC

The PCR product was ligated at the MluI site in the second exon of *pqn-53* gene in frame, which precedes the glutamine-rich region, to create *CEOP5320::GFP*. When GFP was replaced with mCherry (*CEOP5320::mCherry*) the GFP::UNC-2 defect of *calf-2(ky977)* was partially rescued (three lines tested), indicating that this fusion retains some *calf-2* function (data not shown).

Construction of all other plasmids used in this study was previously described [160].

mRNAseq and RT-PCR

Animals were synchronized by bleaching gravid animals that were grown at 20°C. The eggs were thoroughly washed by M9 buffer and transferred to a new agar plate. The animals were incubated with OP50 at 20°C for 47 hours. L3/L4 mixed animals were collected and washed with M9 buffer, and total RNA was isolated using Trizol (Gibco). Construction of RNA-seq libraries was carried out following manufacture's protocols (Illumina: mRNA-Seq Sample Prep Kit). The cDNA templates were size-fractionated on 2% agarose gel, and the 200 bp fractions were excised. Cluster generation and sequencing was performed on the Illumina cluster station and Illumina GAIIx with Paired-end module following manufacturer's instructions. Paired-end sequences were extracted from the resulting image files using the onboard software application (SCS2.6) run with default parameters. Read lengths were 35 bases from both ends and average insertion size was 30bp. Reads were aligned to WS190 *C. elegans*

genome using Bowtie [193], and splice junctions were detected by TopHat [194]. Gene model used were downloaded from Ensembl. Ensembl Caenorhabditis_elegans.WS190.54.gtf.gz <ftp://ftp.ensembl.org/pub/release-54/gtf/caenorhabditis_elegans/Caenorhabditis_elegans.WS190.54.gtf.gz> ftp.ensembl.org/pub/release-54/gtf/caenorhabditis_elegans/. RPKM values were obtained using Cufflink (http://cufflinks.cbcb.umd.edu/). UCSC genome browser was used to visualize reads coverage, predicted splicing junctions and gene models.

For RT-PCR, poly(A)+ RNA was isolated from total RNA by using the oligotex mRNA kit (QIAGEN). We used the oligo-dT primers from the SuperScript III First-Strand Synthesis System (Invitrogen) to generate a cDNA template. PCR was performed to amplify full-length cDNAs by using following primers,

5' NheI *pqn-53*: GAATCGTAGCTAGCatggctgaaaaaatcaacatg

3' KpnI *pqn-53*: GATTGGAAGGTACCttagaaggcacggaatccacg

5' NheI *pqn-54c*: GAATCGTAGCTAGCatgcgcttcacctccctcgccattgc

3' KpnI Stop *pqn-54c*: GATTGGAAGGTACCtcactttcttctacagcactgtccat

5' NheI *pqn-74c*: GAATCGTAGCTAGCatggcgcgcttcctcctcattatcgg

3' KpnI Stop *pqn-74c*: GATTGGAAGGTACCttagaaacgacgggccttcttgcgga

5' NheI *abu-10c*: GAATCGTAGCTAGCatgttccgctctgcattttcaatttttg

3' KpnI Stop *abu-10c*: GATTGGAAGGTACCttaggcgatcgatcgctttgccttgc

*act-1*F: GTGTGACGACGAGGTTGCCGCTCTTGTTGTAGAC

*act-1*R: GGTAAGGATCTTCATGAGGTAATCAGTAAGATCAC

cDNA samples were 10-fold serially diluted three times. A total of 30 cycles were used

for PCR of *act-1* control primers. A total of 40 cycles were used for PCR of candidate genes. Cycle parameters used were 96°C 3min, "94°C 30sec, 60°C 30sec, 72°C 3min, (x the number of cycles)" 72°C 5min.

C. elegans Killing Assay

The *Escherichia coli* OP50 [189] and *Salmonella enterica* serovar Typhimurium 1344 [195]strains were used. Nematodes were maintained at 20°C on nematode growth medium (NGM, minimal medium containing NaCl, agar, peptone, cholesterol, CaCl2, MgSO4, and potassium phosphate [189]) that contains a lawn of OP50. Synchronous populations were obtained either by bleaching gravid animals or by placing gravid adults on NGM plates containing OP50 for 5 hours at 20°C. The gravid adults were removed, and the eggs were allowed to hatch and develop into young adults at 20°C.

Individual bacterial colonies were inoculated into LB and grown overnight on a rotary wheel at 26°C, and a drop of the LB was put on each NGM plate. Young adult hermaphrodites were transferred to lawns of the bacteria and transferred daily to a fresh lawn until progeny were no longer produced. All experiments were performed at 25°C. Animals were considered dead upon failure to respond to touch, and animals missing from the agar plate were censored on the day of loss.

Statistical Analysis

For fluorescent images, statistical analysis was performed using Student's unpaired t-test or Bonferroni t-test as appropriate.

References

1. Bidaud, I., Mezghrani, A., Swayne, L.A., Monteil, A. & Lory, P. Voltage-gated calcium channels in genetic diseases. *Biochim Biophys Acta* **1763**, 1169-1174 (2006).
2. Smith, L.A.*, et al.* A Drosophila calcium channel alpha1 subunit gene maps to a genetic locus associated with behavioral and visual defects. *J Neurosci* **16**, 7868-7879 (1996).
3. Mathews, E.A.*, et al.* Critical residues of the Caenorhabditis elegans unc-2 voltage-gated calcium channel that affect behavioral and physiological properties. *J Neurosci* **23**, 6537-6545 (2003).
4. Vaughn, J.E. Fine structure of synaptogenesis in the vertebrate central nervous system. *Synapse* **3**, 255-285 (1989).
5. Couteaux, R. The Differentiation of Synaptic Areas. *Proc R Soc Lond B Biol Sci* **158**, 457-480 (1963).
6. Jin, Y. & Garner, C.C. Molecular mechanisms of presynaptic differentiation. *Annu Rev Cell Dev Biol* **24**, 237-262 (2008).
7. Pielage, J.*, et al.* A presynaptic giant ankyrin stabilizes the NMJ through regulation of presynaptic microtubules and transsynaptic cell adhesion. *Neuron* **58**, 195-209 (2008).
8. Kittel, R.J.*, et al.* Bruchpilot promotes active zone assembly, Ca2+ channel clustering, and vesicle release. *Science* **312**, 1051-1054 (2006).
9. Biederer, T. & Stagi, M. Signaling by synaptogenic molecules. *Curr Opin Neurobiol* **18**, 261-269 (2008).
10. Gerrow, K. & El-Husseini, A. Cell adhesion molecules at the synapse. *Front Biosci* **11**, 2400-2419 (2006).
11. Scheiffele, P., Fan, J., Choih, J., Fetter, R. & Serafini, T. Neuroligin expressed in nonneuronal cells triggers presynaptic development in contacting axons. *Cell* **101**, 657-669 (2000).
12. Biederer, T.*, et al.* SynCAM, a synaptic adhesion molecule that drives synapse assembly. *Science* **297**, 1525-1531 (2002).
13. Varoqueaux, F.*, et al.* Neuroligins determine synapse maturation and function. *Neuron* **51**, 741-754 (2006).
14. Li, J., Ashley, J., Budnik, V. & Bhat, M.A. Crucial role of Drosophila neurexin in proper active zone apposition to postsynaptic densities, synaptic growth, and synaptic transmission. *Neuron* **55**, 741-755 (2007).
15. Zeng, X.*, et al.* Neurexin-1 is required for synapse formation and larvae associative learning in Drosophila. *FEBS Lett* **581**, 2509-2516 (2007).
16. Missler, M.*, et al.* Alpha-neurexins couple Ca2+ channels to synaptic vesicle exocytosis. *Nature* **423**, 939-948 (2003).
17. Hall, A.C., Lucas, F.R. & Salinas, P.C. Axonal remodeling and synaptic differentiation in the cerebellum is regulated by WNT-7a signaling. *Cell* **100**, 525-535 (2000).
18. Ahmad-Annuar, A.*, et al.* Signaling across the synapse: a role for Wnt and Dishevelled in presynaptic assembly and neurotransmitter release. *J Cell Biol* **174**, 127-139 (2006).

19. Umemori, H., Linhoff, M.W., Ornitz, D.M. & Sanes, J.R. FGF22 and its close relatives are presynaptic organizing molecules in the mammalian brain. *Cell* **118**, 257-270 (2004).
20. Christopherson, K.S.*, et al.* Thrombospondins are astrocyte-secreted proteins that promote CNS synaptogenesis. *Cell* **120**, 421-433 (2005).
21. Butz, S., Okamoto, M. & Sudhof, T.C. A tripartite protein complex with the potential to couple synaptic vesicle exocytosis to cell adhesion in brain. *Cell* **94**, 773-782 (1998).
22. Shen, K. & Bargmann, C.I. The immunoglobulin superfamily protein SYG-1 determines the location of specific synapses in C. elegans. *Cell* **112**, 619-630 (2003).
23. Shen, K., Fetter, R.D. & Bargmann, C.I. Synaptic specificity is generated by the synaptic guidepost protein SYG-2 and its receptor, SYG-1. *Cell* **116**, 869-881 (2004).
24. Patel, M.R.*, et al.* Hierarchical assembly of presynaptic components in defined C. elegans synapses. *Nat Neurosci* **9**, 1488-1498 (2006).
25. Crump, J.G., Zhen, M., Jin, Y. & Bargmann, C.I. The SAD-1 kinase regulates presynaptic vesicle clustering and axon termination. *Neuron* **29**, 115-129 (2001).
26. Zhen, M. & Jin, Y. The liprin protein SYD-2 regulates the differentiation of presynaptic termini in C. elegans. *Nature* **401**, 371-375 (1999).
27. Zhen, M., Huang, X., Bamber, B. & Jin, Y. Regulation of presynaptic terminal organization by C. elegans RPM-1, a putative guanine nucleotide exchanger with a RING-H2 finger domain. *Neuron* **26**, 331-343 (2000).
28. Hallam, S.J., Goncharov, A., McEwen, J., Baran, R. & Jin, Y. SYD-1, a presynaptic protein with PDZ, C2 and rhoGAP-like domains, specifies axon identity in C. elegans. *Nat Neurosci* **5**, 1137-1146 (2002).
29. Liao, E.H., Hung, W., Abrams, B. & Zhen, M. An SCF-like ubiquitin ligase complex that controls presynaptic differentiation. *Nature* **430**, 345-350 (2004).
30. Nakata, K.*, et al.* Regulation of a DLK-1 and p38 MAP kinase pathway by the ubiquitin ligase RPM-1 is required for presynaptic development. *Cell* **120**, 407-420 (2005).
31. Patel, M.R. & Shen, K. RSY-1 is a local inhibitor of presynaptic assembly in C. elegans. *Science* **323**, 1500-1503 (2009).
32. Colon-Ramos, D.A., Margeta, M.A. & Shen, K. Glia promote local synaptogenesis through UNC-6 (netrin) signaling in C. elegans. *Science* **318**, 103-106 (2007).
33. Meyer, M.P., Niell, C.M. & Smith, S.J. Brain imaging: how stable are synaptic connections? *Curr Biol* **13**, R180-182 (2003).
34. Sankaranarayanan, S., Atluri, P.P. & Ryan, T.A. Actin has a molecular scaffolding, not propulsive, role in presynaptic function. *Nat Neurosci* **6**, 127-135 (2003).
35. Kalla, S.*, et al.* Molecular dynamics of a presynaptic active zone protein studied in Munc13-1-enhanced yellow fluorescent protein knock-in mutant mice. *J Neurosci* **26**, 13054-13066 (2006).
36. Inaki, M., Yoshikawa, S., Thomas, J.B., Aburatani, H. & Nose, A. Wnt4 is a local repulsive cue that determines synaptic target specificity. *Curr Biol* **17**, 1574-1579 (2007).
37. Klassen, M.P. & Shen, K. Wnt signaling positions neuromuscular connectivity by inhibiting synapse formation in C. elegans. *Cell* **130**, 704-716 (2007).

38. Poon, V.Y., Klassen, M.P. & Shen, K. UNC-6/netrin and its receptor UNC-5 locally exclude presynaptic components from dendrites. *Nature* **455**, 669-673 (2008).
39. Stevens, B.*, et al.* The classical complement cascade mediates CNS synapse elimination. *Cell* **131**, 1164-1178 (2007).
40. Ding, M., Chao, D., Wang, G. & Shen, K. Spatial regulation of an E3 ubiquitin ligase directs selective synapse elimination. *Science* **317**, 947-951 (2007).
41. Yao, I.*, et al.* SCRAPPER-dependent ubiquitination of active zone protein RIM1 regulates synaptic vesicle release. *Cell* **130**, 943-957 (2007).
42. van Roessel, P., Elliott, D.A., Robinson, I.M., Prokop, A. & Brand, A.H. Independent regulation of synaptic size and activity by the anaphase-promoting complex. *Cell* **119**, 707-718 (2004).
43. Wheeler, T.C., Chin, L.S., Li, Y., Roudabush, F.L. & Li, L. Regulation of synaptophysin degradation by mammalian homologues of seven in absentia. *J Biol Chem* **277**, 10273-10282 (2002).
44. Chin, L.S., Vavalle, J.P. & Li, L. Staring, a novel E3 ubiquitin-protein ligase that targets syntaxin 1 for degradation. *J Biol Chem* **277**, 35071-35079 (2002).
45. Malinow, R. & Malenka, R.C. AMPA receptor trafficking and synaptic plasticity. *Annu Rev Neurosci* **25**, 103-126 (2002).
46. Rongo, C., Whitfield, C.W., Rodal, A., Kim, S.K. & Kaplan, J.M. LIN-10 is a shared component of the polarized protein localization pathways in neurons and epithelia. *Cell* **94**, 751-759 (1998).
47. Burbea, M., Dreier, L., Dittman, J.S., Grunwald, M.E. & Kaplan, J.M. Ubiquitin and AP180 regulate the abundance of GLR-1 glutamate receptors at postsynaptic elements in C. elegans. *Neuron* **35**, 107-120 (2002).
48. Rongo, C. & Kaplan, J.M. CaMKII regulates the density of central glutamatergic synapses in vivo. *Nature* **402**, 195-199 (1999).
49. Dreier, L., Burbea, M. & Kaplan, J.M. LIN-23-mediated degradation of beta-catenin regulates the abundance of GLR-1 glutamate receptors in the ventral nerve cord of C. elegans. *Neuron* **46**, 51-64 (2005).
50. Chun, D.K., McEwen, J.M., Burbea, M. & Kaplan, J.M. UNC-108/Rab2 regulates postendocytic trafficking in Caenorhabditis elegans. *Mol Biol Cell* **19**, 2682-2695 (2008).
51. Grunwald, M.E. & Kaplan, J.M. Mutations in the ligand-binding and pore domains control exit of glutamate receptors from the endoplasmic reticulum in C. elegans. *Neuropharmacology* **45**, 768-776 (2003).
52. Juo, P., Harbaugh, T., Garriga, G. & Kaplan, J.M. CDK-5 regulates the abundance of GLR-1 glutamate receptors in the ventral cord of Caenorhabditis elegans. *Mol Biol Cell* **18**, 3883-3893 (2007).
53. Catterall, W.A. Structure and regulation of voltage-gated Ca2+ channels. *Annu Rev Cell Dev Biol* **16**, 521-555 (2000).
54. Arikkath, J. & Campbell, K.P. Auxiliary subunits: essential components of the voltage-gated calcium channel complex. *Curr Opin Neurobiol* **13**, 298-307 (2003).
55. Jeziorski, M.C., Greenberg, R.M. & Anderson, P.A. The molecular biology of invertebrate voltage-gated Ca(2+) channels. *J Exp Biol* **203**, 841-856 (2000).
56. Brooks, I.M., Felling, R., Kawasaki, F. & Ordway, R.W. Genetic analysis of a synaptic calcium channel in Drosophila: intragenic modifiers of a temperature-sensitive paralytic mutant of cacophony. *Genetics* **164**, 163-171 (2003).

57. Kawasaki, F., Zou, B., Xu, X. & Ordway, R.W. Active zone localization of presynaptic calcium channels encoded by the cacophony locus of Drosophila. *J Neurosci* **24**, 282-285 (2004).
58. Schafer, W.R. & Kenyon, C.J. A calcium-channel homologue required for adaptation to dopamine and serotonin in Caenorhabditis elegans. *Nature* **375**, 73-78 (1995).
59. Richmond, J.E., Weimer, R.M. & Jorgensen, E.M. An open form of syntaxin bypasses the requirement for UNC-13 in vesicle priming. *Nature* **412**, 338-341 (2001).
60. Hell, J.W.*, et al.* Identification and differential subcellular localization of the neuronal class C and class D L-type calcium channel alpha 1 subunits. *J Cell Biol* **123**, 949-962 (1993).
61. Westenbroek, R.E.*, et al.* Biochemical properties and subcellular distribution of an N-type calcium channel alpha 1 subunit. *Neuron* **9**, 1099-1115 (1992).
62. Llinas, R., Sugimori, M., Hillman, D.E. & Cherksey, B. Distribution and functional significance of the P-type, voltage-dependent Ca2+ channels in the mammalian central nervous system. *Trends Neurosci* **15**, 351-355 (1992).
63. Trimmer, J.S. & Rhodes, K.J. Localization of voltage-gated ion channels in mammalian brain. *Annu Rev Physiol* **66**, 477-519 (2004).
64. Bech-Hansen, N.T.*, et al.* Loss-of-function mutations in a calcium-channel alpha1-subunit gene in Xp11.23 cause incomplete X-linked congenital stationary night blindness. *Nat Genet* **19**, 264-267 (1998).
65. Platzer, J.*, et al.* Congenital deafness and sinoatrial node dysfunction in mice lacking class D L-type Ca2+ channels. *Cell* **102**, 89-97 (2000).
66. Maximov, A. & Bezprozvanny, I. Synaptic targeting of N-type calcium channels in hippocampal neurons. *J Neurosci* **22**, 6939-6952 (2002).
67. Canti, C.*, et al.* The metal-ion-dependent adhesion site in the Von Willebrand factor-A domain of alpha2delta subunits is key to trafficking voltage-gated Ca2+ channels. *Proc Natl Acad Sci U S A* **102**, 11230-11235 (2005).
68. Dickman, D.K., Kurshan, P.T. & Schwarz, T.L. Mutations in a Drosophila alpha2delta voltage-gated calcium channel subunit reveal a crucial synaptic function. *J Neurosci* **28**, 31-38 (2008).
69. Ly, C.V., Yao, C.K., Verstreken, P., Ohyama, T. & Bellen, H.J. straightjacket is required for the synaptic stabilization of cacophony, a voltage-gated calcium channel alpha1 subunit. *J Cell Biol* **181**, 157-170 (2008).
70. Bichet, D.*, et al.* The I-II loop of the Ca2+ channel alpha1 subunit contains an endoplasmic reticulum retention signal antagonized by the beta subunit. *Neuron* **25**, 177-190 (2000).
71. Viard, P.*, et al.* PI3K promotes voltage-dependent calcium channel trafficking to the plasma membrane. *Nat Neurosci* **7**, 939-946 (2004).
72. Nishimune, H., Sanes, J.R. & Carlson, S.S. A synaptic laminin-calcium channel interaction organizes active zones in motor nerve terminals. *Nature* **432**, 580-587 (2004).
73. Bahls, F.H.*, et al.* Contact-dependent regulation of N-type calcium channel subunits during synaptogenesis. *J Neurobiol* **35**, 198-208 (1998).
74. Long, A.A.*, et al.* Presynaptic calcium channel localization and calcium-dependent synaptic vesicle exocytosis regulated by the Fuseless protein. *J Neurosci* **28**, 3668-3682 (2008).

75. Lai, M.*, et al.* A tctex1-Ca2+ channel complex for selective surface expression of Ca2+ channels in neurons. *Nat Neurosci* **8**, 435-442 (2005).
76. Maximov, A., Sudhof, T.C. & Bezprozvanny, I. Association of neuronal calcium channels with modular adaptor proteins. *J Biol Chem* **274**, 24453-24456 (1999).
77. Atasoy, D.*, et al.* Deletion of CASK in mice is lethal and impairs synaptic function. *Proc Natl Acad Sci U S A* **104**, 2525-2530 (2007).
78. Ho, A.*, et al.* Genetic analysis of Mint/X11 proteins: essential presynaptic functions of a neuronal adaptor protein family. *J Neurosci* **26**, 13089-13101 (2006).
79. Olsen, O.*, et al.* Neurotransmitter release regulated by a MALS-liprin-alpha presynaptic complex. *J Cell Biol* **170**, 1127-1134 (2005).
80. Littleton, J.T. & Ganetzky, B. Ion channels and synaptic organization: analysis of the Drosophila genome. *Neuron* **26**, 35-43 (2000).
81. Bargmann, C.I. Neurobiology of the Caenorhabditis elegans genome. *Science* **282**, 2028-2033 (1998).
82. Mochida, S.*, et al.* Requirement for the synaptic protein interaction site for reconstitution of synaptic transmission by P/Q-type calcium channels. *Proc Natl Acad Sci U S A* **100**, 2819-2824 (2003).
83. Szabo, Z., Obermair, G.J., Cooper, C.B., Zamponi, G.W. & Flucher, B.E. Role of the synprint site in presynaptic targeting of the calcium channel CaV2.2 in hippocampal neurons. *Eur J Neurosci* **24**, 709-718 (2006).
84. Spafford, J.D.*, et al.* Calcium channel structural determinants of synaptic transmission between identified invertebrate neurons. *J Biol Chem* **278**, 4258-4267 (2003).
85. Spafford, J.D. & Zamponi, G.W. Functional interactions between presynaptic calcium channels and the neurotransmitter release machinery. *Curr Opin Neurobiol* **13**, 308-314 (2003).
86. Goodman, M.B., Hall, D.H., Avery, L. & Lockery, S.R. Active currents regulate sensitivity and dynamic range in C. elegans neurons. *Neuron* **20**, 763-772 (1998).
87. Lee, R.Y., Lobel, L., Hengartner, M., Horvitz, H.R. & Avery, L. Mutations in the alpha1 subunit of an L-type voltage-activated Ca2+ channel cause myotonia in Caenorhabditis elegans. *Embo J* **16**, 6066-6076 (1997).
88. Suzuki, H.*, et al.* In vivo imaging of C. elegans mechanosensory neurons demonstrates a specific role for the MEC-4 channel in the process of gentle touch sensation. *Neuron* **39**, 1005-1017 (2003).
89. Hilliard, M.A.*, et al.* In vivo imaging of C. elegans ASH neurons: cellular response and adaptation to chemical repellents. *Embo J* **24**, 63-72 (2005).
90. Hall, D.H. & Hedgecock, E.M. Kinesin-related gene unc-104 is required for axonal transport of synaptic vesicles in C. elegans. *Cell* **65**, 837-847 (1991).
91. Frokjaer-Jensen, C.*, et al.* Effects of voltage-gated calcium channel subunit genes on calcium influx in cultured C. elegans mechanosensory neurons. *J Neurobiol* **66**, 1125-1139 (2006).
92. Bauer Huang, S.L.*, et al.* Left-right olfactory asymmetry results from antagonistic functions of voltage-activated calcium channels and the Raw repeat protein OLRN-1 in C. elegans. *Neural Develop* **2**, 24 (2007).

93. Schaefer, A.M., Hadwiger, G.D. & Nonet, M.L. rpm-1, a conserved neuronal gene that regulates targeting and synaptogenesis in C. elegans. *Neuron* **26**, 345-356 (2000).
94. Pan, C.L.*, et al.* C. elegans AP-2 and retromer control Wnt signaling by regulating mig-14/Wntless. *Dev Cell* **14**, 132-139 (2008).
95. Charlie, N.K., Schade, M.A., Thomure, A.M. & Miller, K.G. Presynaptic UNC-31 (CAPS) is required to activate the G alpha(s) pathway of the Caenorhabditis elegans synaptic signaling network. *Genetics* **172**, 943-961 (2006).
96. Richmond, J.E., Davis, W.S. & Jorgensen, E.M. UNC-13 is required for synaptic vesicle fusion in C. elegans. *Nat Neurosci* **2**, 959-964 (1999).
97. Koushika, S.P.*, et al.* A post-docking role for active zone protein Rim. *Nat Neurosci* **4**, 997-1005 (2001).
98. Lee, J., Jongeward, G.D. & Sternberg, P.W. unc-101, a gene required for many aspects of Caenorhabditis elegans development and behavior, encodes a clathrin-associated protein. *Genes Dev* **8**, 60-73 (1994).
99. Dwyer, N.D., Adler, C.E., Crump, J.G., L'Etoile, N.D. & Bargmann, C.I. Polarized dendritic transport and the AP-1 mu1 clathrin adaptor UNC-101 localize odorant receptors to olfactory cilia. *Neuron* **31**, 277-287 (2001).
100. Whitfield, C.W., Benard, C., Barnes, T., Hekimi, S. & Kim, S.K. Basolateral localization of the Caenorhabditis elegans epidermal growth factor receptor in epithelial cells by the PDZ protein LIN-10. *Mol Biol Cell* **10**, 2087-2100 (1999).
101. Rolls, M.M., Hall, D.H., Victor, M., Stelzer, E.H. & Rapoport, T.A. Targeting of rough endoplasmic reticulum membrane proteins and ribosomes in invertebrate neurons. *Mol Biol Cell* **13**, 1778-1791 (2002).
102. Chalasani, S.H.*, et al.* Dissecting a circuit for olfactory behaviour in Caenorhabditis elegans. *Nature* **450**, 63-70 (2007).
103. Zerangue, N., Schwappach, B., Jan, Y.N. & Jan, L.Y. A new ER trafficking signal regulates the subunit stoichiometry of plasma membrane K(ATP) channels. *Neuron* **22**, 537-548 (1999).
104. Schwappach, B., Zerangue, N., Jan, Y.N. & Jan, L.Y. Molecular basis for K(ATP) assembly: transmembrane interactions mediate association of a K+ channel with an ABC transporter. *Neuron* **26**, 155-167 (2000).
105. Troemel, E.R., Sagasti, A. & Bargmann, C.I. Lateral signaling mediated by axon contact and calcium entry regulates asymmetric odorant receptor expression in C. elegans. *Cell* **99**, 387-398 (1999).
106. Mello, C. & Fire, A. DNA transformation. *Methods Cell Biol* **48**, 451-482 (1995).
107. Chudakov, D.M., Lukyanov, S. & Lukyanov, K.A. Tracking intracellular protein movements using photoswitchable fluorescent proteins PS-CFP2 and Dendra2. *Nat Protoc* **2**, 2024-2032 (2007).
108. Yeh, E.*, et al.* A putative cation channel, NCA-1, and a novel protein, UNC-80, transmit neuronal activity in C. elegans. *PLoS Biol* **6**, e55 (2008).
109. Grunwald, M.E., Mellem, J.E., Strutz, N., Maricq, A.V. & Kaplan, J.M. Clathrin-mediated endocytosis is required for compensatory regulation of GLR-1 glutamate receptors after activity blockade. *Proc Natl Acad Sci U S A* **101**, 3190-3195 (2004).
110. Schwappach, B. An overview of trafficking and assembly of neurotransmitter receptors and ion channels (Review). *Mol Membr Biol* **25**, 270-278 (2008).

111. Hendrich, J.*, et al.* Pharmacological disruption of calcium channel trafficking by the alpha2delta ligand gabapentin. *Proc Natl Acad Sci U S A* **105**, 3628-3633 (2008).
112. Herrmann, J.M., Malkus, P. & Schekman, R. Out of the ER--outfitters, escorts and guides. *Trends Cell Biol* **9**, 5-7 (1999).
113. Fromme, J.C., Orci, L. & Schekman, R. Coordination of COPII vesicle trafficking by Sec23. *Trends Cell Biol* **18**, 330-336 (2008).
114. Kota, J. & Ljungdahl, P.O. Specialized membrane-localized chaperones prevent aggregation of polytopic proteins in the ER. *J Cell Biol* **168**, 79-88 (2005).
115. Michelsen, K., Yuan, H. & Schwappach, B. Hide and run. Arginine-based endoplasmic-reticulum-sorting motifs in the assembly of heteromultimeric membrane proteins. *EMBO Rep* **6**, 717-722 (2005).
116. Schutze, M.P., Peterson, P.A. & Jackson, M.R. An N-terminal double-arginine motif maintains type II membrane proteins in the endoplasmic reticulum. *Embo J* **13**, 1696-1705 (1994).
117. Chuang, C.F., Vanhoven, M.K., Fetter, R.D., Verselis, V.K. & Bargmann, C.I. An innexin-dependent cell network establishes left-right neuronal asymmetry in C. elegans. *Cell* **129**, 787-799 (2007).
118. Troemel, E.R., Chou, J.H., Dwyer, N.D., Colbert, H.A. & Bargmann, C.I. Divergent seven transmembrane receptors are candidate chemosensory receptors in C. elegans. *Cell* **83**, 207-218 (1995).
119. Vanhoven, M.K., Bauer Huang, S.L., Albin, S.D. & Bargmann, C.I. The claudin superfamily protein nsy-4 biases lateral signaling to generate left-right asymmetry in C. elegans olfactory neurons. *Neuron* **51**, 291-302 (2006).
120. Pierce-Shimomura, J.T., Faumont, S., Gaston, M.R., Pearson, B.J. & Lockery, S.R. The homeobox gene lim-6 is required for distinct chemosensory representations in C. elegans. *Nature* **410**, 694-698 (2001).
121. Yu, S., Avery, L., Baude, E. & Garbers, D.L. Guanylyl cyclase expression in specific sensory neurons: a new family of chemosensory receptors. *Proc Natl Acad Sci U S A* **94**, 3384-3387 (1997).
122. Johnston, R.J., Jr., Chang, S., Etchberger, J.F., Ortiz, C.O. & Hobert, O. MicroRNAs acting in a double-negative feedback loop to control a neuronal cell fate decision. *Proc Natl Acad Sci U S A* **102**, 12449-12454 (2005).
123. Wes, P.D. & Bargmann, C.I. C. elegans odour discrimination requires asymmetric diversity in olfactory neurons. *Nature* **410**, 698-701 (2001).
124. Torayama, I., Ishihara, T. & Katsura, I. Caenorhabditis elegans integrates the signals of butanone and food to enhance chemotaxis to butanone. *J Neurosci* **27**, 741-750 (2007).
125. Heitzler, P. & Simpson, P. The choice of cell fate in the epidermis of Drosophila. *Cell* **64**, 1083-1092 (1991).
126. Chuang, C.F. & Bargmann, C.I. A Toll-interleukin 1 repeat protein at the synapse specifies asymmetric odorant receptor expression via ASK1 MAPKKK signaling. *Genes Dev* **19**, 270-281 (2005).
127. Sagasti, A.*, et al.* The CaMKII UNC-43 activates the MAPKKK NSY-1 to execute a lateral signaling decision required for asymmetric olfactory neuron fates. *Cell* **105**, 221-232 (2001).

128. Tanaka-Hino, M.*, et al.* SEK-1 MAPKK mediates Ca2+ signaling to determine neuronal asymmetric development in Caenorhabditis elegans. *EMBO Rep* **3**, 56-62 (2002).
129. Colosimo, M.E.*, et al.* Identification of thermosensory and olfactory neuron-specific genes via expression profiling of single neuron types. *Curr Biol* **14**, 2245-2251 (2004).
130. Schwarz, E.M.*, et al.* WormBase: better software, richer content. *Nucleic Acids Res* **34**, D475-478 (2006).
131. Shaner, N.C.*, et al.* Improved monomeric red, orange and yellow fluorescent proteins derived from Discosoma sp. red fluorescent protein. *Nat Biotechnol* **22**, 1567-1572 (2004).
132. Byars, C.L., Bates, K.L. & Letsou, A. The dorsal-open group gene raw is required for restricted DJNK signaling during closure. *Development* **126**, 4913-4923 (1999).
133. Kerr, R.*, et al.* Optical imaging of calcium transients in neurons and pharyngeal muscle of C. elegans. *Neuron* **26**, 583-594 (2000).
134. Jack, J. & Myette, G. The genes raw and ribbon are required for proper shape of tubular epithelial tissues in Drosophila. *Genetics* **147**, 243-253 (1997).
135. Kojima, T.*, et al.* Cx32 formation and/or Cx32-mediated intercellular communication induces expression and function of tight junctions in hepatocytic cell line. *Exp Cell Res* **276**, 40-51 (2002).
136. Davies, A.G.*, et al.* A central role of the BK potassium channel in behavioral responses to ethanol in C. elegans. *Cell* **115**, 655-666 (2003).
137. Irisawa, H., Brown, H.F. & Giles, W. Cardiac pacemaking in the sinoatrial node. *Physiol Rev* **73**, 197-227 (1993).
138. Verheijck, E.E.*, et al.* Pacemaker synchronization of electrically coupled rabbit sinoatrial node cells. *J Gen Physiol* **111**, 95-112 (1998).
139. Thomas, A.P., Bird, G.S., Hajnoczky, G., Robb-Gaspers, L.D. & Putney, J.W., Jr. Spatial and temporal aspects of cellular calcium signaling. *FASEB J* **10**, 1505-1517 (1996).
140. West, A.E.*, et al.* Calcium regulation of neuronal gene expression. *Proc Natl Acad Sci U S A* **98**, 11024-11031 (2001).
141. Brizuela, B.J., Wessely, O. & De Robertis, E.M. Overexpression of the Xenopus tight-junction protein claudin causes randomization of the left-right body axis. *Dev Biol* **230**, 217-229 (2001).
142. Levin, M. & Mercola, M. Gap junctions are involved in the early generation of left-right asymmetry. *Dev Biol* **203**, 90-105 (1998).
143. Levin, M., Thorlin, T., Robinson, K.R., Nogi, T. & Mercola, M. Asymmetries in H+/K+-ATPase and cell membrane potentials comprise a very early step in left-right patterning. *Cell* **111**, 77-89 (2002).
144. Knecht, S.*, et al.* Handedness and hemispheric language dominance in healthy humans. *Brain* **123 Pt 12**, 2512-2518 (2000).
145. Bien, C.G.*, et al.* Pathogenesis, diagnosis and treatment of Rasmussen encephalitis: a European consensus statement. *Brain* **128**, 454-471 (2005).
146. Ophoff, R.A.*, et al.* Familial hemiplegic migraine and episodic ataxia type-2 are caused by mutations in the Ca2+ channel gene CACNL1A4. *Cell* **87**, 543-552 (1996).
147. Ellgaard, L. & Helenius, A. Quality control in the endoplasmic reticulum. *Nat Rev Mol Cell Biol* **4**, 181-191 (2003).

148. Ma, D. & Jan, L.Y. ER transport signals and trafficking of potassium channels and receptors. *Curr Opin Neurobiol* **12**, 287-292 (2002).
149. Taylor, S.C., Ferguson, A.D., Bergeron, J.J. & Thomas, D.Y. The ER protein folding sensor UDP-glucose glycoprotein-glucosyltransferase modifies substrates distant to local changes in glycoprotein conformation. *Nat Struct Mol Biol* **11**, 128-134 (2004).
150. Anelli, T. & Sitia, R. Protein quality control in the early secretory pathway. *EMBO J* **27**, 315-327 (2008).
151. Ron, D. & Walter, P. Signal integration in the endoplasmic reticulum unfolded protein response. *Nat Rev Mol Cell Biol* **8**, 519-529 (2007).
152. Hollien, J.*, et al.* Regulated Ire1-dependent decay of messenger RNAs in mammalian cells. *J Cell Biol* **186**, 323-331 (2009).
153. Kopito, R.R. Biosynthesis and degradation of CFTR. *Physiol Rev* **79**, S167-173 (1999).
154. Shen, X.*, et al.* Complementary signaling pathways regulate the unfolded protein response and are required for C. elegans development. *Cell* **107**, 893-903 (2001).
155. Richardson, C.E., Kooistra, T. & Kim, D.H. An essential role for XBP-1 in host protection against immune activation in C. elegans. *Nature* **463**, 1092-1095.
156. Urano, F.*, et al.* A survival pathway for Caenorhabditis elegans with a blocked unfolded protein response. *J Cell Biol* **158**, 639-646 (2002).
157. Shim, J., Umemura, T., Nothstein, E. & Rongo, C. The unfolded protein response regulates glutamate receptor export from the endoplasmic reticulum. *Mol Biol Cell* **15**, 4818-4828 (2004).
158. Michelitsch, M.D. & Weissman, J.S. A census of glutamine/asparagine-rich regions: implications for their conserved function and the prediction of novel prions. *Proc Natl Acad Sci U S A* **97**, 11910-11915 (2000).
159. Bianchi, L., Miller, D.M., 3rd & George, A.L., Jr. Expression of a CIC chloride channel in Caenorhabditis elegans gamma-aminobutyric acid-ergic neurons. *Neurosci Lett* **299**, 177-180 (2001).
160. Saheki, Y. & Bargmann, C.I. Presynaptic CaV2 calcium channel traffic requires CALF-1 and the alpha(2)delta subunit UNC-36. *Nat Neurosci* **12**, 1257-1265 (2009).
161. McKinney, S.A., Murphy, C.S., Hazelwood, K.L., Davidson, M.W. & Looger, L.L. A bright and photostable photoconvertible fluorescent protein. *Nat Methods* **6**, 131-133 (2009).
162. Hillier, L.W.*, et al.* Massively parallel sequencing of the polyadenylated transcriptome of C. elegans. *Genome Res* **19**, 657-666 (2009).
163. Wang, Z., Gerstein, M. & Snyder, M. RNA-Seq: a revolutionary tool for transcriptomics. *Nat Rev Genet* **10**, 57-63 (2009).
164. Huang da, W., Sherman, B.T. & Lempicki, R.A. Systematic and integrative analysis of large gene lists using DAVID bioinformatics resources. *Nat Protoc* **4**, 44-57 (2009).
165. Haskins, K.A., Russell, J.F., Gaddis, N., Dressman, H.K. & Aballay, A. Unfolded protein response genes regulated by CED-1 are required for Caenorhabditis elegans innate immunity. *Dev Cell* **15**, 87-97 (2008).
166. Zhou, Z., Hartwieg, E. & Horvitz, H.R. CED-1 is a transmembrane receptor that mediates cell corpse engulfment in C. elegans. *Cell* **104**, 43-56 (2001).

167. Todd, D.J., Lee, A.H. & Glimcher, L.H. The endoplasmic reticulum stress response in immunity and autoimmunity. *Nat Rev Immunol* **8**, 663-674 (2008).
168. Bischof, L.J.*, et al.* Activation of the unfolded protein response is required for defenses against bacterial pore-forming toxin in vivo. *PLoS Pathog* **4**, e1000176 (2008).
169. Calfon, M.*, et al.* IRE1 couples endoplasmic reticulum load to secretory capacity by processing the XBP-1 mRNA. *Nature* **415**, 92-96 (2002).
170. Vembar, S.S. & Brodsky, J.L. One step at a time: endoplasmic reticulum-associated degradation. *Nat Rev Mol Cell Biol* **9**, 944-957 (2008).
171. Viswanathan, M., Kim, S.K., Berdichevsky, A. & Guarente, L. A role for SIR-2.1 regulation of ER stress response genes in determining C. elegans life span. *Dev Cell* **9**, 605-615 (2005).
172. Gravato-Nobre, M.J. & Hodgkin, J. Caenorhabditis elegans as a model for innate immunity to pathogens. *Cell Microbiol* **7**, 741-751 (2005).
173. Irazoqui, J.E., Urbach, J.M. & Ausubel, F.M. Evolution of host innate defence: insights from Caenorhabditis elegans and primitive invertebrates. *Nat Rev Immunol* **10**, 47-58.
174. Kim, D.H.*, et al.* A conserved p38 MAP kinase pathway in Caenorhabditis elegans innate immunity. *Science* **297**, 623-626 (2002).
175. Kim, D.H.*, et al.* Integration of Caenorhabditis elegans MAPK pathways mediating immunity and stress resistance by MEK-1 MAPK kinase and VHP-1 MAPK phosphatase. *Proc Natl Acad Sci U S A* **101**, 10990-10994 (2004).
176. Powell, J.R., Kim, D.H. & Ausubel, F.M. The G protein-coupled receptor FSHR-1 is required for the Caenorhabditis elegans innate immune response. *Proc Natl Acad Sci U S A* **106**, 2782-2787 (2009).
177. Means, T.K.*, et al.* Evolutionarily conserved recognition and innate immunity to fungal pathogens by the scavenger receptors SCARF1 and CD36. *J Exp Med* **206**, 637-653 (2009).
178. Sudarsanam, P., Iyer, V.R., Brown, P.O. & Winston, F. Whole-genome expression analysis of snf/swi mutants of Saccharomyces cerevisiae. *Proc Natl Acad Sci U S A* **97**, 3364-3369 (2000).
179. Du, Z., Park, K.W., Yu, H., Fan, Q. & Li, L. Newly identified prion linked to the chromatin-remodeling factor Swi1 in Saccharomyces cerevisiae. *Nat Genet* **40**, 460-465 (2008).
180. Tyedmers, J., Madariaga, M.L. & Lindquist, S. Prion switching in response to environmental stress. *PLoS Biol* **6**, e294 (2008).
181. Ahmari, S.E., Buchanan, J. & Smith, S.J. Assembly of presynaptic active zones from cytoplasmic transport packets. *Nat Neurosci* **3**, 445-451 (2000).
182. Shapira, M.*, et al.* Unitary assembly of presynaptic active zones from Piccolo-Bassoon transport vesicles. *Neuron* **38**, 237-252 (2003).
183. Anderson, P. Mutagenesis. *Methods Cell Biol* **48**, 31-58 (1995).
184. Wicks, S.R., Yeh, R.T., Gish, W.R., Waterston, R.H. & Plasterk, R.H. Rapid gene mapping in Caenorhabditis elegans using a high density polymorphism map. *Nat Genet* **28**, 160-164 (2001).
185. Tallini, Y.N.*, et al.* Imaging cellular signals in the heart in vivo: Cardiac expression of the high-signal Ca2+ indicator GCaMP2. *Proc Natl Acad Sci U S A* **103**, 4753-4758 (2006).

186. Chen, C.C., *et al.* RAB-10 is required for endocytic recycling in the Caenorhabditis elegans intestine. *Mol Biol Cell* **17**, 1286-1297 (2006).
187. Richardson, S.M., Wheelan, S.J., Yarrington, R.M. & Boeke, J.D. GeneDesign: rapid, automated design of multikilobase synthetic genes. *Genome Res* **16**, 550-556 (2006).
188. Hobert, O. PCR fusion-based approach to create reporter gene constructs for expression analysis in transgenic C. elegans. *Biotechniques* **32**, 728-730 (2002).
189. Brenner, S. The genetics of Caenorhabditis elegans. *Genetics* **77**, 71-94 (1974).
190. Mello, C.C., Kramer, J.M., Stinchcomb, D. & Ambros, V. Efficient gene transfer in C.elegans: extrachromosomal maintenance and integration of transforming sequences. *Embo J* **10**, 3959-3970 (1991).
191. Roayaie, K., Crump, J.G., Sagasti, A. & Bargmann, C.I. The G alpha protein ODR-3 mediates olfactory and nociceptive function and controls cilium morphogenesis in C. elegans olfactory neurons. *Neuron* **20**, 55-67 (1998).
192. Horton, R.M., Hunt, H.D., Ho, S.N., Pullen, J.K. & Pease, L.R. Engineering hybrid genes without the use of restriction enzymes: gene splicing by overlap extension. *Gene* **77**, 61-68 (1989).
193. Langmead, B., Trapnell, C., Pop, M. & Salzberg, S.L. Ultrafast and memory-efficient alignment of short DNA sequences to the human genome. *Genome Biol* **10**, R25 (2009).
194. Trapnell, C., Pachter, L. & Salzberg, S.L. TopHat: discovering splice junctions with RNA-Seq. *Bioinformatics* **25**, 1105-1111 (2009).
195. Wray, C. & Sojka, W.J. Experimental Salmonella typhimurium infection in calves. *Res Vet Sci* **25**, 139-143 (1978).